MASTERARBEIT | MASTER'S THESIS

Titel | Title

Incorporating beyond ΛCDM Models into Fast Predictions of the Cosmic Large Scale Structure

verfasst von | submitted by

Szymon Juszczak BSc

angestrebter akademischer Grad | in partial fulfilment of the requirements for the degree of

Master of Science (MSc)

Wien | Vienna, 2025

Studienkennzahl lt. Studienblatt | Degree programme code as it appears on the student record sheet:	UA 066 876
Studienrichtung lt. Studienblatt | Degree programme as it appears on the student record sheet:	Masterstudium Physics
Betreut von | Supervisor:	Univ.-Prof. Dipl.-Phys. Dr. sc. ETH Oliver Hahn

This thesis has been created in close collaboration and under guidance of Dr. Cornelius Rampf.

Acknowledgements

First and foremost, I would like to thank Cornelius Rampf and Oliver Hahn for their supervision my thesis. While Cornelius could not be the official co-supervisor, due to formalities, he invested an enormous amount of time into guiding me, answering my questions and giving me feedback to my work. It is not an exaggeration to say that my understanding of both the field of cosmology and the formalities of academic work have been majorly shaped and improved by him. I would like to thank Oliver for explaining key concepts of cosmological simulations, fuelling my interest in cosmology through this thesis and previous seminars, and funny conversations during meetings and lunch. While very busy, he always took his time to patiently answer my inquiries. I could not have wished for better supervisors.

I would also like to thank Florian List for answering all my (often trivial) questions about Disco-DJ, Lukas Winkler, without whom my simulations would still not work, Agata for nice conversations, and the entirety of the group for their advise during my time there.

Next I would like to thank my peers and more importantly friends, Anni, David, Isak, Konsti, Lilly, Magda and Serafin who have accompanied and supported me throughout my five years of studying physics. I am very grateful to have met such wonderful people to spend time with and look up to. I look back very fondly on the last five years and these people are a major reason why :)

Lastly, I would like to thank my mother for supporting me and giving me the opportunity to study, when she was not given the same privilege and for patiently listening to my tirades about physics and studying in general.

Kurzfassung

Das Feld der Kosmologie hat in den letzten Jahrzehnten einen bedeutenden Zustrom an neuen Daten aus Beobachtungen erfahren. Um diese Daten angemessen nutzen zu können und die Lücke zu theoretischen Vorhersagen zu überbrücken, verwendet man üblicherweise N-Körper-Simulationen der großräumigen Strukturen des Kosmos. Diese sind jedoch sowohl durch die Hardware der Rechencluster als auch durch die Effizienz der N-Körper-Simulationscodes begrenzt.

Um Letzteres zu adressieren, kann man die Zeitschritt-berechnung in diesen N-Körper-Simulationen ändern, um bei gleicher Genauigkeit (oder sogar verbesserter), durch den Einsatz der Lagrangeschen Störungstheorie, die Anzahl der notwendigen Zeitschritte zu reduzieren.

Diese Masterarbeit präsentiert in erster Linie die Theorie hinter der erweiterten Version des auf der Lagrangeschen Störungstheorie basierenden BULLFROG-Integrators, wie er in das Simulationsekosystem Disco-DJ (Differentiable Simulations in COsmology, Done by Jax) der Kosmologiegruppe der Universität Wien implementiert wurde, sowie die Tests dieser Implementierung. Dieses Upgrade umfasst ein dynamisches Dunkle-Energie-Modell, gegeben durch die Chevallier-Polarski-Linder-Parametrisierung unter Hinzufügung einer nicht verschwindenden Krümmung. Zweitens werden neue theoretische Einsichten diskutiert, die für die Implementierung weiterer Modelle in das BULLFROG-Integrationsschema relevant sein werden.

Wir stellen fest, dass das nichtlineare spektrale Materie-leistungsspektrum unserer BULLFROG-Implementierung, unter Annahme eines dynamischen Dunkle-Energie-Modells, mit dem nichtlinearen Leistungsspektrum von „baccoemu“ innerhalb von 1% auf linearen Skalen übereinstimmt und eine deutliche Verbesserung der Genauigkeit gegenüber dem FASTPM-Integrationsschema zeigt, wobei ungefähr halb so viele BULLFROG-Schritte erforderlich sind, um die gleiche Genauigkeit zu erreichen. Dadurch wird auch die Simulationsdauer erheblich reduziert.

Abstract

The field of cosmology has experienced a significant influx of new observational data in the last decades. In order to adequately utilise this data and bridge the gap to theoretical predictions, one usually employs N-body simulations of the large scale structure. These, however, are limited by the hardware of computational clusters, and the efficiency of N-body simulation codes.

To address the latter of these issues one can change the time-stepping in these N-body simulations, to maintain (or even improve) the accuracy of these, reducing the amount of time steps necessary through the use of Lagrangian perturbation theory.

This master thesis then primarily, presents the theory behind the upgraded version of the Lagrangian perturbation theory informed BULLFROG integrator scheme as implemented into the university of Vienna's cosmology group's simulation ecosystem Disco-DJ (Differentiable Simulations in COsmology, Done by Jax), and the tests of this implementation. This upgrade includes a dynamical dark energy model, as given through the Chevallier-Polarski-Linder parametrisation with the addition of non-zero curvature. Secondly, it discusses new theoretical insights, which will be relevant for the implementations of further models into the BULLFROG integration scheme.

We find that our BULLFROG implementation's non-linear power spectrum, assuming a dynamical dark energy model, is consistent with the non-linear-power spectrum of "baccoemu" within 1% on linear scales and shows a significant improvement in accuracy to the FASTPM integration scheme, where roughly half as many BULLFROG steps are required to reach the same accuracy, therefore also reducing the simulation duration significantly.

Contents

List of Figures

1 Introduction

The Λ cold dark matter (ΛCDM) model [1, 2] has seen stunning success in describing the observed evolution of the universe in the past [3], while remaining a very simple and mathematically well behaved model. It has therefore been termed the standard model of cosmology. The model is built upon the basic assumptions that:

- The universe is statistically homogeneous and isotropic on large scales, i.e., it satisfies the cosmological principle.
- General relativity is the correct gravitational theory on cosmological scales.
- The energy content of the universe is given by radiation, baryonic matter, cold dark matter and dark energy (DE), with the last one being governed by the cosmological constant Λ.

These assumptions yield a minimal condensed model (excluding massive neutrinos), which is dependent only on six free independent parameters (massive neutrinos would add a seventh parameter [4]): the baryonic and cold dark matter energy densities Ω_b and Ω_CDM, the angular diameter distance to the sound horizon at the time of last scattering θ_s, the primordial scalar fluctuations amplitude A_s, spectral index n_s and finally the optical depth of re-ionization τ [5].

The successes include, but are not limited to strong agreement with the cosmic microwave background (CMB), predictions of the baryonic acoustic oscillations (BAO) in the early universe and “survival” of a variety of observational stress tests [3]. Increasingly precise measurements have yielded a variety of tensions, most prominently the so-called Hubble tension [5, 6], which is the tension in measurements of the Hubble constant H_0, and is currently at $\approx 4\sigma$. The Hubble constant relates the velocity, with which objects move away from us today to their distance [5]. Additionally, the Dark Energy Spectroscopic Instrument (DESI) observations, seem to favour a dynamical DE, rather than one governed by a constant [7]. Whether DE is time-dependent or constant, ΛCDM remains a "unsatisfying" theory from a naturalness point of view (i.e. it is not derivable by some more fundamental theory): the cosmological constant (which is thought to be interpretable as the vacuum energy density) can be calculated from the standard model of particle physics (SM) in an effective field theory (EFT) approach, which yields a discrepancy of 10^{55} between calculated and measured values for Λ, which is part of the so-called cosmological constant (CC) problem [3]. It is not certain what the correct approach is to alleviate the various tensions and the CC problem. Proposals range from modifying DE, for example through an early dark energy model [8], modifying GR [3], eternal inflation [9] and, in the case of the Hubble tension, it might also be systematic problems with the measurements, although it is not believed to be the only source of the discrepancy [5, 6, 9].

These recent results and considerations have renewed interest in models beyond ΛCDM. One of the most precise methods to bridge the gap between observations and the theory is through

N-body simulations. These, however, have the distinct disadvantage of being computationally expensive. One can approach this problem by improving the strength of the hardware and/or by optimising the code. Recently, multiple research groups around the globe have been developing so-called fast N-body simulation techniques [10, 11, 12, 13, 14, 15]. This reduces the amount of time steps required, while maintaining a very high standard of accuracy compared to regular integrators, which have a far inferior scaling.

This thesis then presents two of these fast (D-time) integration schemes, BULLFROG and FASTPM applied to a dynamical DE model with non-zero curvature in the form of the Chevalier-Polarski-Lindner (CPL) DE model [16]. Our implementation of these is then compared with the cosmological simulation code CO*N*CEPT [17] and with the power spectrum emulator Bacco [18] as well.

The novelty lies in the extension of BULLFROG towards the CPL model, and the analytical discussion, which is a necessary prerequisite for each new model one would like to include in the BULLFROG integration scheme. Previous implementations have included matter and DE given through the cosmological constant Λ only [15].

Within cosmological simulations a very broad spectrum of numerical and discretisation problems can arise, the suppression of which is an ongoing research topic, see [19] for an overview. In this work we focus on the time evolution and assume that numerical inaccuracies are sufficiently suppressed.

The structure is as follows: Chapter 1 gives a general introduction to the parts of cosmology, which are relevant to the thesis, for readers new to the field and explains the "position" of the thesis within the context of cosmological research. In chapter 2 we introduce theoretical considerations and the models which we have been simulated. Chapter 3 covers the Lagrangian perturbation theory, that is essential to the implementation of BULLFROG, which is then the focus of chapter 4. In chapter 5 we then compare our implementation against CO*N*CEPT and Bacco, and discuss our findings in chapter 6.

1.1 Cosmology

The nature of the universe as a whole has been a mystery which humans have been wondering about, dating as far back as far as the 16th century B.C. [20] in Mesopotamia, and most likely even earlier. Proposed explanations have varied over time, from the geocentric model in the medieval ages, formally established in the 5th century A.D. [21], to the heliocentric model proposed by Copernicus [22] in 1543. Ever since the 17th century onwards there was mounting evidence that the milky way consists of stars and is thus the center of our universe, which is also known as the galactocentric model. However the precise structure of the milky way and our position in it remained elusive. At the turn of the 20th century the question about the nature of "spirals" in the sky became central with one side arguing that these are small objects within the milky way and the other arguing for so-called "island universes" which correspond to our own milky way. The conflict was resolved by Edwin Hubble in 1924 (formally published in a paper in 1925) who used the Leavitt Law to measure the distance to cepheids within these "spirals" and showed that they are in fact galaxies just as our milky way, thus creating the "acentric" model [23]. This answer of course only raised further questions, as the universe, according to our understanding, became a lot larger. Five years later Hubble discovered what later become known as "Hubble's Law" which showed that the velocity of a galaxy is proportional to its distance (isotropically), a property that is most easily explained by an expanding universe [24]. This can be regarded as the beginning of modern cosmology. Many more different explanations have been offered to explain the nature of the universe in the early 20th century, which have not been confirmed by later observations, but were plausible at the given time. As Lev Landau very famously remarked: "Cosmologists are often in error, but never in doubt."[25], a very critical opinion on the state of early modern cosmology during a time when observations of the distant universe were very scarce. Results from multiple recent space and ground based experiments, like for example COBE [26], WMAP [27] and PLANCK [28] have given us data about the CMB and therefore the early universe, and, combined with surveys of the late universe like e.g. the HSC [29], Euclid [30], LSST [31] and various Hubble space Telescope surveys have then led to the establishment of the "standard model of cosmology" ΛCDM. In what follows we will explain key parts of the theory behind cosmology and the ΛCDM model. Readers familiar with this topic can skip towards chapter 2, which is the starting point of the main work for this thesis.

1.1.1 Introductory Elements of Modern Cosmology

Central to our study of the universe is the cosmological principle, which was initially postulated for mathematical convenience, but has since been confirmed by a multitude of observations [4]. It states that the universe is statistically **homogenous** and **isotropic** on large scales. Heuristically, one can say that the universe looks statistically the same in every direction (isotropic) and it does so at every point in space (homogenous) (see [2] for a more formal approach). Specifying now that our universe is spatially isotropic and homogenous, the topology of our universe becomes restricted to three possibilities: $\mathbb{H}^3$, $\mathbb{R}^3$, and $\mathbb{S}^3$, which will be specified through a parameter $k = \{-1, 0, 1\}$ (Note that these are the simplest topologies, as technically $k = 0$, which means flat space, can also correspond to something like a three torus $S_1 \times S_1 \times S_1$. The theoretical number of topologies is therefore slightly larger [2]). One can derive a metric that encapsulates all of these, dependent on this curvature parameter k, and additionally includes the expansion of space itself. This is the known as the Friedmann-Lemaitre-Robertson-Walker (FLRW) metric, and given through the following line element:

$$ds^2 = -\mathrm{d}t^2 + a^2(t)\left(\frac{\mathrm{d}r^2}{1-kr^2} + r^2(\mathrm{d}\theta^2 + \sin^2(\theta)\mathrm{d}\varphi^2)\right), \tag{1.1}$$

which we have written in temporal radial coordinates (t, r, θ, φ) (see [2, 4, 32] for possible ways of deriving this metric). Here $a(t)$ is the scale factor which is usually normalised as $a \in [0, 1]$ with $a(t = 0) = 0$, where $t = 0$ corresponds to the big bang and $a(t_{\mathrm{today}}) = 1$ is the scale factor today. We can see from this, that instead of using the cosmic time t as our time variable we can use the measure of how much the universe has expanded (given through a) as a time variable instead, which we shall do in later sections, as it turns out to be more convenient. The explicit form of the scale factor can be determined by solving a set of differential equations, which depend on the energy content within our universe, the so-called Friedmann equations. These equations are derived by inserting all energy contributions into the stress energy tensor $T_{\mu\nu}$ on the right hand side (RHS) of the Einstein field equations (EFE) 1.2 below and our FLRW metric from above 1.1

$$R_{\mu\nu} - \frac{1}{2}Rg_{\mu\nu} + \Lambda g_{\mu\nu} = 8\pi G T_{\mu\nu}\,, \tag{1.2}$$

where, $g_{\mu\nu}$ is the metric, $R_{\mu\nu}$ the Ricci tensor R ,the Ricci scalar [33] and we have set $c = 1$. Here we have already written the EFE with the Λ term included, which signifies a constant dark energy. Since $\nabla_\mu T^{\mu\nu} = 0$, adding and removing a term, which is proportional to a constant times the metric, is always possible, because the Levi-Civita connection implies $\boldsymbol{\nabla g} = 0$ [34]. The dynamics with this Λ term included are of course different to a model with its absence. Assuming the minimal ΛCDM model contributions to the stress-energy tensor, i.e. matter and radiation, will yield a stress energy tensor of the following form $T_{\mu\nu} = \mathrm{diag}(-\rho, p, p, p)$, where we do not distinguish between species densities, but summarize them into one total density ρ and one total pressure p. Note that we only have one p in each spatial direction, which is a consequence of isotropy. One can also absorb the Λ term into the $T_{\mu\nu}$ on the RHS and view dark energy as a part of the energy content rather than a part of the curvature on the left hand side (LHS) (hence the name "dark energy"). In this standard way we can derive the Friedmann equations by inserting into the 00-component of the EFE and into the spatial components of the EFE respectively, which yields the following:

$$H^2 = \left(\frac{\dot{a}}{a}\right)^2 = \frac{8\pi G}{3}\rho - \frac{k}{a^2}\,, \tag{1.3}$$

$$\frac{\ddot{a}}{a} = -\frac{4\pi G}{3}\left(\rho + 3p\right) = -\frac{4\pi G}{3}\rho\left(1 + 3w\right)\,, \tag{1.4}$$

where $w = p/\rho$ is the equation of state parameter and H is the Hubble function. Additionally, inserting into $\nabla_\mu T^{\mu\nu} = 0$, we get the continuity equation:

$$\dot{\rho} + 3\frac{\dot{a}}{a}\rho\left(1 + w\right) = 0\,. \tag{1.5}$$

Each species has its own density ρ_i, pressure p_i and therefore its own equation of state parameter w_i. Within our minimal ΛCDM model this means that $\rho_{\mathrm{matter}} \propto a^{-3}$, $\rho_{\mathrm{rad}} \propto a^{-4}$, $\rho_k \propto a^{-2}$ and $\rho_{\mathrm{DE}} \propto a^{-3(1+w_{\mathrm{DE}})}$, where $w_{\mathrm{DE}} = -1$ and therefore $\rho_{\mathrm{DE}} \propto$ some constant. The radiation density includes all relativistic particles, which include photons, massless neutrinos and gravitons. The total density ρ is then simply a linear combination of all the species densities and so is the total pressure. To study simple solutions of the respective epochs, one usually assumes that within a given time frame it is sufficient to consider only the dominant component in the universe. Therefore, one would first look at a radiation dominated universe, which has a equation of state parameter $w_{\mathrm{rad}} = 1/3$, followed by a matter dominated universe with $w_{\mathrm{matter}} \approx 0$ and lastly, a Λ dominated universe with $w_{\mathrm{DE}} = -1$, which also corresponds to the epoch today [4] (see also [4] for a derivation of these parameters). Solving the first Friedmann equation for these single component universes yields the following scale factors:

$$a(t) \propto t^{1/2}\,, \quad w = 1/3\,, \tag{1.6}$$

$$a(t) \propto t^{2/3}\,, \quad w = 0\,, \tag{1.7}$$

$$a(t) \propto \mathrm{e}^{H_0 t}\,, \quad w = -1\,. \tag{1.8}$$

An essential definition for the subsequent discussion is that of the critical density $\rho_{\text{crit}} = 3H^2/(8\pi G)$ of the universe, for which $k = 0$, i.e. it determines the density of a flat universe. This can be seen from the first Friedmann equation (1.3). We can use the critical density today ρ_{crit0} as a "reference density" and talk about energy densities relative to the critical one $\Omega_i = \rho_i/\rho_{\text{crit0}}$, which are normalised as $\sum_i \Omega_i = 1$. If we now explicitly write out (1.3) with the component densities explicitly we arrive at:

$$H^2 = \frac{8\pi G}{3}\left(\rho_{\text{r0}}a^{-4} + \rho_{\text{m0}}a^{-3} + \rho_{k0}a^{-2} + \rho_{\text{DE0}}\right) , \tag{1.9}$$

where we have defined $\rho_{\text{k0}} = -3k/(8\pi G)$. By multiplying (1.9) with $\rho_{\text{crit0}}/\rho_{\text{crit0}}$ and using the fact that $H_0^2 = 8\pi G\rho_{\text{crit0}}/3$, we arrive at the alternative formulation of the first Friedmann equation:

$$\left(\frac{H}{H_0}\right)^2 = \Omega_{\text{r0}}a^{-4} + \Omega_{\text{m0}}a^{-3} + \Omega_{\text{k0}}a^{-2} + \Omega_{\text{DE}} . \tag{1.10}$$

Different models with various contributions in their Friedmann equations shall be discussed further in chapter 2.

Redshift and Scale Factor The redshift z that light experiences when the source moves away from the observer is given by the following relation:

$$z = \frac{\lambda_{\text{observed}} - \lambda_{\text{emitted}}}{\lambda_{\text{emitted}}} . \tag{1.11}$$

We know from Hubble's observations that space is expanding and therefore objects which are further away, move away with higher velocities and are redshifted stronger [24]. This effect is referred to as the "cosmological redshift" in contrast to the "gravitational redshift", which light experiences, when it moves away from massive objects [35]. In this sense the redshift is a measure of the distance to objects in the sky. However, since the speed of light is finite, light emitted from objects further away has also been emitted when the universe was "younger", and arrives with a stronger redshift. Therefore, redshift can also be used as a measure of time in the universe, with a higher redshift corresponding to an earlier cosmic time in the universe [4]. It is therefore also possible to derive a (surprisingly simple) relation between the redshift and the scale factor:

$$a = \frac{1}{1+z} . \tag{1.12}$$

(see [4] chapter 2.5.4 or [32] chapter 1.2 for derivations). We have now established the topology of space, its expansion and ways to quantify at what point in time we are throughout the evolution of the universe, given the validity of the ΛCDM model. We will now move on to discuss important events within the history of the universe.

1.1.2 Hot Big Bang and Inflation

The hot Big Bang model is the currently accepted explanation for the "start" of the universe and its validity is based on the so-called "three pillars of the Big Bang model":

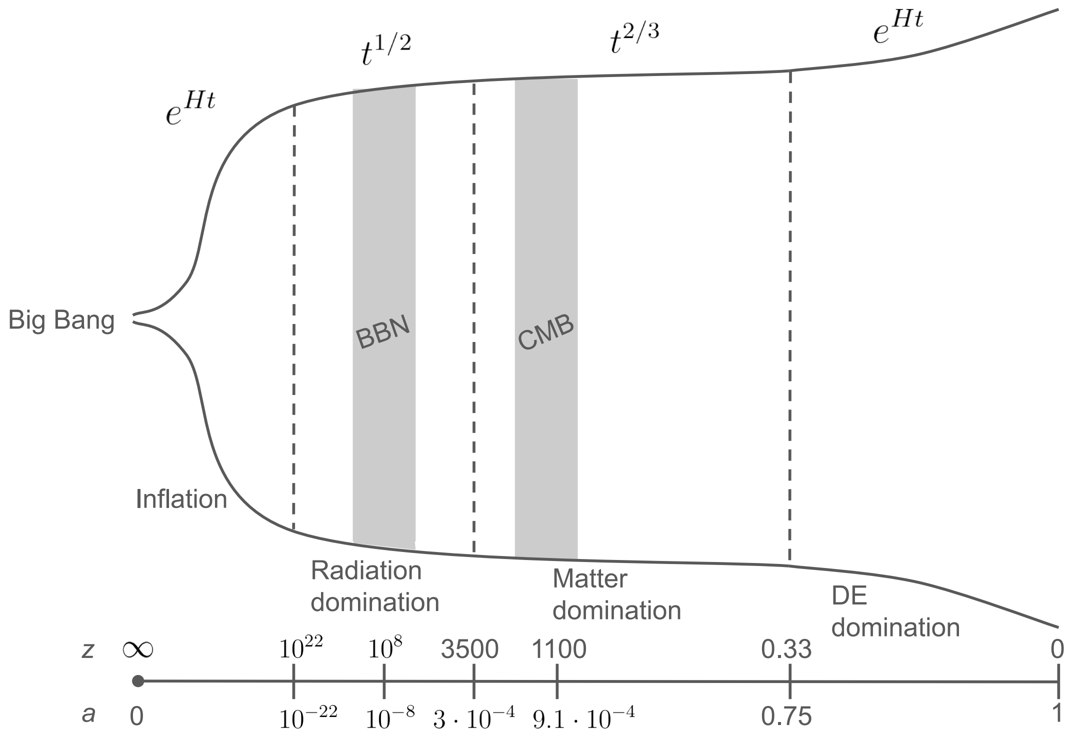

Figure 1.1: Timeline of the universe, with values of the scale factor a and their corresponding redshift values z below the figure. At the top one can see how $a(t)$ increases with cosmic time t during each epoch. The figure was inspired by [4].

1. Expansion of the universe, as firstly measured by Hubble [24]

2. Existence of the CMB measured by a variety of missions [26, 27, 28],

3. Light element abundances due to the high initial temperature and an appropriate scaling of temperatures with the expansion rate of the universe, also known as Big Bang Nucleosynthesis (BBN) [4].

Explaining all three simultaneously is possible through the hot Big Bang model. It is therefore viewed as part of the standard model. The only real alternative to this, the steady-state model, which proposed that the universe is infinitely old and mostly unchanging, has been discarded some time ago, since the three pillars above are well established by measurements. The consensus among cosmologists is therefore, that this is currently the appropriate model for the early time of the universe [4].

Simply assuming a hot Big Bang, which immediately moves into a radiation dominated era, creates multiple problems with observations:

1. Flatness Problem,

2. Horizon Problem,

3. Magnetic Monopole Problem.

We shall briefly discuss them here, and how inflation can be used to solve them all in one framework, but more detailed explanations can be found in [2, 4, 32, 36].

Flatness Problem CMB measurements imply that the universe is close to flat with very high certainty [28], i.e.

$$\Omega_{\text{tot0}} = 0.999 \pm 0.002\,, \tag{1.13}$$

where Ω_{tot0} is the sum of all energy densities today, except for curvature. For any arbitrary time we can rewrite the first Friedmann equation (1.10) into:

$$1 - \Omega_{\text{tot}}(t) = -\frac{k}{a^2H^2}\,, \tag{1.14}$$

where $\Omega_{\text{tot}}(t)$ is just the sum of all non-curvature energy density terms times $(H_0/H)^2$. We can see that if the universe is flat at some point in time, it will remain so continuously. From the definition of Ω_{tot0} we can also write:

$$1 - \Omega_{\text{tot0}} = -\frac{k}{H_0^2}\,. \tag{1.15}$$

Dividing (1.14) by (1.15) yields:

$$1 - \Omega_{\text{tot}}(t) = (1 - \Omega_{\text{tot0}})\left(\frac{H_0^2}{a^2H^2}\right)\,. \tag{1.16}$$

By approximating our universe as having single fluid contents for evaluating a and H, and using our knowledge of Ω_{tot0}, H_0^2, one can find bounds on the LHS of the equation, which we quote from [4] for different times in the universe:

$$|1 - \Omega_{\text{tot}}(t_{\text{rec}})| \lesssim 10^{-5}\,, \tag{1.17}$$

$$|1 - \Omega_{\text{tot}}(t_{\text{BBN}})| \lesssim 10^{-18}\,, \tag{1.18}$$

$$|1 - \Omega_{\text{tot}}(t_{\text{Planck}})| \lesssim 10^{-63}\,, \tag{1.19}$$

where a matter only universe is assumed in the first estimate and a radiation dominated universe in the other two; $t_{\text{rec}} \approx 0.4$ Myr refers to the time of recombination, when electrons and protons within the plasma of the universe first combined into hydrogen, $t_{\text{BBN}} \approx 100$ s to the beginning of BBN, when the fusion of light elements happened and t_{Planck} the Planck time. We can see that if our universe had non-zero curvature, which is compatible with our current measurement, it had to be extremely fine-tuned, in order to remain as small as it is today [4].

Horizon Problem Uniformity of the CMB and the fact that its anisotropies $\delta T/T$ are of order 10^{-5}, imply that the photon plasma was almost in thermal equilibrium at last scattering, the event signifying the end of recombination. From the particle horizon at- and the angular diameter distance to last scattering we can deduce the angle subtended on the sky that corresponds to the particle horizon on the surface of last scattering:

$$\theta \approx 1.8^\circ \,. \tag{1.20}$$

This means that only regions with a diameter 2° on the CMB could be causally connected, which is necessary to achieve thermal equilibrum. However, there are about $40 \cdot 10^3$ square degrees on the entire sky, which means that $40 \cdot 10^3/(2 \cdot 2) = 10^4$ patches should be causally disconnected, even though they show an almost perfectly uniform temperature. It is very unlikely, that this is an coincidence and therefore requires a mechanism that explains this phenomenon [4, 36].

Magnetic Monopole Problem The framework of Grand Unified Theories (GUT) tries to unify the strong nuclear force with the electroweak force into one symmetry group, that is broken at very high energies. These energies would have been present during the initial stages of the hot big bang, and one of the GUT predictions is that this symmetry breaking should produce a sizeable amount of magnetic monopoles. At the time of GUT symmetry breaking $\sim 10^{-37}$s [35] their density should be $\sim 10^{76}\mathrm{cm}^{-3}$ with a particle mass of $10^{13} - 10^{18}$GeV. This means that the universe should have been dominated by magnetic monopoles and we should see an abundance of them (Their mass density should larger than that of baryons by a factor of 10^{14} [35]). However, not a single one has been found so [36].

Inflation In order to see how inflation can solve these problems we shall assume that the universe underwent an exponential expasion with an equation of state parameter $w \approx -1$. In this case the first Friedmann equation (1.3) is equal to the second one (1.4) i.e. $\ddot{a}/a = (\dot{a}/a)^2$, which is equivalent to saying:

$$\frac{\mathrm{d}}{\mathrm{d}t}\left(\frac{\dot{a}}{a}\right) = 0\,, \tag{1.21}$$

$$\Leftrightarrow H = \frac{\dot{a}}{a} = \text{const.}\,, \tag{1.22}$$

which means that $a \propto \mathrm{e}^{Ht}$. One can now introduce the number of e-folds N, which is defined as $N := \int H\mathrm{d}t \simeq H\Delta t$, where the second equality is valid during inflation, Δt is the duration of inflation and therefore $a \propto \mathrm{e}^N$. It turns out that assuming $N \gtrsim 60$ e-folds is sufficient to make the observable universe appear flat, even though it could be curved globally [4, 36]. It also means that the entire sky we observe today had a chance of being in contact with itself and therefore the possibility to establish thermal equilibrium [4, 36]. Lastly, the amount of magnetic monopoles gets diluted very strongly, such that we should at most be able to detect at most one within the observable universe [35]. The greatest success of inflation has, however not just been the fact that it solves these so-called "coincidence problems" of the universe, but also the fact that its predictions of the spectral index n_s (one of the cosmological parameters of ΛCDM) is in very good agreement with measurements $n_s = 0.966 \pm 0.005$, when assuming a slow-roll model of inflation [4], which we very briefly outline in the next section. It has therefore become part of the standard model of cosmology.

Graceful Exit and Reheating In modern inflation one assumes that the exponential expansion is caused by the so-called "inflaton" scalar field ϕ_I, which proceeds via second order phase transition, in contrast to the originally proposed first order phase transition. This inflaton moves in a potential $V(\phi_\mathrm{I})$ and its density ρ_I and pressure p_I are given by:

$$\rho_\mathrm{I} = \frac{1}{2}\dot{\phi}_\mathrm{I}^2 + V(\phi_\mathrm{I})\,, \quad p_\mathrm{I} = \frac{1}{2}\dot{\phi}_\mathrm{I}^2 - V(\phi_\mathrm{I})\,. \tag{1.23}$$

Its "motion" in the potential follows the differential equation:

$$\ddot{\phi}_\mathrm{I} + 3H\dot{\phi}_\mathrm{I} + \partial_{\phi_\mathrm{I}} V(\phi_\mathrm{I}) = 0\,, \tag{1.24}$$

which is often referred to as "Slow-Roll Model", since this differential equation is equivalent to the motion of a ball rolling down a hill. In the modern picture, inflation ends with a so-called "Graceful Exit", where $V(\phi_\mathrm{I}) \to 0$ smoothly and, due to oscillations around this minimum, produces fermions and bosons in phases which are referred to as "Reheating" and "Preheating" respectively. In this sense, the energy of the Inflaton is the origin of the matter and radiation we see today [4].

1.1.3 Plasma Phase

After reheating, the universe is an plasma with a high temperature and expands as $a(t) \propto t^{1/2}$. Note that this transition from Inflation to radiation domination in the scale factor cannot be done through an analytical Taylor expansion of the scale factor. The most notable events during this epoch of the universe are the neutrino decoupling, Big Bang nucleosynthesis, matter-radiation equality and finally Recombination. We will briefly discuss each of these in what follows.

Massive Neutrino Decoupling Roughly one second after the Big Bang, once the universe has cooled down to about 1 MeV, the Hubble factor becomes large enough such that neutrino interactions through the weak force freeze out, and their number density starts scaling $\propto a^{-3}$, while their momentum decreases as $\propto a^{-1}$, just like their temperature. Since radiation temperature scales as $\propto (a \cdot g_{*\mathrm{S}}^{1/3})^{-1}$, where $g_{*\mathrm{S}}$ is the effective number of relativistic degrees of freedom, these two species become decoupled at this stage and the so-called "cosmic neutrino background" (CNB) is emitted. Note that massive neutrinos remain relativistic even well beyond the matter-radiation equality, which means that neutrinos behave as radiation would. It is predicted that the CNB has a temperature of 1.96K today, and while it was not detected as of yet, it is in principle possible to do so and would signify a strong confirmation of the Big Bang model [4].

Big Bang Nucleosynthesis A few minutes ($z = 10^8$) after the Big Bang, or when the universe cooled down to a temperature of 0.1 MeV the so-called "Big Bang nucleosynthesis" (BBN) happened, which is the fusion of protons and neutrons into the light elements of the periodic table. The stable ones of these are Hydrogen $^1_1$H, Deuterium $^1_2$H, Helium-4 $^4_2$He and Lithium $^7_3$Li. This resulted in the majority of baryonic matter consisting of elementary hydrogen $\approx 75\%$ and Helium-4 with $\approx 24\%$. The first three elements are in good agreement with BBN predictions, while the Lithium abundance is discrepant with it. This so-called "lithium problem" is one of the tensions to the ΛCDM model [4].

Matter-Radiation Equality The moment when the contribution of matter towards the total energy density becomes dominant is referred to as the "matter-radiation equality" and happened $\approx$ 50 000 years or at redshift $z = 3500$ after the Big Bang. The epoch of matter domination begins as of that point, the epoch during which matter perturbations could begin to grow [4]. It is therefore the moment when the scale factor moves towards growing as $a \propto t^{2/3}$.

Recombination During the plasma phase of the universe baryons and photons were very tightly coupled through Thomson scattering:

$$\gamma + e^- \rightleftharpoons \gamma + e^- \,, \tag{1.25}$$

where γ is a photon and e^- is an electron. The latter is then coupled to protons via electromagnetic force, therefore resulting in the combined baryon-photon plasma. Once the temperature in the universe is low enough the ionised nuclei from BBN combine with the electrons to form neutral atoms. This reduces the density of electrons in the universe and therefore also the Thomson scattering rate. This means that photons can then freely propagate through the vacuum until today, which is referred to as the cosmic microwave background (CMB). This phase is referred to as "recombination" and is a process that started at $z = 1450$ where 90% of the hydrogen was still ionised and ended somewhere around $z = 1060$ when only 10% was still ionised, which is a time frame of about 300 000 years. This time period is essential for modern cosmology, as the CMB is one of the strongest foundations of the ΛCDM model's validity [4].

1.1.4 Structure Formation

The matter domination era is of central importance for the way structure growth. It is in this time period that the so-called "cosmic web" formed, see figure 1.2. We shall briefly discuss the most important findings here, while more detailed derivations, which are also more closely related to the work of this thesis can be found in chapter 2. We start of by stating the ordinary differential equation (ODE) that describes the linear growth of perturbations in the universe (for sub-horizon scales):

$$\ddot{\delta} + 2H\dot{\delta} - 4\pi G\bar{\rho}(t)\delta = 0\,, \tag{1.26}$$

where H is the Hubble factor, G the gravitational constant and $\bar{\rho}$ the average density of matter. A precise derivation of this equation can be found in [4] or in sections 2.2-2.3. During radiation domination, we know that $a \propto t^{1/2}$, and where we can neglect the last term in the ODE, to find the following solution:

$$\delta_{\text{rad}} = C_1 + C_2 \ln(t)\,, \tag{1.27}$$

where C_1 and C_2 are functions of space, but constant in time. We can see that structures grow logarithmically during this time epoch. Meanwhile, during matter domination, when the last term is not negligible, and yields the following solution:

$$\delta_{\text{matter}} = C_1 t^{2/3} + C_2 t^{-1} \propto C_1 a + C_2 a^{-3/2}\,, \tag{1.28}$$

where we have used that during matter domination $a \propto t^{2/3}$ and therefore the Hubble function in 1.26 is now different than when we considered radiation domination. As we can see, the growth of structures is proportional to the matter domination scale factor or $t^{2/3}$ and therefore significantly faster than during radiation domination. This is incredibly relevant, as the matter domination era lasted about 10 billion years. For comparison, the total age of the universe is estimated to be about 13.8 billion years [5]. It is therefore in this time frame, in which the majority of structures formed. Finally, assuming the standard minimal ΛCDM model we can also look at what happens deeply in the DE dominated phase, where again we can neglect the contribution from the last term in 1.26:

$$\delta_{\text{DE}} = C_1 + C_2 e^{-2Ht} \simeq C_1\,. \tag{1.29}$$

This now tells us, that structures remain constant, i.e. stop growing. Suppression of structure growth can be already observed in our universe at $z \lesssim 1$ [4]. Note that this discussion assumes single component universes. In chapter 2, we shall numerically investigate combined models, which yield more detailed results, allowing for smooth transitions between the various epochs.

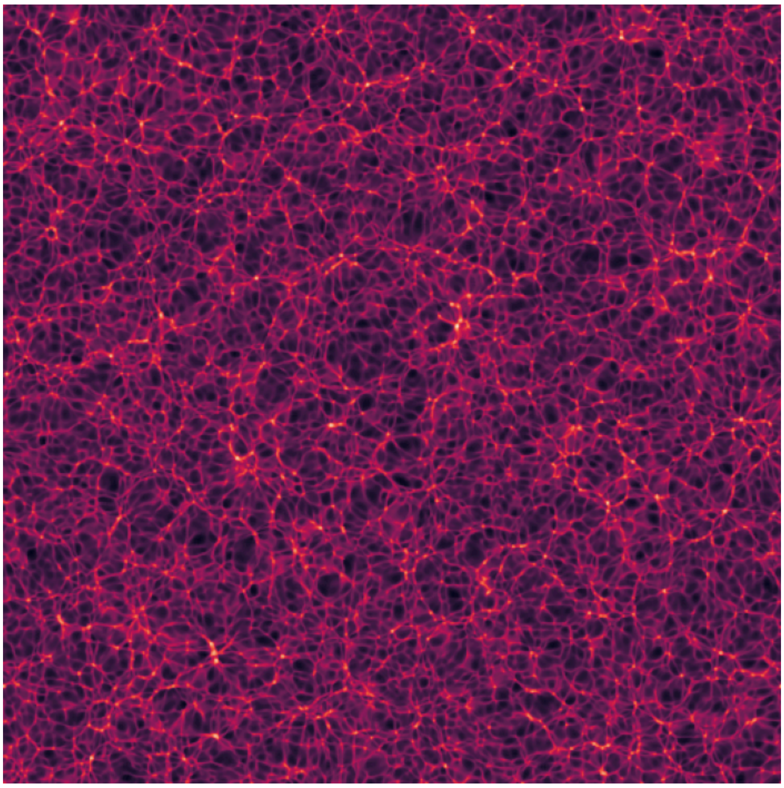

Figure 1.2: Slice along x-axis of the simulated universe using the BullFrog time-integration scheme with 50 steps at $a = 1$ (within the Disco-DJ ecosystem). The web-like structure is easily discernible, which is a consequence of matter clustering due to gravity. The length of one side of the box equals $L = 1.024$ Gpc.

2 Eulerian Fluid Equations in Cosmology

Before we attempt to simulate the universe, we must first clarify the dynamics, which govern it on the relevant scales. In this chapter we first discuss the evolution of the background spacetime through the Friedmann equations, which we derive from general relativistic considerations, in section 2.1. Afterwards we derive dynamics of matter in the universe through the formalism of fluid equations on both the background and fluctuation level in section 2.2. Next, we derive the ODE for the time evolution of matter perturbations in the universe 2.3. In sections 2.3.1-2.3.4 we discuss the growth of perturbation for different models and discuss the early time and initial conditions for our dynamical dark energy (DDE) model with non-zero curvature in sections 2.3.5 and 2.3.6. These last four subsections contain the novel theoretical work of this thesis. We set $c = 1$ for the entire work.

2.1 Derivation of Background Equations

We would like to derive the Friedmann equations in the presence of a DE component and non-zero curvature $k = \{-1, 0, 1\}$ for the background metric. These will then tell us the evolution of the scale factor $a(t)$. Our metric in spatial polar coordinates (r, θ, φ) and cosmic time t is given by:

$$ds^2 = -\mathrm{d}t^2 + a^2(t)\left(\frac{\mathrm{d}r^2}{1-kr^2} + r^2(\mathrm{d}\theta^2 + sin^2(\theta)\mathrm{d}\varphi^2)\right) . \tag{2.1}$$

This is used to calculate the Christoffel symbols $\Gamma^{\lambda}_{\mu\nu}$, the Ricci tensor $R_{\mu\nu}$ and the Ricci scalar R [2, 4, 32]. Later we will turn towards Cartesian coordinates. Next we write the EFE, with the DDE being a part of the total stress-energy tensor:

$$(T^{\mu}_{\nu}) = \mathrm{diag}(-\rho_{\mathrm{matter}}, 0, 0, 0) + \mathrm{diag}(-\bar{\rho}_{\mathrm{DE}}, \bar{p}_{\mathrm{DE}}, \bar{p}_{\mathrm{DE}}, \bar{p}_{\mathrm{DE}}) . \tag{2.2}$$

Here ρ_i denote the density of a certain species and p_i the corresponding pressure. A bar above a given quantity means that it affects the background evolution only. We consider DE to be part of the background evolution only, so it has no fluctuating component, in contrast to matter, which can be split into: $\rho_{\mathrm{matter}} = \bar{\rho}_{\mathrm{matter}}(1 + \delta)$, as we will see later on. Note that we assume the matter part to be pressure-free, since we are not including baryonic matter (or assume it to behave like dark matter, i.e. we assume it to be collisionless). Alternatively, we can assume that DE is a single real scalar field with an unspecified potential $V(\phi)$ such that:

$$T^{\phi}_{\mu\nu} = \partial_\mu\phi\partial_\nu\phi - g_{\mu\nu}\left(\frac{1}{2}g^{\alpha\beta}\partial_\alpha\phi\partial_\beta\phi + V(\phi)\right) . \tag{2.3}$$

This is very similar to the approach one would use to model inflation [4]. Since both inflation and DE describe an exponential expansion of space, it is not surprising, that their mathematical treatment turns out to be similar. One can then write:

$$T^{\phi}_{00} = \frac{1}{2}\dot{\phi}^2 + V(\phi) + \frac{1}{2}g^{kl}(\partial_k\phi)(\partial_l\phi)\,, \tag{2.4}$$

$$T^{\phi}_{ij} = (\partial_i\phi)(\partial_j\phi) + \frac{1}{2}g_{ij}\dot{\phi}^2 - g_{ij}V(\phi) - g_{ij}g^{kl}(\partial_k)(\partial_l\phi)\,, \tag{2.5}$$

where latin indices run over spatial components $i = (1, 2, 3)$ and greek indices run over space-time components $\mu = (0, 1, 2, 3)$. If we then assume the scalar field to be part of the background evolution only, $\phi = \bar{\phi}$, with no fluctuating component, it follows that $\partial_i\phi = 0$ and thus:

$$\bar{T}^{\phi}_{00} = \frac{1}{2}\dot{\phi}^2 + V(\phi) = \bar{\rho}_{\phi}\,, \tag{2.6}$$

$$\bar{T}^{\phi}_{ij} = \frac{1}{2}g_{ij}\dot{\phi}^2 - g_{ij}V(\phi) = g_{ij}\bar{p}_{\phi}\,. \tag{2.7}$$

One can see that these are very similar to the scalar field equations in modern inflation 1.23. We can then identify, by imposing $\bar{T}^{\mathrm{DE}} = \bar{T}^{\phi}$, with $\bar{T}^{\mathrm{DE}}$ being the DE part of the previous stress-energy tensor 2.2:

$$\bar{\rho}_{\mathrm{DE}} = -\bar{\rho}_{\phi}\,, \quad \bar{p}_{\mathrm{DE}}\delta_{ij} = \bar{p}_{\phi}g_{ij}\,. \tag{2.8}$$

Which means that, at the background level, a perfect fluid Ansatz is equivalent to a scalar field Ansatz for DE. Now we want to derive the evolution of the scale factor in the form of the Friedmann equations. To do this we insert the background contributions into the EFE.

$$R_{\mu\nu} - \frac{1}{2}Rg_{\mu\nu} = 8\pi G(\bar{T}^{\mathrm{matter}}_{\mu\nu} + \bar{T}^{\mathrm{DE}}_{\mu\nu})\,. \tag{2.9}$$

Inserting into the 00 component of the field equations gives us:

$$\left(\frac{\dot{a}}{a}\right)^2 = \frac{8\pi G}{3}(\bar{\rho}_{\mathrm{matter}} + \bar{\rho}_{\mathrm{DE}}) - \frac{k}{a^2}\,, \tag{2.10}$$

which is the first Friedmann equation [2]. With the spatial components of the Ricci tensor and the first Friedmann equation we can arrive at:

$$\frac{\ddot{a}}{a} = -\frac{4\pi G}{3}\left(\bar{\rho}_{\mathrm{matter}} + \bar{\rho}_{\mathrm{DE}} + 3\bar{p}_{\mathrm{DE}}\right)\,, \tag{2.11}$$

the second Friedmann equation [2]. The continuity equations can be calculated from:

$$\nabla_{\mu}T^{\mu\nu} = 0\,. \tag{2.12}$$

It can be immediately seen, that for no interactions between DE and matter, the continuity equation will be a linear combination of the matter only and the DE continuity equation.

$$\partial_t\bar{\rho}_{\mathrm{matter}} + 3\frac{\dot{a}}{a}\bar{\rho}_{\mathrm{matter}} = 0\,, \tag{2.13a}$$

$$\partial_t\bar{\rho}_{\mathrm{DE}} + 3\frac{\dot{a}}{a}\bar{\rho}_{\mathrm{DE}}\,(1 + w_{\mathrm{DE}}) = 0\,. \tag{2.13b}$$

where we have defined the DE equation of state $w_{\mathrm{DE}} = \bar{p}_{\mathrm{DE}}/\bar{\rho}_{\mathrm{DE}}$[2]. These are now all required prerequisites for our background evolution.

2.2 Fluid Equations

Let us begin with stating the fluid equations for matter in the presence of DE and spatial curvature, but assume zero velocity dispersion of matter. The latter means that shell-crossing, i.e. the crossing of particle trajectories, has not yet occurred. In the following, we start with functions that all depend on the *physical coordinate* $\boldsymbol{r}$; throughout this chapter we will switch to the *comoving coordinate* $\boldsymbol{x} = \boldsymbol{r}/a$ where we will explicitly write out the coordinate dependencies. In subsequent chapters we will remain in comoving coordinates until we switch to Lagrangian comoving coordinates in chapter 3; see [1, 37] for similar treatments. To make the equations more readable we have dropped the subscript in ρ_{matter} and $\bar{\rho}_{\text{matter}}$ for the matter densities, which makes all (background) densities without a subscript matter by default. In the following chapters up to and including 2.3 we shall generalise the derivations found in [37]. In physical coordinates $\boldsymbol{r}$, the fluid equations are:

$$\partial_t \boldsymbol{U} + (\boldsymbol{U} \cdot \boldsymbol{\nabla}_{\boldsymbol{r}})\, \boldsymbol{U} = -\boldsymbol{\nabla}_{\boldsymbol{r}} \phi\,, \tag{2.14}$$

$$\partial_t \rho + \boldsymbol{\nabla}_{\boldsymbol{r}} \cdot (\rho \boldsymbol{U}) = 0\,, \tag{2.15}$$

$$4\pi G \left[\rho + \bar{\rho}_{\text{DE}} + 3\bar{p}_{\text{DE}}\right] = \boldsymbol{\nabla}_{\boldsymbol{r}}^2 \phi\,. \tag{2.16}$$

Here $\boldsymbol{U} = \boldsymbol{U}(\boldsymbol{r}, t)$ denotes the total velocity field of matter, $\phi = \phi(\boldsymbol{r}, t)$ denotes the cosmological potential, $\rho = \rho(\boldsymbol{r}, t)$ is the total matter fluid density. It should be noted, that introducing an additional radiation energy momentum tensor $\bar{T}_{\mu\nu}^{\text{rad}} = diag(-\bar{\rho}_{\text{rad}}, \bar{p}_{\text{rad}}, \bar{p}_{\text{rad}}, \bar{p}_{\text{rad}})$ to the total energy momentum tensor $T_{\mu\nu}$ would simply give 2 more terms in (2.11) another continuity equation and change the Poisson equation (2.16) to the following:

$$4\pi G \left[\rho + \bar{\rho}_{\text{DE}} + 3\bar{p}_{\text{DE}} + \bar{\rho}_{\text{rad}} + 3\bar{p}_{\text{rad}}\right] = \boldsymbol{\nabla}_{\boldsymbol{r}}^2 \phi\,. \tag{2.17}$$

We remind the reader that we assume that every fluid, except for matter, affects the background only. Therefore, all subsequent derivations at both the background and fluctuation level will hold, even with the addition of a radiation component, assuming it only affects the background and does not interact with our dark matter and dark energy components. This will be useful to us later, when we turn to specific models, as it justifies the inclusion of radiation components in our cosmological models.

2.2.1 Background Fluid Equations

Let us solve these equations for the *background variables* in an exactly homogeneous and isotropic universe, where $\rho = \bar{\rho}(t)$, $\boldsymbol{U} = H(t)\,\boldsymbol{r} \equiv (\dot{a}/a)\boldsymbol{r}$, and $\phi = \bar{\phi}(\boldsymbol{r}, t)$. Inserting these into (2.14):

$$\partial_t \left(\frac{\dot{a}}{a}\right) \boldsymbol{r} + \left(\frac{\dot{a}}{a}\boldsymbol{r} \cdot \boldsymbol{\nabla}_{\boldsymbol{r}}\right) \frac{\dot{a}}{a}\boldsymbol{r} = -\boldsymbol{\nabla}_{\boldsymbol{r}} \bar{\phi}\,, \tag{2.18a}$$

$$\left(\frac{\ddot{a}a - \dot{a}^2}{a^2}\right) \boldsymbol{r} + \left(\frac{\dot{a}}{a}\right)^2 \boldsymbol{r} = -\boldsymbol{\nabla}_{\boldsymbol{r}} \bar{\phi}\,, \tag{2.18b}$$

$$\frac{\ddot{a}}{a}\boldsymbol{r} = -\boldsymbol{\nabla}_{\boldsymbol{r}} \bar{\phi}\,. \tag{2.18c}$$

Now taking the divergence of (2.18c):

$$3\frac{\ddot{a}}{a} = -\nabla_{\boldsymbol{r}}^2\bar{\phi} = -4\pi G\left[\bar{\rho} + \bar{\rho}_{\mathrm{DE}} + 3\bar{p}_{\mathrm{DE}}\right] . \tag{2.19}$$

Interestingly, $\nabla_{\boldsymbol{r}}^2\bar{\phi}$ is equal to the R_{00} component of the Ricci tensor [2]. Now we only have to insert into (2.15):

$$\begin{aligned} \partial_t\bar{\rho} + \nabla_{\boldsymbol{r}} \cdot \left(\bar{\rho}\frac{\dot{a}}{a}\boldsymbol{r}\right) = 0\,, \\ \partial_t\bar{\rho} + 3\frac{\dot{a}}{a}\bar{\rho} = 0\,. \end{aligned} \tag{2.20}$$

To summarize, our background equations are as follows:

$$\frac{\ddot{a}}{a}\boldsymbol{r} = -\nabla_{\boldsymbol{r}}\bar{\phi}\,, \tag{2.21a}$$

$$\partial_t\bar{\rho} + 3\frac{\dot{a}}{a}\bar{\rho} = 0\,, \tag{2.21b}$$

$$3\frac{\ddot{a}}{a} = -\nabla_{\boldsymbol{r}}^2\bar{\phi} = -4\pi G\left[\bar{\rho} + \bar{\rho}_{\mathrm{DE}} + 3\bar{p}_{\mathrm{DE}}\right] . \tag{2.21c}$$

Equation (2.21b) states mass conservation at the background level, while Eq. (2.21c) is the well-known second Friedmann equation, here "re-derived" from a Newtonian perspective. Equivalent formulations of these can be found in [37]. Equations (2.21) will be of use in the subsequent section when determining the fluctuation equations for matter.

2.2.2 Fluctuation Equations

Now we include the fluctuations as well, i.e., $\rho = \rho(1+\delta)$, $\boldsymbol{U} = \frac{\dot{a}}{a}\boldsymbol{r} + a\boldsymbol{u}$ and $\phi = \bar{\phi} + \tilde{\phi}$, where $\tilde{\phi}$ denotes the fluctuation part and $\delta = (\rho - \bar{\rho})/\bar{\rho}$ is the density contrast. We insert this into (2.14) and remind the reader, that this means starting with the $\boldsymbol{r}$ dependence again:

$$\partial_t\left(\frac{\dot{a}}{a}\boldsymbol{r} + a\boldsymbol{u}\right) + \left[\left(\frac{\dot{a}}{a}\boldsymbol{r} + a\boldsymbol{u}\right)\cdot\nabla_{\boldsymbol{r}}\right]\left(\frac{\dot{a}}{a}\boldsymbol{r} + a\boldsymbol{u}\right) = -\nabla_{\boldsymbol{r}}\phi\,. \tag{2.22}$$

Let us first consider the LHS:

$$\begin{aligned} &\left(\frac{\ddot{a}a - \dot{a}^2}{a^2}\right)\boldsymbol{r} + \dot{a}\boldsymbol{u} + a\partial_t\boldsymbol{u} + \frac{\dot{a}}{a}\boldsymbol{r}\left(\boldsymbol{r}\cdot\nabla_{\boldsymbol{r}}\right)\left(\frac{\dot{a}}{a}\boldsymbol{r} + a\boldsymbol{u}\right) + a\left(\boldsymbol{u}\cdot\nabla_{\boldsymbol{r}}\right)\left(\frac{\dot{a}}{a}\boldsymbol{r} + a\boldsymbol{u}\right) = \\ &= \frac{\ddot{a}}{a}\boldsymbol{r} - \left(\frac{\dot{a}}{a}\right)^2\boldsymbol{r} + \dot{a}\boldsymbol{u} + a\partial_t\boldsymbol{u} + \left(\frac{\dot{a}}{a}\right)^2\boldsymbol{r} + \dot{a}(\boldsymbol{r}\cdot\nabla_{\boldsymbol{r}})\boldsymbol{u} + \dot{a}\boldsymbol{u} + a^2(\boldsymbol{u}\cdot\nabla_{\boldsymbol{r}})\boldsymbol{u} = \\ &= \frac{\ddot{a}}{a}\boldsymbol{r} + 2\dot{a}\boldsymbol{u} + a\partial_t\boldsymbol{u} + \dot{a}(\boldsymbol{r}\cdot\nabla_{\boldsymbol{r}})\boldsymbol{u} + a^2(\boldsymbol{u}\cdot\nabla_{\boldsymbol{r}})\boldsymbol{u}\,. \end{aligned} \tag{2.23}$$

We can now see by comparing with (2.19) which part is contributing to the background potential and which part is relevant for the perturbation. Therefore:

$$2\dot{a}\boldsymbol{u}(\boldsymbol{r},t) + a\partial_t\boldsymbol{u}(\boldsymbol{r},t) + \dot{a}(\boldsymbol{r}\cdot\nabla_{\boldsymbol{r}})\boldsymbol{u}(\boldsymbol{r},t) + a^2(\boldsymbol{u}(\boldsymbol{r},t)\cdot\nabla_{\boldsymbol{r}})\boldsymbol{u}(\boldsymbol{r},t) = -\nabla_{\boldsymbol{r}}\tilde{\phi}(\boldsymbol{r},t)\,, \tag{2.24}$$

where we have reintroduced the dependencies for $\boldsymbol{u}$. We can now change to *comoving coordinates* $\boldsymbol{x} = \frac{\boldsymbol{r}}{a}$ and use that for any function $f(\boldsymbol{r}, t) = f(a(t)\boldsymbol{x}, t)$ the following holds:

$$\partial_t f|_{\boldsymbol{x} \text{ fixed}} = \partial_t f|_{\boldsymbol{r} \text{ fixed}} + \dot{a}(\boldsymbol{x} \cdot \boldsymbol{\nabla}_{\boldsymbol{r}}) f|_{t \text{ fixed}} \,. \tag{2.25}$$

Inserting into (2.24) and additionally considering $\boldsymbol{\nabla}_{\boldsymbol{x}} = a\boldsymbol{\nabla}_{\boldsymbol{r}}$ We arrive at:

$$\begin{aligned} 2\dot{a}\boldsymbol{u} + a\left(\partial_t \boldsymbol{u}|_{\boldsymbol{x} \text{ fixed}} - \dot{a}\left(\frac{\boldsymbol{x}}{a} \cdot \boldsymbol{\nabla}_x\right) \boldsymbol{u}|_{t \text{ fixed}}\right) + \dot{a}\,(\boldsymbol{x} \cdot \boldsymbol{\nabla}_x)\,\boldsymbol{u} + a(\boldsymbol{u} \cdot \boldsymbol{\nabla}_x)\boldsymbol{u} &= -\frac{1}{a}\boldsymbol{\nabla}_x\tilde{\phi}\,, \\ 2\dot{a}\boldsymbol{u}(\boldsymbol{x}, t) + a\partial_t \boldsymbol{u}(\boldsymbol{x}, t) + a(\boldsymbol{u}(\boldsymbol{x}, t) \cdot \boldsymbol{\nabla}_x)\boldsymbol{u}(\boldsymbol{x}, t) &= -\frac{1}{a}\boldsymbol{\nabla}_x\tilde{\phi}(\boldsymbol{x}, t)\,. \end{aligned} \tag{2.26}$$

This is the expression in comoving coordinates. We will now continue using these coordinates, but without explicitly writing the dependencies. Dividing the last expression by the scale factor yields:

$$2\frac{\dot{a}}{a}\boldsymbol{u} + \partial_t \boldsymbol{u} + (\boldsymbol{u} \cdot \boldsymbol{\nabla}_x)\boldsymbol{u} = -\frac{1}{a^2}\boldsymbol{\nabla}_x\tilde{\phi}\,. \tag{2.27}$$

With this we have derived the Euler equation for the comoving peculiar velocity $\boldsymbol{u}$. We would also like to derive the mass conservation for the peculiar velocity, which means taking the background with a fluctuation part as before and inserting into (2.15):

$$\begin{aligned} 0 &= \partial_t\,[\bar{\rho}\,(1+\delta)] + \boldsymbol{\nabla}_{\boldsymbol{r}} \cdot \left\{[\bar{\rho}(1+\delta)]\left[\frac{\dot{a}}{a}\boldsymbol{r} + a\boldsymbol{u}\right]\right\}\,, \\ 0 &= (\partial_t\bar{\rho})(1+\delta) + \bar{\rho}(\partial_t\delta) + (\boldsymbol{\nabla}_{\boldsymbol{r}}\,[\bar{\rho}(1+\delta)]) \cdot \left(\frac{\dot{a}}{a}\boldsymbol{r} + a\boldsymbol{u}\right) + \bar{\rho}(1+\delta)\boldsymbol{\nabla}_{\boldsymbol{r}} \cdot \left(\frac{\dot{a}}{a}\boldsymbol{r} + a\boldsymbol{u}\right)\,, \\ 0 &= \partial_t\bar{\rho} + 3\frac{\dot{a}}{a}\bar{\rho} + \left(\partial_t\bar{\rho} + 3\frac{\dot{a}}{a}\bar{\rho}\right)\delta + \bar{\rho}(\partial_t\delta) + \bar{\rho}(\boldsymbol{\nabla}_{\boldsymbol{r}}\delta) \cdot \left(\frac{\dot{a}}{a}\boldsymbol{r} + a\boldsymbol{u}\right) + \bar{\rho}(1+\delta)a\boldsymbol{\nabla}_{\boldsymbol{r}}\boldsymbol{u}\,. \end{aligned} \tag{2.28}$$

Note that we are still in *physical coordinates*, since we started from our initial form of the mass conservation, which was written in these. We can now see that the first three terms contain the background mass conservation relation (2.21b) and are thus 0. Using this and dividing by $\bar{\rho}$ on both sides yields:

$$0 = \partial_t\delta + (\boldsymbol{\nabla}_{\boldsymbol{r}}\delta) \cdot \left(\frac{\dot{a}}{a}\boldsymbol{r} + a\boldsymbol{u}\right) + (1+\delta)a\boldsymbol{\nabla}_{\boldsymbol{r}} \cdot \boldsymbol{u}\,. \tag{2.29}$$

As previously we can use (2.25) and transform this expression into *comoving coordinates* $\boldsymbol{x}$:

$$\begin{aligned} 0 &= \partial_t\delta - \frac{\dot{a}}{a}(\boldsymbol{x} \cdot \boldsymbol{\nabla}_x)\delta + \frac{\dot{a}}{a}\boldsymbol{x} \cdot (\boldsymbol{\nabla}_x\delta) + (\boldsymbol{\nabla}_x\delta) \cdot \boldsymbol{u} + (1+\delta)\boldsymbol{\nabla}_x\boldsymbol{u}\,, \\ 0 &= \partial_t\delta + \boldsymbol{\nabla}_{\boldsymbol{x}} \cdot [(1+\delta)\boldsymbol{u}]\,, \end{aligned} \tag{2.30}$$

which is the final expression for our mass conservation. The only thing left now is the Poisson equation. For this we insert the perturbed objects into (2.16):

$$\boldsymbol{\nabla}_{\boldsymbol{r}}^2(\bar{\phi} + \tilde{\phi}) = 4\pi G\,[\bar{\rho}(1+\delta) + \bar{\rho}_{\mathrm{DE}} + 3\bar{p}_{\mathrm{DE}}]\,. \tag{2.31}$$

After removing the background part we arrive at:

$$\nabla_{\boldsymbol{r}}^2 \tilde{\phi} = 4\pi G \bar{\rho}(\boldsymbol{r}, t)\delta(\boldsymbol{r}, t)\,, \tag{2.32}$$

$$\nabla_{\boldsymbol{x}}^2 \tilde{\phi} = 4\pi G \bar{\rho}(\boldsymbol{x}, t) a^2 \delta(\boldsymbol{x}, t)\,, \tag{2.33}$$

where we have again transformed to *comoving coordinates* in the last line. So to summarize, our peculiar Euler–Poisson equations for the fluid variables in comoving coordinates are given by:

$$\partial_t \boldsymbol{u} + (\boldsymbol{u} \cdot \nabla_x)\boldsymbol{u} = -2\frac{\dot{a}}{a}\boldsymbol{u} - \frac{1}{a^2}\nabla_x \tilde{\phi}\,, \tag{2.34a}$$

$$\partial_t \delta + \nabla_{\boldsymbol{x}} \cdot [(1+\delta)\boldsymbol{u}] = 0\,, \tag{2.34b}$$

$$\nabla_{\boldsymbol{x}}^2 \tilde{\phi} = 4\pi G \bar{\rho} a^2 \delta\,. \tag{2.34c}$$

As mentioned above, this derivation for the fluctuations would also be valid if we included the radiation component, as all radiation contributions would be removed with the background potential. It should also be mentioned that one could include a massive neutrino contribution to the background and arrive at the same conclusion, assuming that there is no interaction between the neutrinos and the other contributions to the total energy momentum tensor. The fluid equations (2.34) were also derived by [1] for ΛCDM, by starting from a transformed action.

2.3 Linearisation and Structure Growth

Next, we derive a differential equation for our fluctuation. For this we linearise the previously derived equations (2.34) which yields:

$$\partial_t \boldsymbol{u} + 2H\boldsymbol{u} = -\frac{1}{a^2}\nabla_x \tilde{\phi}\,, \tag{2.35a}$$

$$\partial_t \delta + \nabla_{\boldsymbol{x}} \cdot \boldsymbol{u} = 0\,, \tag{2.35b}$$

$$\nabla_{\boldsymbol{x}}^2 \tilde{\phi} = 4\pi G \bar{\rho} a^2 \delta\,. \tag{2.35c}$$

Inserting these equations into one another we arrive at the following differential equation:

$$\ddot{\delta} + 2H\dot{\delta} - 4\pi G \bar{\rho}\delta = 0\,. \tag{2.36}$$

See also [1, 4] and [38] as alternatives to the derivation from [37] and above. Since this ODE is now autonomous in the spatial dependence, we can infer that its solution will be of the form $\delta(t, \boldsymbol{x}) = D_+(t)C_+(\boldsymbol{x}) + D_-(t)C_-(\boldsymbol{x})$, where $D(t)$ is the linear growth function and $C_{+/-}(\boldsymbol{x})$ is are space-dependent functions and the plus and minus subscript specify the growing and decaying mode solution respectively [38]. Using this we can rewrite the ODE (2.36) as:

$$\ddot{D} + 2H\dot{D} - 4\pi G \bar{\rho} D = 0\,, \tag{2.37}$$

where $D = D(t)$. This D-time ODE can also be found in [1, 37, 38, 39]. We can see that the entire cosmology is "encrypted" in the time derivative and the Hubble factor. Here and in the following, we will omit the temporal dependencies, unless we change the time variable. In that case, the change will be explicitly mentioned. Before analysing various solutions to this ODE we will reformulate it in a more convenient way.

Alternative Formulation of the Euler-Poisson system and D-time ODE. As previously shown in section 1.1.1, we can introduce the energy density parameters Ω_i and the total density parameter Ω, which are normalized as $\Omega = \sum_i \Omega_i = 1$, where $\Omega_i = \bar{\rho}_i/\rho_c$ with $\rho_c = 3H^2/(8\pi G)$ the critical energy density of the universe. This allows us to rewrite the first Friedmann equation for a given model. For kDDE model (i.e. time evolving DE + curvature + matter) this translates to:

$$\left(\frac{H}{H_0}\right)^2 = \Omega_{\mathrm{m}0} a^{-3} + \Omega_\Lambda(a) + \Omega_{\mathrm{k}0} a^{-2} . \tag{2.38}$$

When we compare this to the previously derived Friedmann equation, which we repeat here:

$$\left(\frac{\dot{a}}{a}\right)^2 = \frac{8\pi G}{3}\bar{\rho}_0 a^{-3} + \frac{8\pi G}{3}\bar{\rho}_{\mathrm{DE}} - \frac{k}{a^2} , \tag{2.39}$$

and by comparing coefficients we can conclude that $(3/2)H_0^2\Omega_{\mathrm{m}0} = 4\pi G\bar{\rho}_0$ and $-kH_0^2 = \Omega_{\mathrm{k}0}$, where we have used that $\bar{\rho} = \bar{\rho}_0 a^{-3}$. We can then use this to write (2.37) as:

$$\boxed{\ddot{D} + 2H\dot{D} - \frac{3}{2}H_0^2\Omega_{\mathrm{m}0}a^{-3}D = 0 .} \tag{2.40}$$

At the level of the Euler-Poisson system of equations this translates to:

$$\partial_t \boldsymbol{u} + (\boldsymbol{u}\cdot\boldsymbol{\nabla}_x)\boldsymbol{u} = -2H\boldsymbol{u} - \frac{1}{a^2}\boldsymbol{\nabla}_x\tilde{\phi} , \tag{2.41a}$$

$$\partial_t\delta + \boldsymbol{\nabla}_x \cdot [(1+\delta)\boldsymbol{u}] = 0 , \tag{2.41b}$$

$$\frac{3}{2}H_0^2\Omega_{\mathrm{m}0}\frac{\delta}{a} = \boldsymbol{\nabla}_x^2\tilde{\phi} . \tag{2.41c}$$

This formulation is valid for all models, that satisfy our initial assumptions of non-interacting fluids, as only the constants in the last term (2.40) and the last equation in (2.41) change, and these are determined by the matter components only. All other changes are encoded in the Hubble factor, and these we will study case by case. Therefore, we will use this formulation, to study the solutions of the D-time ODE for all models, as it turns out to be more convenient.

2.3.1 Einstein-de-Sitter (EdS) Model

Before solving this ODE for DDE model with non-zero curvature, we will first solve this for the EdS model ($\Omega_{\mathrm{m}0} = 1$), which is the simplest case and is a very well known result [1]. In this cosmology the first Friedmann equation is given by:

$$\left(\frac{\dot{a}}{a}\right)^2 = H_0^2\Omega_{\mathrm{m}0}a^{-3} . \tag{2.42}$$

In order to solve the ODE for the D-time (2.40) in the EdS model it is more convenient to write it with a temporal dependence on the scale factor a. This is also the case for the other cosmologies.

The transformation law is given by $\partial_t = \dot{a}\partial_a$. The first Friedmann equation (2.42) can be written as:

$$\dot{a} = aH_0\sqrt{\Omega_{\mathrm{m0}}a^{-3}} = H_0\sqrt{\Omega_{\mathrm{m0}}a^{-1}}\,, \tag{2.43}$$

which can be used in the transformation law to obtain an expression for $\dot{a}$:

$$\partial_t D(t) = \dot{a}\partial_a D(a) = H_0\sqrt{\Omega_{\mathrm{m0}}a^{-1}}\partial_a D(a)\,. \tag{2.44}$$

We can use this expression to convert temporal dependencies of temporal functions and their time derivatives from cosmic time t to a-time, which will simplify the derivation of analytical solutions. Calculating the second derivative:

$$\begin{aligned}
\partial_t^2 D(t) &= \dot{a}\partial_a(\dot{a}\partial_a D(a))\,,\\
&= H_0^2\Omega_{m0}a^{-1/2}\partial_a\left(a^{-1/2}\partial_a D\right)\,,\\
&= H_0^2\Omega_{m0}a^{-1/2}\left(-\frac{1}{2}a^{-3/2}\partial_a D + a^{-1/2}\partial_a^2 D\right)\,,\\
&= H_0^2\Omega_{m0}\left(a^{-1}\partial_a^2 D - \frac{1}{2}a^{-2}\partial_a D\right)\,,
\end{aligned} \tag{2.45}$$

which is the first term of (2.40) in a-time. Combining this with the other two terms in a-time, we get:

$$\begin{aligned}
\dot{a}\partial_a(\dot{a}\partial_a D) + 2\dot{a}^2 a^{-1}\partial_a D - \frac{3}{2}H_0^2\Omega_{\mathrm{m0}}a^{-3}D &= 0\,,\\
H_0^2\Omega_{\mathrm{m0}}\left(a^{-1}\partial_a^2 D - \frac{1}{2}a^{-2}\partial_a D\right) + 2H_0^2\Omega_{\mathrm{m0}}a^{-2}\partial_a D - \frac{3}{2}H_0^2\Omega_{\mathrm{m0}}a^{-3}D &= 0\,,\\
\partial_a^2 D - \frac{1}{2}a^{-1}\partial_a D - \frac{3}{2}a^{-2}D + 2a^{-1}\partial_a D &= 0\,,\\
\partial_a^2 D + \frac{3}{2}a^{-1}\partial_a D - \frac{3}{2}a^{-2}D &= 0\,.
\end{aligned} \tag{2.46}$$

This ODE is solvable by taking the Ansatz $D(a) = a^c$ and using that $a \neq 0$:

$$\begin{aligned}
\partial_a^2(a^c) + \frac{3}{2}a^{-1}\partial_a(a^c) - \frac{3}{2}a^{c-2} &= 0\,,\\
c(c-1)a^{c-2} + \frac{3}{2}ca^{c-2} - \frac{3}{2}a^{c-2} &= 0\,,\\
c^2 + \frac{1}{2}c - \frac{3}{2} &= 0\,.
\end{aligned} \tag{2.47}$$

Here we can now solve for c using the quadratic formula. The final solution for the D-time in EdS cosmology is then given by:

$$D(a) = c_1 a + c_2 a^{-3/2}\,. \tag{2.48}$$

See also [39]. We can see that the solution consists of a term that grows with a and one that decreases with it, hence one usually refers to them as the growing and decaying mode respectively. Since we would like to start simulations at $a = 0$, the decaying mode is problematic, as it diverges there, which implies a breakdown of our linearisation, as can be seen in figure (2.1). However, through appropriate choice of initial conditions (ICs) we can circumvent this problem [37, 40, 41]:

$$D(a_{\mathrm{ini}}) = a_{\mathrm{ini}} \,, \qquad \partial_a D(a_{\mathrm{ini}}) = 1 \,. \tag{2.49}$$

We will refer to this set of initial conditions as EdS initial conditions (EdS ICs) from now on. Consequently, our solution is given by:

$$D(a) = a \,, \tag{2.50}$$

which is just the growing-mode solution and has also been visualised in figure (2.1).

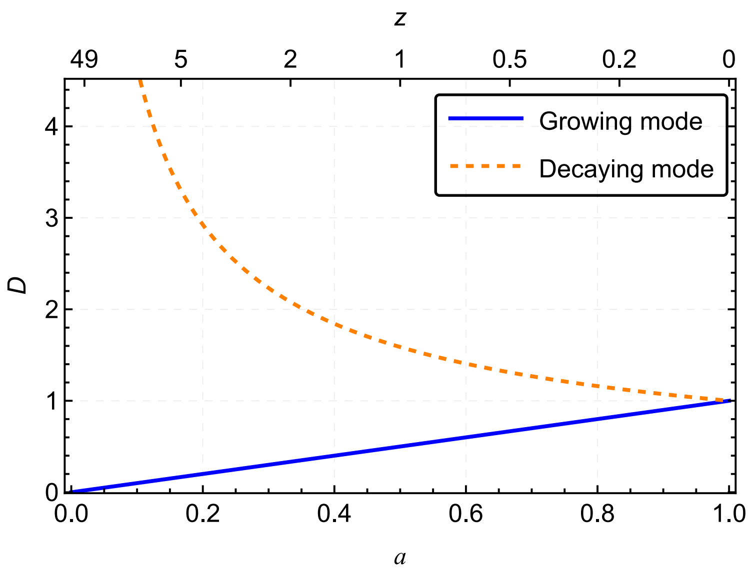

Figure 2.1: Growing- and decaying-mode solutions of D as a function of a in the EdS model.

2.3.2 ΛCDM Model

We would now like to solve the D-time ODE (2.40) for the slightly more complicated ΛCDM model. Note that in this case we only include matter and DE given by the CC, since these contribute the almost all of the energy density of the universe in this model. The derivation here follows [37]. For this, we start again with the first Friedmann equation, formulated using the energy density parameters,

$$\left(\frac{H}{H_0}\right)^2 = \Omega_{\mathrm{m}0} a^{-3} + \Omega_{\Lambda 0} \,. \tag{2.51}$$

This can be rearranged to:

$$\dot{a} = H_0\sqrt{\Omega_{\mathrm{m}0}a^{-1} + \Omega_{\Lambda 0}a^2}\,. \tag{2.52}$$

Let us now consider just the first term in (2.40). Just like for EdS we transform it to a-time using $\dot{D} = \partial_t D(t) = \dot{a}\partial_a D(a)$:

$$\begin{aligned}
\ddot{D} &= \dot{a}\partial_a(\dot{a}\partial_a D(a)) = \\
&= \dot{a}^2\partial_a^2 D + \dot{a}\partial_a(\dot{a})\partial_a D = \\
&= H_0^2\left(\Omega_{\mathrm{m}0}a^{-1} + \Omega_{\Lambda 0}a^2\right)\partial_a^2 D + \\
&+ H_0^2\sqrt{\Omega_{\mathrm{m}0}a^{-1} + \Omega_{\Lambda 0}a^2}\left[\frac{1}{2}\frac{1}{\sqrt{\Omega_{\mathrm{m}0}a^{-1} + \Omega_{\Lambda 0}a^2}}\left(-\Omega_{\mathrm{m}0}a^{-2} + 2\Omega_{\Lambda 0}a\right)\right]\partial_a D = \\
&= H_0^2\Omega_{\mathrm{m}0}a^{-1}\left(1 + f_{\Lambda 0}a^3\right)\partial_a^2 D + H_0^2\Omega_{\mathrm{m}0}a^{-2}\left(-\frac{1}{2} + f_{\Lambda 0}a^3\right)\partial_a D\,,
\end{aligned} \tag{2.53}$$

where $f_{\Lambda 0} := \Omega_{\Lambda 0}/\Omega_{\mathrm{m}0}$. Next we look at the other two terms in Eq. (2.40):

$$\begin{aligned}
&2\frac{\dot{a}}{a}\dot{D} - \frac{3}{2}H_0^2\Omega_{\mathrm{m}0}a^{-3}D = \\
&= 2\frac{\dot{a}^2}{a}\partial_a D - \frac{3}{2}H_0^2\Omega_{\mathrm{m}0}a^{-3}D = \\
&= H_0^2\Omega_{\mathrm{m}0}a^{-2}\left(2 + 2f_{\Lambda 0}a^3\right)\partial_a D - \frac{3}{2}H_0^2\Omega_{\mathrm{m}0}a^{-3}D\,.
\end{aligned} \tag{2.54}$$

Inserting Eqs. (2.53) and (2.54) into (2.40) and dividing the resulting expression by $H_0^2\Omega_{\mathrm{m}0}$, we find

$$\begin{aligned}
a^{-1}\left(1 + f_{\Lambda 0}a^3\right)\partial_a^2 D + a^{-2}\left(-\frac{1}{2} + f_{\Lambda 0}a^3\right)\partial_a D + a^{-2}\left(2 + 2f_{\Lambda 0}a^3\right)\partial_a D - \frac{3}{2}a^{-3}D = 0\,,\\
\left(1 + f_{\Lambda 0}a^3\right)\partial_a^2 D + a^{-1}\left(\frac{3}{2} + 3f_{\Lambda 0}a^3\right)\partial_a D - \frac{3}{2}a^{-2}D = 0\,,\\
\left(1 + f_{\Lambda 0}a^3\right)\partial_a^2 D + \frac{3}{2a}\left(1 + 2f_{\Lambda 0}a^3\right)\partial_a D - \frac{3}{2a^2}D = 0\,,\\
\left(1 + f_{\Lambda 0}a^3\right)\left(\partial_a^2 D + \frac{3}{2a}\partial_a D\right) + \frac{3}{2}a^2 f_{\Lambda 0}\partial_a D - \frac{3}{2a^2}D = 0\,,
\end{aligned} \tag{2.55}$$

which, notably, is independent of H_0. Our final expression of the D-time ODE for ΛCDM is then given by the following:

$$\left(1 + f_{\Lambda 0}a^3\right)\left(\partial_a^2 D + \frac{3}{2a}\partial_a D\right) + \frac{3}{2}a^2 f_{\Lambda 0}\partial_a D - \frac{3}{2a^2}D = 0\,. \tag{2.56}$$

The solution to the ODE (2.56) is given by:

$$D(a) = c_1\, a\; {}_2F_1\left(1/3, 1, 11/6, -f_{\Lambda 0}a^3\right) + c_2\sqrt{1 + f_{\Lambda 0}a^3}\,a^{-3/2}\,, \tag{2.57}$$

where ${}_2F_1$ is the Gauss hypergeometric function. This result can also be found in [39], in addition to [37].

As for the EdS solution (See chapter 2.3.1) we have a decaying mode in the second term and a growing mode in the first one, where the second one breaks our linearisation for early times. We would like to set ICs such that the first one gets removed. We can do this using the EdS ICs, as we did earlier (2.49). We then arrive at the well-known solution (see e.g. [39]):

$$D(a) = a\ {}_2F_1(1/3, 1, 11/6, -f_{\Lambda 0}a^3)\ . \tag{2.58}$$

The comparison between both solutions can be seen in figure (2.2), where we have used $\Omega_{m0} = 0.3$ and $\Omega_{\Lambda 0} = 0.7$. One can clearly see that for early times both solutions align, but for late times

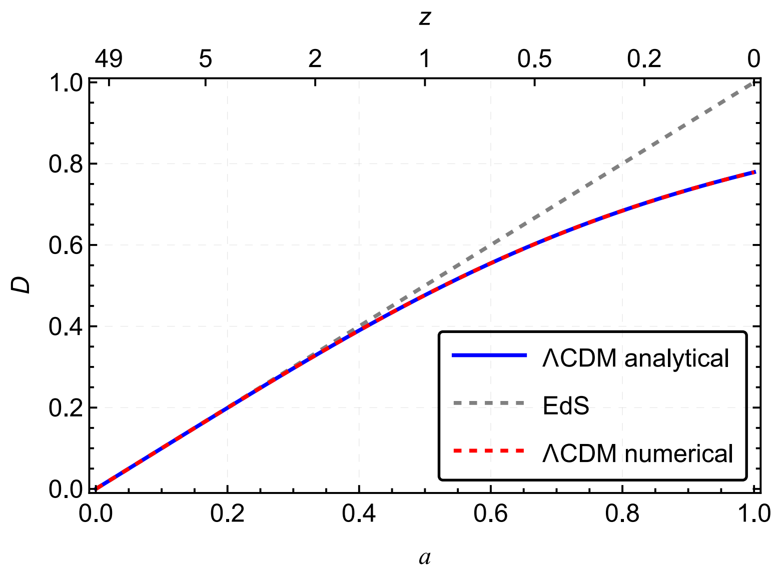

Figure 2.2: Numerical solution of the D-time ODE for ΛCDM compared to the analytical solution, as implemented in Mathematica. The choice of cosmological parameters for ΛCDM is given by the fiducial values $\Omega_{m0} = 0.3$, $\Omega_{\Lambda 0} = 0.7$ and the numerical ODE solver is initialised at scale factor $a_{\text{ini}} = 10^{-5}$.

their difference increases. It is possible to integrate the ODE (2.56) numerically using very small values in the initial conditions (2.49) for a_{ini}. The resulting ODE can be seen in Fig. 2.2. Here we can see that the numerical solution looks very consistent with the analytical solution. For this we have used $a_{\text{ini}} = 10^{-5}$. We can also compare the solutions for different initial times. To do this we use the relative difference or D Difference, which in our case is defined as the ratio between the numerical and analytical solution minus one $D_{\text{num}}/D_{\text{ana}} - 1$. This is visualised in Fig. 2.3. Here we can see the difference clearly, especially for $a_{\text{ini}} = 10^{-2}$. This is a consequence of not being precisely in the growing mode, but getting a small contribution from the decaying mode as well, which could be reduced by initialising with e.g. $D(a_{\text{ini}}) = a_{\text{ini}} - (2/11) f_{\Lambda 0} a_{\text{ini}}^4$ or by initialising at earlier times. The other two initial times, however, align very well with one the analytical one. It should be noted, that even for $a_{\text{ini}} = 0.01$ the difference between the analytical and numerical solution is of order $\approx 10^{-6}$, which is still very small.

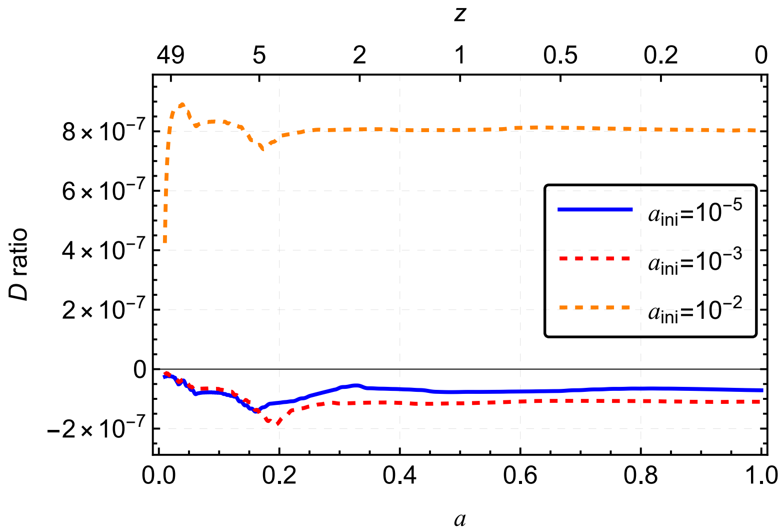

Figure 2.3: Relative difference (D Difference) $D_{\mathrm{num}}/D_{\mathrm{ana}} - 1$ for different a_{ini} in the ΛCDM model. One can see that the error increases with initialisation time.

2.3.3 Matter+Radiation (M+R) Model

We know that the energy density of the universe was dominated by a radiation contribution $\propto a^{-4}$ at early times. We can derive a solution to the D-time for such a model. For simplicity we take a Friedmann equation of the following form:

$$\left(\frac{H}{H_0}\right)^2 = \Omega_{\mathrm{r}0}a^{-4} + \Omega_{\mathrm{m}0}a^{-3}\,, \tag{2.59}$$

which gives us a radiation and matter only universe, where as usual $\Omega_{\mathrm{r}0} + \Omega_{\mathrm{m}0} = 1$. From this it follows that:

$$\dot{a} = H_0\sqrt{\Omega_{\mathrm{m}0}a^{-1} + \Omega_{\mathrm{r}0}a^{-2}}\,. \tag{2.60}$$

We can now insert this into our ODE ($\boxed{2.40}$) and transform to a-time. The first term in the ODE is then given by:

$$\begin{aligned}\ddot{D} &= \dot{a}\partial_a(\dot{a}\partial_a D(a)) = \\ &= H_0^2\Omega_{\mathrm{m}0}a^{-1}\left(1 + f_{\mathrm{R}0}a^{-1}\right)\partial_a^2 D + H_0^2\Omega_{\mathrm{m}0}a^{-1}\left(-\frac{1}{2}a^{-1} - f_{\mathrm{R}0}a^{-2}\right)\partial_a D\,,\end{aligned} \tag{2.61}$$

where we have defined $f_{\mathrm{R}0} := \Omega_{\mathrm{r}0}/\Omega_{\mathrm{m}0}$. The second and third terms are then given by:

$$\begin{aligned}&2\frac{\dot{a}^2}{a}\partial_a D - \frac{3}{2}H_0^2\Omega_{\mathrm{m}0}a^{-3} = \\ &= H_0^2\Omega_{\mathrm{m}0}a^{-1}\left(2a^{-1} + 2f_{\mathrm{R}0}a^{-2}\right)\partial_a D - \frac{3}{2}H_0^2\Omega_{\mathrm{m}0}a^{-3}D\,.\end{aligned} \tag{2.62}$$

Finally, combining all three into the ODE and dividing by $H_0^2\Omega_{\mathrm{m}0}a^{-1}$ on both sides yields:

$$\begin{aligned}
&\left(1+f_{\mathrm{R}0}a^{-1}\right)\partial_a^2 D+\left(-\frac{1}{2}a^{-1}-f_{\mathrm{R}0}a^{-2}\right)\partial_a D+\left(2a^{-1}+2f_{\mathrm{R}0}a^{-2}\right)\partial_a D-\frac{3}{2}a^{-2}D=0\,,\\
&\left(1+\Lambda_R a^{-1}\right)\left(\partial_a^2 D+\frac{3}{2a}\partial_a D\right)-\frac{1}{2a^2}\Lambda_R\partial_a D-\frac{3}{2a^2}D=0\,. \qquad (2.63)
\end{aligned}$$

The solution to the above ODE is then given by:

$$\begin{aligned}
D(a)=&\,c_1\left(a+\frac{2}{3}f_{\mathrm{R}0}\right)+\\
&-c_2 f_{\mathrm{R}0}^{-5/2}\left[(3a+2f_{\mathrm{R}0})\tanh^{-1}\left(\sqrt{\frac{a+f_{\mathrm{R}0}}{f_{\mathrm{R}0}}}\right)-3\sqrt{f_{\mathrm{R}0}(a+f_{\mathrm{R}0})}\right] \qquad (2.64)
\end{aligned}$$

(see [39] for a different, but equivalent presentation of this result). The growing mode solution is visualised in figure 2.4. Here we have used the energy densities $\Omega_{\mathrm{m}0}=0.99$ and $\Omega_{\mathrm{r}0}=0.01$ for the radiation solution. Note that this choice of $\Omega_{\mathrm{r}0}$ is exaggerated as data implies an $\Omega_{\mathrm{r}0}\approx 10^{-5}$ [39].

Novel slaving argument. We can write the fluid equations (2.34) using the a-time and the variables $\boldsymbol{u}=\dot{a}\boldsymbol{v}$ and a rescaled potential $(3/2)H_0^2\Omega_{\mathrm{m}0}\varphi=\tilde{\phi}$ to get the following:

$$\left(1+f_{\mathrm{R}0}a^{-1}\right)\left[\partial_a\boldsymbol{v}+(\boldsymbol{v}\cdot\nabla_x)\boldsymbol{v}\right]=-\frac{3}{2a}\left(\boldsymbol{v}+\nabla_x\varphi\right)-\Lambda_{\mathrm{R}0}a^{-2}\boldsymbol{v}\,, \qquad (2.65a)$$

$$\partial_a\delta+\nabla_x\cdot\left[(1+\delta)\boldsymbol{v}\right]=0\,, \qquad (2.65b)$$

$$\nabla_x^2\varphi=\frac{\delta}{a}\,. \qquad (2.65c)$$

We can easily identify multiple terms, that diverge for $a\to 0$, which require a vanishing numerator at $a=0$, to remove the divergences. A similar treatment for this in the case of ΛCDM can be found in [37] (and see also [40, 41] for slaving in EdS). There the choice of ICs is immediately discernible from the ΛCDM equivalent of (2.65a). For the M+R model this is at this stage highly non-trivial, so to make progress we approach this problem by starting with the fluid equations (2.34) in comoving coordinates, using the cosmological energy density formulation and linearising them:

$$\partial_t^2\boldsymbol{x}+2H\partial_t\boldsymbol{x}=-\frac{1}{a^2}\boldsymbol{\nabla}_x\tilde{\phi}\,, \qquad (2.66a)$$

$$\boldsymbol{\nabla}_x^2\tilde{\phi}=\frac{3}{2}H_0^2\Omega_{\mathrm{m}0}\frac{\delta}{a}\,, \qquad (2.66b)$$

together with the D-time ODE Eq. (2.40). By now transforming to the D-time variable through $\partial_t=\dot{D}\partial_D$ and $\partial_t^2=\ddot{D}\partial_D+\dot{D}\partial_t\partial_D=\left(\frac{3}{2}H_0^2\Omega_{\mathrm{m}0}a^{-3}D-2H\dot{D}\right)\partial_D+\dot{D}^2\partial_D^2$ we get an expression, which, when inserted into Eq (2.66a), yields:

$$\left(\frac{3}{2}H_0^2\Omega_{\mathrm{m}0}a^{-3}D-2H\dot{D}\right)\partial_D\boldsymbol{x}+\dot{D}^2\partial_D^2\boldsymbol{x}+2H\dot{D}\partial_D\boldsymbol{x}=-\frac{1}{a^2}\boldsymbol{\nabla}_x\tilde{\phi}\,. \qquad (2.67)$$

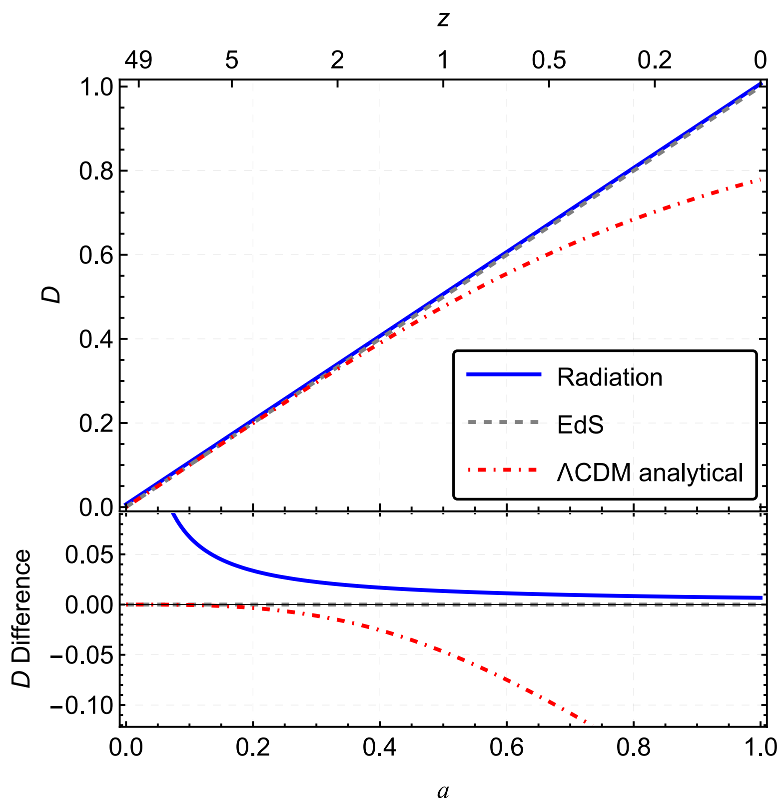

Figure 2.4: Numerical solution of $D(a)$ in the M+R model for $\Omega_{\mathrm{m0}} = 0.99$ and $\Omega_{\mathrm{r0}} = 0.01$. The relative difference is w.r.t. the analytical EdS solution. The ODE solver was initialised with $a_{\mathrm{ini}} = 10^{-5}$.

By redefining our potential according to $\tilde{\phi} = \frac{3}{2}H_0^2\Omega_{\mathrm{m0}}\frac{D}{a}\varphi_r$ we can simplify this expression to:

$$\partial_D^2 \boldsymbol{x} = -\frac{3}{2}\frac{DH_0^2\Omega_{\mathrm{m0}}}{\dot{D}^2 a^3}\left(\partial_D \boldsymbol{x} + \boldsymbol{\nabla}_x \varphi_r\right) . \tag{2.68}$$

This simple expression is still a mixture of a-time and D-time. We can now transform back to the a-time, by simply inverting the growing mode solution from Eq. (2.64), realising from this that $\partial_D = (\partial a/\partial D)\partial_a = \partial_a$ and inserting it together with the Friedmann equation (2.60) into the above equation:

$$\partial_a^2 \boldsymbol{x} = -\frac{3}{2}\frac{a + (2/3)f_{\mathrm{R0}}}{a(a + f_{\mathrm{R0}})}\left(\partial_D \boldsymbol{x} + \boldsymbol{\nabla}_x \varphi_r\right) . \tag{2.69}$$

For the new potential the Poisson equation (2.66b) reads:

$$\boldsymbol{\nabla}_x^2 \varphi_r = \frac{\delta}{D} = \frac{\delta}{a + (2/3)f_{\mathrm{R0}}} . \tag{2.70}$$

These equations read in Eulerian coordinates as follows:

$$-\partial_a^2\delta = -\frac{3(a+(2/3)f_{R0})}{2a(a+f_{R0})}\left(-\partial_a\delta + \frac{\delta}{a+(2/3)f_{R0}}\right). \tag{2.71}$$

To arrive here we have transformed to Lagrangian coordinates first, where $\boldsymbol{x}(\boldsymbol{q},t) = \boldsymbol{q} + \boldsymbol{\psi}(\boldsymbol{q},t)$, where $\boldsymbol{q}$ are the initial Lagrangian positions and $\boldsymbol{\psi}$ is the Lagrangian displacement, then applied the divergence with respect to the comoving coordinates. To simplify we used the perturbative relations $J = \det[\boldsymbol{\nabla_q x}] \simeq 1 + \boldsymbol{\nabla_q}\cdot\boldsymbol{\psi}$; $\boldsymbol{\nabla_x} = J^{-1}\boldsymbol{\nabla_q} \simeq \boldsymbol{\nabla_q}$ and $\delta = 1/J - 1 \simeq -\boldsymbol{\nabla_q}\cdot\boldsymbol{\psi}$. We took these relations from chapter 3, where we introduce them step by step. The ODE for δ (2.71) has the following growing mode solution:

$$\delta_+(a,\boldsymbol{x}) = \left(a + \frac{2}{3}f_{R0}\right)C(\boldsymbol{x}). \tag{2.72}$$

From this and the above ODE (2.71) we can read out the slaving conditions for matter + radiation cosmology:

$$v^{\rm ini} = -\nabla\varphi^{\rm ini} = -\nabla^{-1}C(\boldsymbol{x}), \qquad \delta^{\rm ini} = \frac{2}{3}f_{R0}C(\boldsymbol{x}), \qquad [\text{ini:}\, a \to 0^+] \tag{2.73}$$

where $\nabla^{-1} := \nabla\nabla^{-2}$, with ∇^{-2} denoting the inverse Laplacian. It should be mentioned that this slaving argument was previously assumed to be impossible [37] because of the a^{-4} term in the Friedmann equation which produces a^{-1} and a^{-2} terms in the Euler equation (2.65a). While neither the subsequent models, nor the numerical implementation, include a radiation component, this section shows that it is in principle possible and, for the sake of completeness, desirable, to realise this numerically in the future. Eventually, it should be possible to combine all the contributions into one model.

2.3.4 Dynamical Dark Energy and Curvature (*k*DDE) Model

We now want to move towards a DEE model, also allowing for non-zero spatial curvature (k); we call the combined model with collisionless matter loosely kDDE in the following, which is also known as the $o\omega_0\omega_a$CDM model. For this, we require an expression for $\bar\rho_{\rm DE}$. As previously we use the first Friedmann equation, formulated with the cosmological energy densities, which we repeat below:

$$\left(\frac{H}{H_0}\right)^2 = \Omega_{m0}a^{-3} + \Omega_\Lambda(a) + \Omega_{k0}a^{-2}. \tag{2.74}$$

To make progress, it is constructive to change the temporal dependence in the continuity equation (2.13b) from t to a-time:

$$\begin{aligned}
\partial_t\bar\rho_{\rm DE} + 3\frac{\dot a}{a}\bar\rho_{\rm DE}\,(1+w_{\rm DE}) &= 0\,,\\
\dot a\partial_a\bar\rho_{\rm DE} + 3\frac{\dot a}{a}\bar\rho_{\rm DE}\,(1+w_{\rm DE}) &= 0\,,\\
\partial_a\bar\rho_{\rm DE} + 3a^{-1}\bar\rho_{\rm DE}\,(1+w_{\rm DE}) &= 0\,,
\end{aligned} \tag{2.75}$$

where, notably, the $\dot{a}$ has dropped out. Up until now we have not specified whether w_{DE} is constant or some function of a. We shall now employ the Chevallier-Polarski-Linder (CPL) model [16], which is commonly used when discussing dynamical dark energy observations, where

$$w_{\mathrm{DE}} = w_0 + (1-a)w_a \,, \tag{2.76}$$

which reduces to ΛCDM when we take $w_0 = -1$ and $w_a = 0$. We can insert this model into our ODE (2.75) and use separation of variables again. We then get the following expression:

$$\begin{aligned}\ln\left(\frac{\bar{\rho}_{\mathrm{DE}}(a)}{\bar{\rho}_{\mathrm{DE}0}}\right) &= -3\int_1^a [1+w_0+(1-a')w_a]a'^{-1}da' = \\ &= -3\int_1^a (1+w_0+w_a)a'^{-1}da' + 3\int_1^a w_a da' \,.\end{aligned} \tag{2.77}$$

The last expression can be explicitly integrated, yielding

$$\bar{\rho}_{\mathrm{DE}}(a) = \bar{\rho}_{\mathrm{DE}0}\, a^{-3(1+w_0+w_a)} \mathrm{e}^{3w_a(a-1)} \,. \tag{2.78}$$

It should be noted that using a beyond CPL model with a higher polynomial in a, as was suggested in [42], would simply yield additional exponential terms, which would turn out to be unproblematic for the subsequent analysis, as these never lead to divergences, but simply complicate the expressions. Now that we know the $\bar{\rho}_{\mathrm{DE}}$ we can write the Friedmann equation as follows:

$$\left(\frac{H}{H_0}\right)^2 = \Omega_{\mathrm{m}0}a^{-3} + \Omega_{\mathrm{DE}0}a^{-3(1+w_0+w_a)}\mathrm{e}^{3w_a(a-1)} + \Omega_{\mathrm{k}0}a^{-2} \,, \tag{2.79}$$

where we have just inserted $\Omega_{\mathrm{DE}}(a) = \Omega_{\mathrm{DE}0}\, a^{-3(1+w_0+w_a)}\mathrm{e}^{3w_a(a-1)}$ explicitly. For the following derivations, it is convenient to recast Eq. (2.79) as follows,

$$\dot{a} = H_0\sqrt{\Omega_{\mathrm{m}0}a^{-1} + \Omega_{\mathrm{DE}0}a^{-1}a^{-3(w_0+w_a)}\mathrm{e}^{3w_a(a-1)} + \Omega_{\mathrm{k}0}} \,. \tag{2.80}$$

Using this expression, it straightforward to convert the temporal dependencies of the governing ODE (2.40) from t to a-time. Specifically, for the first term we have:

$$\begin{aligned}\ddot{D} &= \dot{a}^2\partial_a^2 D + \dot{a}(\partial_a\dot{a})\partial_a D = \\ &= H_0^2\left(\Omega_{\mathrm{m}0}a^{-1} + \Omega_{\mathrm{DE}0}a^{-1}a^{-3(w_0+w_a)}\mathrm{e}^{3w_a(a-1)} + \Omega_{\mathrm{k}0}\right)\partial_a^2 D + \\ &+ \frac{1}{2}H_0^2[-\Omega_{\mathrm{m}0}a^{-2} + \Omega_{\mathrm{DE}0}(-a^{-2}a^{-3(w_0+w_a)}\mathrm{e}^{3w_a(a-1)} - 3(w_0+w_a)a^{-2}a^{-3(w_0+w_a)}\mathrm{e}^{3w_a(a-1)} + \\ &+ 3w_a a^{-1}a^{-3(w_0+w_a)}\mathrm{e}^{3w_a(a-1)})]\partial_a D = \\ &= H_0^2\Omega_{\mathrm{m}0}a^{-1}\left(1 + f_{\mathrm{DE}0}a^{-3(w_0+w_a)}\mathrm{e}^{3w_a(a-1)} + f_{\mathrm{k}0}a\right)\partial_a^2 D + \\ &+ H_0^2\Omega_{\mathrm{m}0}a^{-1}\left[-\frac{1}{2}a^{-1} - \frac{1}{2}a^{-1}f_{\mathrm{DE}0}a^{-3(w_0+w_a)}\mathrm{e}^{3w_a(a-1)}\right]\partial_a D + \\ &+ H_0^2\Omega_{\mathrm{m}0}a^{-1}\left[-\frac{3}{2}f_{\mathrm{DE}0}(w_0+w_a)a^{-1}a^{-3(w_0+w_a)}\mathrm{e}^{3w_a(a-1)}\right]\partial_a D + \\ &+ H_0^2\Omega_{\mathrm{m}0}a^{-1}\left[\frac{3}{2}f_{\mathrm{DE}0}w_a a^{-3(w_0+w_a)}\mathrm{e}^{3w_a(a-1)}\right]\partial_a D \,,\end{aligned} \tag{2.81}$$

where we have defined $f_{\mathrm{DE}0} = \Omega_{\mathrm{DE}0}/\Omega_{\mathrm{m}0}$ and $f_{\mathrm{k}0} = \Omega_{\mathrm{k}0}/\Omega_{\mathrm{m}0}$. Next, we calculate the second term in Eq. (2.40):

$$
\begin{aligned}
2\frac{\dot{a}^2}{a}\partial_a D &= 2H_0^2\left(\Omega_{\mathrm{m}0}a^{-2} + \Omega_{\mathrm{DE}0}a^{-2}a^{-3(w_0+w_a)}\mathrm{e}^{3w_a(a-1)} + \Omega_{\mathrm{k}0}a^{-1}\right) = \\
&= H_0^2\Omega_{\mathrm{m}0}a^{-1}\left(2a^{-1} + 2f_{\mathrm{DE}0}a^{-1}a^{-3(w_0+w_a)}\mathrm{e}^{3w_a(a-1)} + 2f_{\mathrm{k}0}\right)\partial_a D\,.
\end{aligned} \tag{2.82}
$$

Combining these into the ODE (2.40) and dividing by $H_0^2\Omega_{\mathrm{m}0}a^{-1}$ we get:

$$
\begin{aligned}
0 &= \left(1 + f_{\mathrm{DE}0}a^{-3(w_0+w_a)}\mathrm{e}^{3w_a(a-1)} + f_{\mathrm{k}0}a\right)\partial_a^2 D + \\
&+ \left(-\frac{1}{2}a^{-1} - \frac{1}{2}a^{-1}f_{\mathrm{DE}0}a^{-3(w_0+w_a)}\mathrm{e}^{3w_a(a-1)}\right)\partial_a D + \\
&+ \left(-\frac{3}{2}f_{\mathrm{DE}0}(w_0+w_a)a^{-1}a^{-3(w_0+w_a)}\mathrm{e}^{3w_a(a-1)} + \frac{3}{2}f_{\mathrm{DE}0}w_a a^{-3(w_0+w_a)}\mathrm{e}^{3w_a(a-1)}\right)\partial_a D + \\
&+ \left(2a^{-1} + 2f_{\mathrm{DE}0}a^{-1}a^{-3(w_0+w_a)}\mathrm{e}^{3w_a(a-1)} + 2f_{\mathrm{k}0}\right)\partial_a D - \frac{3}{2}a^{-2}D = \\
&= \left(1 + f_{\mathrm{DE}0}a^{-3(w_0+w_a)}\mathrm{e}^{3w_a(a-1)} + f_{\mathrm{k}0}a\right)\left(\partial_a^2 D + \frac{3}{2a}\partial_a D\right) + \frac{1}{2}f_{\mathrm{k}0}\partial_a D + \\
&+ \frac{3}{2}f_{\mathrm{DE}0}\,a^{-3(w_0+w_a)}\mathrm{e}^{3w_a(a-1)}\left(w_a - (w_0+w_a)a^{-1}\right)\partial_a D - \frac{3}{2a^2}D = 0\,.
\end{aligned} \tag{2.83}
$$

So the CPL D-time ODE is then given by:

$$
\begin{aligned}
&\left(1 + f_{\mathrm{DE}0}a^{-3(w_0+w_a)}\mathrm{e}^{3w_a(a-1)} + f_{\mathrm{k}0}a\right)\left(\partial_a^2 D + \frac{3}{2a}\partial_a D\right) + \frac{1}{2}f_{\mathrm{k}0}\partial_a D + \\
&+\frac{3}{2a}\left[w_a a - (w_0+w_a)\right]f_{\mathrm{DE}0}\,a^{-3(w_0+w_a)}\mathrm{e}^{3w_a(a-1)}\partial_a D - \frac{3}{2a^2}D = 0\,.
\end{aligned} \tag{2.84}
$$

This ODE is a novel result, and has not been documented in the literature yet, at the time of writing. It does not have an exact analytical solution so we must rely on numerical solutions instead. One can, however, find solutions for sufficiently early times, as shown in 2.3.5. Using values from DESI 2024 [7] for w_0, w_a, which can be found in table 2.1, the numerical solutions are visualised in the upper part of figure 2.5. To see the difference more clearly, one can also plot the relative difference, i.e. the ratio between the numerical solution and the analytical ΛCDM solution minus 1. The results are visualised in the lower part of figure 2.5. In both cases we have assumed no curvature, i.e $f_{\mathrm{k}0} = 0$.

Model	Ω_{m0}	Ω_{k0}	Ω_{DE0}	Ω_{r0}	w_0	w_a
ΛCDM	0.3	0	0.7	0	-1	0
ΛCDM+C	0.299	0.001	0.7	0	-1	0
ΛCDM-C	0.301	-0.001	0.7	0	-1	0
EdS	1	0	0	0	0	0
M+C	0.999	0.001	0	0	0	0
M-C	1.001	-0.001	0	0	0	0
M+R	0.99	0	0	0.01	0	0
DDE 1	0.3	0	0.7	0	-0.858	-0.68
DDE 2	0.3	0	0.7	0	-0.724	-1.02
DDE 3	0.3	0	0.7	0	-0.761	-0.96
DDE 4	0.3	0	0.7	0	-0.858	-0.3
DDE 5	0.3	0	0.7	0	-0.858	-0.2
DDE 6	0.3	0	0.7	0	-0.858	-0.1
DDE+C	0.299	0.001	0.7	0	-0.858	-0.68
DDE-C	0.301	-0.001	0.7	0	-0.858	-0.68

Table 2.1: Considered parameter choices within this work. To investigate the effects mostly fiducial values were, used except for the DE equation of state parameters, for which precise values from the most recent DESI data release [7] were used.

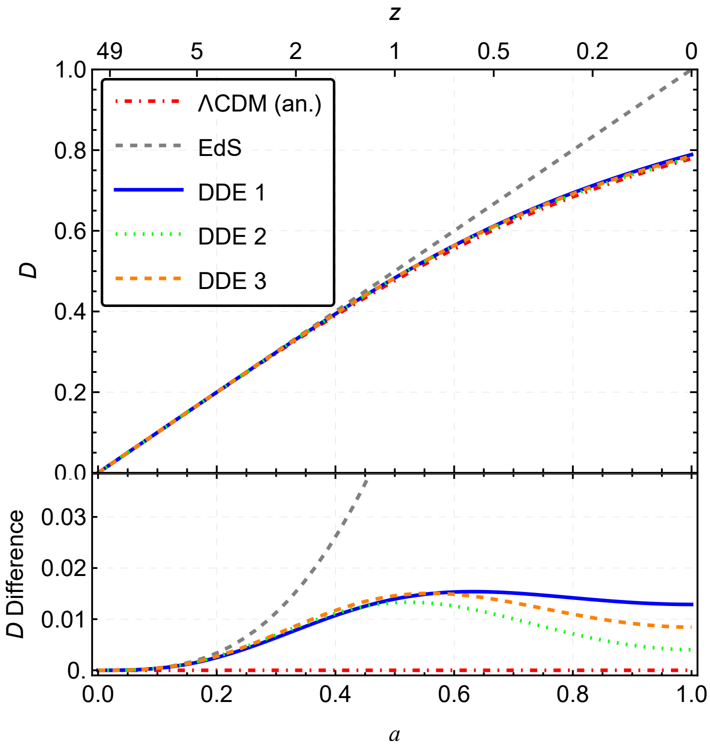

Figure 2.5: Numerical solution of $D(a)$ in the kDDE for different values of w_0, w_a and $k = 0$. One can see that matter perturbations grow stronger for larger values of w_0 and smaller values of w_a. The initialisation time was chosen to be $a_{\text{ini}} = 10^{-5}$. The relative difference is taken w.r.t. the analytical ΛCDM solution.

Using the upper bound value for the curvature energy density from Planck 2018 [28] $\Omega_{K0} = 0.001$ we get a very small suppression of the perturbations, when compared with the analytical ΛCDM solution as can be seen in figures 2.5 and 2.6. Note that this parameter value is a result from the combination of datasets, as the CMB data alone is impacted by geometric degeneracy [28]. All numerical solutions were initiated at $a_{\text{ini}} = 10^{-5}$ unless explicitly specified otherwise. A

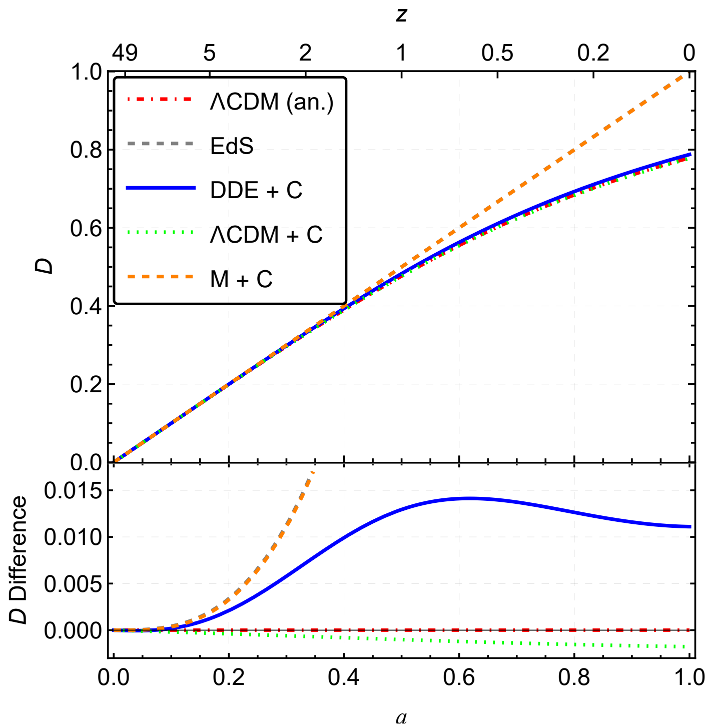

Figure 2.6: Impact of $\Omega_{k0} = 0.001$ on different models, and the relative difference w.r. to the analytical ΛCDM solution. All numerical solutions were initialised at $a_{\text{ini}} = 10^{-5}$.

positive curvature density corresponds to a spherical universe. We can also look at the effects of a negative curvature density, which would correspond to a hyperbolic universe. Numerical solutions of such a case for different models can be seen in the upper half of figure 2.7. The relative difference to ΛCDM - 1 of these is then visualised in the lower half of 2.7. Finally we compare the effects of curvature on a DDE in figure 2.8.

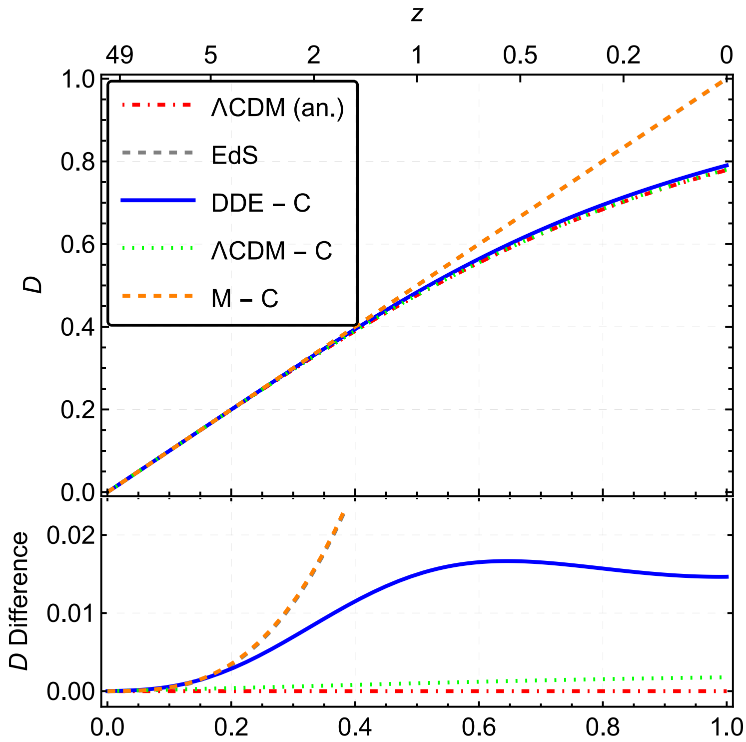

Figure 2.7: Impact of $\Omega_{k0} = -0.001$ on varying cosmological models, with $a_{ini} = 10^{-5}$. The relative difference was taken w.r.t. to the analytical ΛCDM solution.

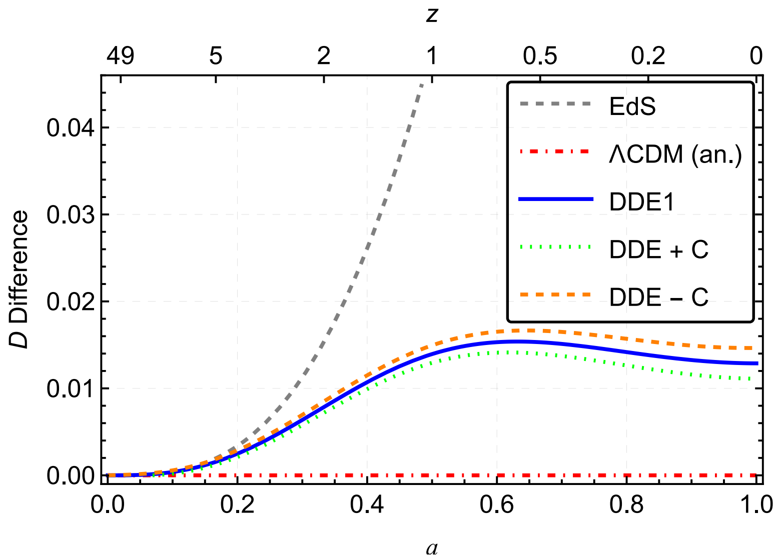

Figure 2.8: Comparison of the effect of $\Omega_{k0} < 0$ and $\Omega_{k0} > 0$ in the kDDE model using relative difference w.r.t. to ΛCDM. One can see that a closed universe ($\Omega_{k0} > 0$) reduces the growth of perturbations, while an open universe ($\Omega_{k0} < 0$) increases it. In both cases $|\Omega_{k0}| = 0.001$. The initialisation time was chosen as $a_{ini} = 10^{-5}$

2.3.5 Early-time Solution for *k*DDE

Equation (2.84) appears to be not analytically solvable. Here we seek ODE solutions that are valid for early times. Such avenues are important also within the numerical context: BullFrog requires the solution of D to be exactly in the growing mode, otherwise initialisations at $a = 0$ through backscaling techniques are ill defined.

To make progress, we define a new time variable through the relations

$$b = a^{-(w_0+w_a)}, \qquad a(b) = b^{-1/(w_0+w_a)}, \tag{2.85}$$

where we note that $b = a$ in ΛCDM by construction. In the b-time variable, the ODE (2.84) becomes

$$p(b)D''(b) + q(b)D'(b) - \frac{3}{2}D(b) = 0, \tag{2.86}$$

where

$$p(b) = (w_0 + w_a)^2 b^2 \Big(1 + f_{\rm DE0} b^3 \exp(3w_a[a(b) - 1]) + f_{\rm k0}\, a(b)\Big), \tag{2.87}$$

$$\begin{aligned} q(b) = \frac{1}{2}a(b)b(w_0 + w_a)\Big[& -3f_{\rm DE0} w_a b^3 \exp(3w_a[a(b) - 1]) + 2f_{\rm k0}(w_0 + w_a - 1) \\ &+ a^{-1}(b)[2w_a + 2w_0 - 1] + f_{\rm DE0} a^{-1}(b) b^3 [5w_a + 5w_0 - 1] \exp(3w_a[a(b) - 1])\Big]. \end{aligned} \tag{2.88}$$

Solving Eq. (2.86) analytically in all generality appears to be still not feasible; to make progress we solve this ODE using perturbation theory. For this we assume that $f_{\rm k0}$ is a perturbed quantity of order $\epsilon > 0$ and impose

$$D = D_0 + \epsilon D_{\rm k}, \qquad p = p_0 + \epsilon p_{\rm k}, \qquad q = q_0 + \epsilon q_{\rm k}, \tag{2.89}$$

where all terms with the index 0 are obtained by setting $f_{\rm k0} = 0$ in the relevant functions, while terms indexed with "k" are of order $f_{\rm k0}$.

Zeroth order. Keeping only terms to zeroth order, i.e., $f_{\rm k0} = 0$, and expanding the various terms about $b = 0$, we find

$$\begin{aligned} p_0(b) &= b^2(w_0 + w_a)^2 + O(b^4), \\ q_0(b) &= \frac{1}{2}(w_0 + w_a)[2w_0 + 2w_a - 1]b + O(b^4) \qquad [f_{\rm k0} = 0]. \end{aligned} \tag{2.90}$$

This is expansion corresponds to an early time expansion only for parameter choices of $w_0+w_a < 0$ due to the definition of $b(a)$. This, however, is of little concern, as the inferred values for these parameters from current measurements satisfy this condition. This leads to the ODE $p_0 D'' + q_0 D' - (3/2)D = 0$ with the following solution:

$$D_0(b) = c_1 b^{3/(2(w_0+w_a))} + c_2 b^{-1/(w_0+w_a)}, \qquad \text{[early-time solution with } f_{\rm k0} = 0] \tag{2.91}$$

which, likewise can be expressed in the a-time

$$D_0(a) = c_1 a^{-3/2} + c_2 a, \tag{2.92}$$

which, formally agrees with the EdS solution – but note again that the derivation seems to be not valid in EdS!

First order. Keeping in the ODE (2.86) terms to order ϵ, and using the results from the zeroth order, we find

$$p_0 D_{\mathrm{k}}'' + q_0 D_{\mathrm{k}}' - \frac{3}{2} D_{\mathrm{k}} = -p_{\mathrm{k}} D_0'' - q_{\mathrm{k}} D_0' \,, \tag{2.93}$$

where p_k and q_k are given by:

$$p_k = a(b)\left[b^2 + O(b^3)\right](w_0 + w_a)^2 f_{\mathrm{k}0} \,. \tag{2.94}$$

$$q_k = a(b)\left[b + O(b^3)\right](w_0 + w_a)[w_0 + w_a - 1] f_{\mathrm{k}0} \,. \tag{2.95}$$

Note that $a(b)$ is not analytical beyond second order and that we applied a Laurent expansion for the above results. Trying to expand this as a Taylor expansion yields to infinities for q_k already at the second order. The treatment of these is then related to singularities in Fuchs' theory, see [43]. This ODE for D_k can be solved analytically, which yields the following early time growing mode solution:

$$D_+(a) = a - \frac{4}{7} f_{\mathrm{k}0} a^2 + O(a^3) \,. \qquad \text{[early-time solution, small } f_{\mathrm{k}0}\text{]} \tag{2.96}$$

From the zeroth order discussion, we can see that the DDE effects are all contained in higher order terms. As a cross check, we can compare the matter and curvature (M+C) solution with our result, which we can get from setting $f_{\mathrm{DE}0} = 0$ in (2.84). This yields the following growing mode solution:

$$D_+^{\mathrm{m+c}}(a) = a \; {}_2F_1(1, 2, 7/2, -a f_{\mathrm{k}0}) \,. \tag{2.97}$$

Expanding this around $a = 0$:

$$D_+^{\mathrm{m+c}} = a - \frac{4}{7} f_{\mathrm{k}0} a^2 + O(a^3) \,. \tag{2.98}$$

In the literature [39], one can also find the following equivalent expression for the growing-mode solution in the same cosmology:

$$D_+(a) = \frac{5}{2 f_{\mathrm{k}0}} + \frac{15}{2 f_{\mathrm{k}0}^2 a} - \frac{15}{2 f_{\mathrm{k}0}^{5/2} a^{3/2}} \sqrt{1 + f_{\mathrm{k}0} a}\, \ln\left(\sqrt{f_{\mathrm{k}0} a} + \sqrt{1 + f_{\mathrm{k}0} a}\right), \tag{2.99}$$

which we have translated into our conventions. The equivalency was verified using Mathematicas "Fullsimplify" function. Expanding this result around $a = 0$ gives us yet again:

$$D_+(a) = a - \frac{4}{7} f_{\mathrm{k}0} a^2 + O(a^3) \,. \tag{2.100}$$

As we can see, approaching this case in three different ways yields the same early time solution, which supports its validity. This is an essential point since Bullfrog needs to be initialised precisely in the growing mode. In the case of ΛCDM this is can be done through EdS initial conditions [37], because the next to leading order contribution is $O(a^4)$, which means it can be safely ignored. In the curvature case however we have an $O(a^2)$ contribution which we might have to treat more carefully. We shall now investigate the difference between initialising with $D(a_{\mathrm{ini}}) = a_{\mathrm{ini}}$, i.e. with EdS ICs, and with $D(a_{\mathrm{ini}}) = a_{\mathrm{ini}} - 4/7 f_{\mathrm{k}0} a_{\mathrm{ini}}$, the early time kDDE solution, which we will call M+C ICs.

Hunt for a Good Initial Time Before we start investigating the impact of the error generated through EdS initial conditions, we must first get a solution that is as close to the exact or "true" solution of the full kDDE ODE as possible. For this we look at the D Difference between a given numerical solution and the early time analytical M+C solution in the regime, where it should be valid i.e. for early times. As we lack a full analytical kDDE solution, this is the closest we can get to the "true" solution at this stage. This analysis is visualised for realistic $\Omega_{k0} = 0.001$

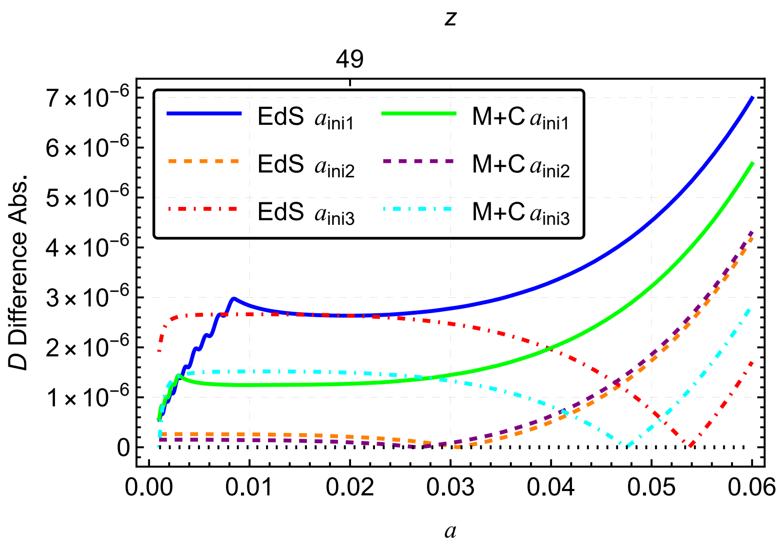

Figure 2.9: Comparison of the relative difference w.r.t. the analytical M+C solution, between numerical solutions of the DDE+C model with three different choices of EdS ICs and three different M+C ICs. The three initial times are chosen as $a_{\text{ini1}} = 10^{-5}$, $a_{\text{ini2}} = 10^{-4}$ and $a_{\text{ini3}} = 10^{-3}$. It follows that earlier initialisation time does not necessarily correspond to a more accurate solution, due to the limited precision of the ODE solver. We can see that the difference rises for larger a, which signifies the breakdown of the early time solution's validity.

in figure 2.9 and for a less realistic $\Omega_{k0} = 0.01$ in figure 2.10. In these numerical runs we have used $a_{\text{ini1}} = 10^{-5}$, $a_{\text{ini2}} = 10^{-4}$ and $a_{\text{ini3}} = 10^{-3}$. The most interesting result is the fact that a_{ini2} performs the best in both cases, even thought it is not the earliest initial time. The reason for the strong deviation is most likely due to the limited precision of Mathematica: since we are subtracting a term $\propto 10^{-5}$ with a term $\propto 10^{-13}$ in the curvature case for example, although the EdS ICs already show a problem with 10^{-5}. A stronger curvature seems to increase this numerical problem, although the EdS error remains in the same order of magnitude. The slight difference between the two EdS errors in different models with the same initialisation time can be explained by the fact that all other energy density parameters are also slightly modified, since the sum of all energy densities is equal to unity, and thus changing one parameter also means changing all of the others. For the latest ICs we can however notice the effect we have predicted: the M+C ICs solution deviates less from the true solution than the Eds ICs solution. We shall therefore take $a_{\text{ini}} = 10^{-4}$ as our reference solution for further analysis. One should note at this stage that even

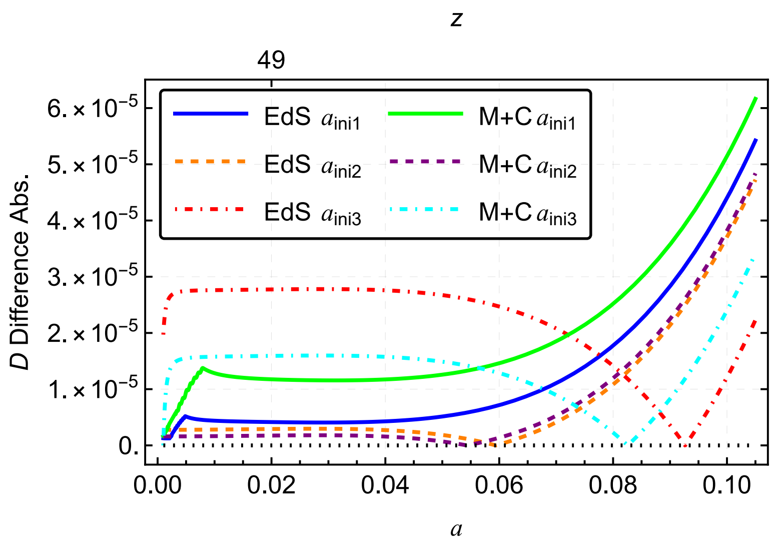

Figure 2.10: Relative difference w.r.t. the analytical M+C solution for parameter choices similar to DDE+C, but with an order of magnitude larger $\Omega_{k0} = 0.01$ and therefore $\Omega_{m0} = 0.29$. The initialisation times for the numerical solution are given by $a_{\text{ini1}} = 10^{-5}$, $a_{\text{ini2}} = 10^{-4}$ and $a_{\text{ini3}} = 10^{-3}$. Just as in the case of realistic curvature, visualised in figure 2.9, we can see that the optimal initialisation time seem so be $a_{\text{ini}} = 10^{-4}$.

the worst early time deviations are of $O(10^{-5})$, which is still very small. All of the numerical solutions start deviating at some point from the early time solution, which is to be expected since at that point the influence of all other parameters in the D-time ODE start to contribute.

Stability of the ODE Solutions With our new starting point $a_{\text{ini}} = 10^{-4}$ we can now try to see how large the error becomes for later times. For this we again choose a new set of initial times: $a_{\text{ini1}} = 10^{-3}$, $a_{\text{ini2}} = 10^{-2}$ and $a_{\text{ini3}} = 10^{-1}$. We now look again at the D difference of the numerical solutions for EdS and M+C ICs but with these later initial times and we use the $a_{\text{ini}} = 10^{-4}$ as our reference and $\Omega_{k0} = 0.001$. The results are visualised in figures 2.11 and 2.12. Here we can clearly see the effects that we have predicted, namely, that the EdS ICs are more susceptible to errors from late initial times than M+C ICs. The error is lower than 1% in each case. We note that this error is amplified when considering stronger curvature contributions.

Comment on Curvature in Simulations We have looked at the impact on the fluid equations from the curvature energy density Ω_{k0} and quantified it. It is however, necessary to point out that cosmological simulations are conducted within a box of a certain size [19], which has no intrinsic curvature and is thus equivalent to flat space ($\Omega_{k0} = 0$). In real curved spacetime with positive Ω_{k0}, trajectories, which start out parallel, could eventually cross one another, even when no forces are involved. This effect is not reflected within our simulations at all. It should, however, not be very significant for realistic choices of Ω_{k0}.

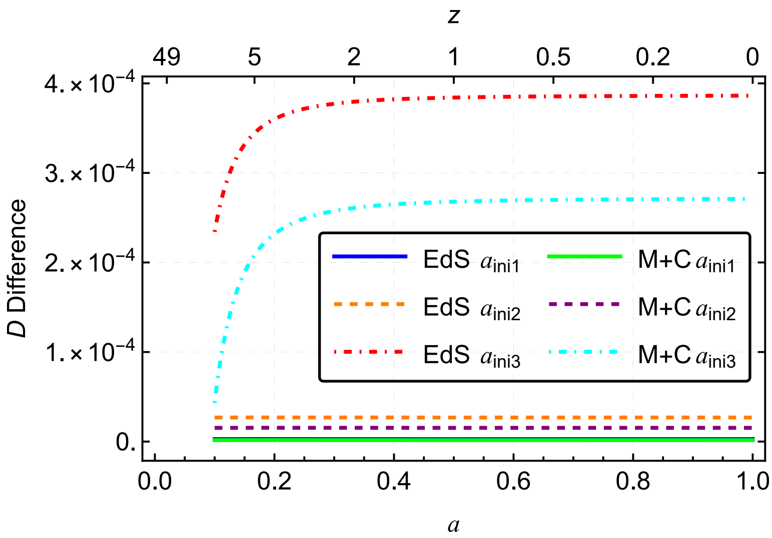

Figure 2.11: Relative difference of numerical solutions with varying initialisation times and ICs w.r.t. the reference solution with $a_{\rm ini} = 10^{-4}$ and M+C ICs, where $\Omega_{\rm k0} = 0.001$. The other starting times are given by $a_{\rm ini1} = 10^{-3}$, $a_{\rm ini2} = 10^{-2}$ and $a_{\rm ini3} = 10^{-1}$. In each case the M+C ICs are more precise than their corresponding EdS IC counterpart. The error introduced by choosing the "wrong" ICs is however always less significant, than the error arising from choosing to start at a later initialisation time.

2.3.6 Slaving Condition for kDDE

While we have discussed the behaviour of the D function for early times, and saw that it is well behaved, we did not discuss an explicit slaving argument. As in section 2.3.3, we start with the linearised fluid equations in comoving coordinates, which we repeat here:

$$\partial_t^2 \boldsymbol{x} + 2H\partial_t \boldsymbol{x} = -\frac{1}{a^2}\boldsymbol{\nabla}_x \tilde{\phi}\,, \tag{2.101a}$$

$$\boldsymbol{\nabla}_x^2 \tilde{\phi} = \frac{3}{2} H_0^2 \Omega_{\rm m0} \frac{\delta}{a}\,, \tag{2.101b}$$

We already saw that transforming the first equation into D-time yields the following:

$$\partial_D^2 \boldsymbol{x} = -\frac{3}{2}\frac{D H_0^2 \Omega_{\rm m0}}{(\partial_t D)^2 a^3}\left(\partial_D \boldsymbol{x} + \boldsymbol{\nabla}_x \varphi_r\right)\,, \tag{2.102}$$

where we have rescaled the potential according to $\tilde{\phi} = \frac{3}{2} H_0^2 \Omega_{\rm m0} \frac{D}{a} \varphi_r$. The expressions so far have specified no model, which is why they are equivalent to the M+R case. In the previous section 2.3.5 we have exhaustively discussed the validity of using the early time solution of the D-time:

$$D(a) = a - \frac{4}{7} f_{\rm k0} a^2 + h.o.t \tag{2.103}$$

Since the slaved initial conditions are important for the limit $a \to 0$ we shall use this, as the expression for D. In order to read off the slaving argument, we shall first start with transforming

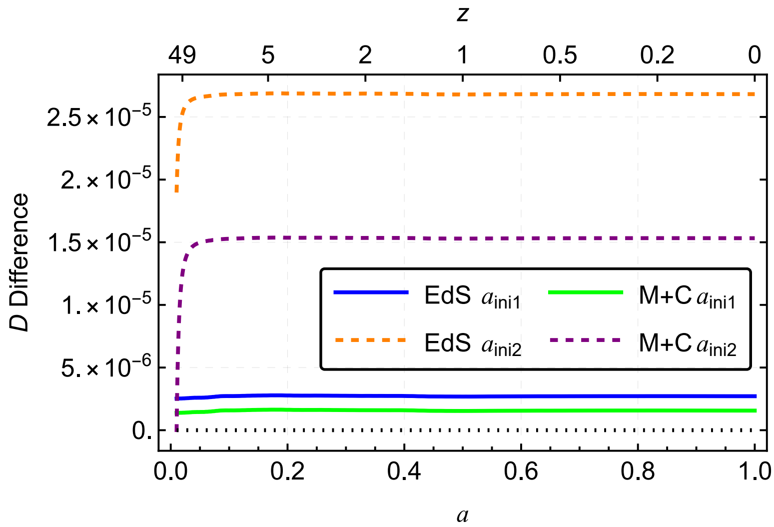

Figure 2.12: The relative differences from figure 2.11, with the two late initialisation times removed. We can again see that the M+C ICs are more accurate, however the largest error arises again from late initialisation times.

back to a-time. This is, however, less straightforward than in the M+R model, since inverting D here can lead to complex solutions for a depending on our choice of $f_{\mathrm{k}0}$. We begin with the transformation law:

$$\partial_D = \frac{\partial a}{\partial D}\partial_a = \left(\frac{\partial D}{\partial a}\right)^{-1}\partial_a = \left(1 - \frac{8}{7}f_{\mathrm{k}0}a\right)^{-1}\partial_a = \frac{1}{D'(a)}\partial_a\,, \tag{2.104}$$

where we have defined $D'(a) := \partial D/\partial a = (1 - 8/7 f_{\mathrm{k}0}a)$. For the second derivative we then have:

$$\partial_D^2 = \frac{1}{D'(a)}\partial_a\left(\frac{1}{D'(a)}\partial_a\right) = \frac{1}{D'(a)^2}\partial_a^2 + \frac{8f_{\mathrm{k}0}}{7D'(a)^3}\partial_a\,. \tag{2.105}$$

Additionally, we have that $\partial_t D = \dot{a}\partial_a D = \dot{a}D'(a)$. If we now also redefine our potential as $\varphi_r = \tilde{\varphi}_r/D'(a)$, we can insert everything into (2.102) to get the following equality:

$$\frac{1}{D'(a)^2}\partial_a^2\boldsymbol{x} + \frac{8f_{\mathrm{k}0}}{7D'(a)^3}\partial_a\boldsymbol{x} = -\frac{3H_0^2\Omega_{\mathrm{m}0}(1-(4/7)f_{\mathrm{k}0}a)}{2a^2\dot{a}^2D'(a)^3}\left(\partial_a\boldsymbol{x} + \nabla_x\tilde{\varphi}_r\right)\,. \tag{2.106}$$

From the Friedmann equation (2.79) we know that $\dot{a}^2 = H_0^2\Omega_{\mathrm{m}0}a^{-1}(1+f_{\mathrm{DE}0}a^{-3(w_0+w_a)}\mathrm{e}^{3w_a(a-1)} + f_{\mathrm{k}0}a) = H_0^2\Omega_{\mathrm{m}0}a^{-1}g(a)$, with $g(a) := (1 + f_{\mathrm{DE}0}a^{-3(w_0+w_a)}\mathrm{e}^{3w_a(a-1)} + f_{\mathrm{k}0}a)$. This further simplifies the denominator on the RHS towards:

$$\frac{1}{D'(a)^2}\partial_a^2\boldsymbol{x} + \frac{8f_{\mathrm{k}0}}{7D'(a)^3}\partial_a\boldsymbol{x} = -\frac{3(1-(4/7)f_{\mathrm{k}0}a)}{2ag(a)D'(a)^3}\left(\partial_a\boldsymbol{x} + \nabla_x\tilde{\varphi}_r\right) \tag{2.107}$$

We shall now discuss the behaviour of the terms in the denominators. We can see that for $a \rightarrow 0$, $D'(a) \rightarrow 1$[1], which means that the LHS shows no divergent behaviour. For $g(a)$, assuming that $w_0 + w_a < 0$, which is both consistent with DESI measurements [7] and also an assumption we made, when deriving the early time solution of D for the kDDE model, we can see that the limit $a \rightarrow 0$ corresponds to $g(a) \rightarrow 1$ too. This means that the only divergent behaviour in the Euler equation can be found in the $1/a$ term on the RHS. This divergence can be resolved by specifying $\partial_a \boldsymbol{x}^{\mathrm{ini}} = -\boldsymbol{\nabla}_x \tilde{\varphi}_r^{\mathrm{ini}}$. Writing the Poisson equation in our redefined potential we find that:

$$\boldsymbol{\nabla}_x^2 \tilde{\varphi}_r = \frac{\delta}{DD'(a)} = \frac{\delta}{a(1-(4/7)f_{\mathrm{k}0}a)D'(a)}\,. \tag{2.108}$$

We can see that the expression in the bracket does not cause a divergence and $D'(a)$ is, as previously discussed, unproblematic, which only leaves the $1/a$. This again can be regularised by setting $\delta^{\mathrm{ini}} = 0$. If we then transform back into the D-time (which is the time variable of BullFrog), the slaving argument for the kDDE model is given by:

$$\partial_D \boldsymbol{x}^{\mathrm{ini}} = -\boldsymbol{\nabla}_x \varphi_r^{\mathrm{ini}}\,, \quad \delta^{\mathrm{ini}} = 0\,, \tag{2.109}$$

which is analogous to the slaving arguments in ΛCDM and EdS cosmologies (see [37] and [40, 41]).

[1] Note that for choices of $f_{\mathrm{k}0} > 7/8$, $D'(a) \rightarrow 0$ for $a \rightarrow 1$, which would yield a divergence in this framework. However, this limit would invalidate the early time approximation, which means that this result is not worrisome.

3 Lagrangian Formulation of the Fluid Equations

As we will see later in chapter 4, the Lagrangian formulation has several advantages, when implemented into N-body codes. In this chapter we will revise the known results from the literature in a systematic way, and see, that they still hold for our modified cosmologies. The structure is as follows: we start by reformulating the mass conservation equation in a more convenient way in section 3.1, then move on to section 3.2, where write the fluid equations in Lagrangian coordinates. In section 3.3 we then apply Lagrangian perturbation theory (LPT).

3.1 Preliminary Considerations

We would now like to recast the peculiar fluid equations (2.34) in Lagrangian coordinates, by using the Lagrangian map $\boldsymbol{q} \mapsto \boldsymbol{x}$ from the initial (Lagrangian) position $\boldsymbol{q}$ to the current position $\boldsymbol{x}(\boldsymbol{q}, t)$ at time t. The map is then defined such that $\dot{\boldsymbol{x}}(\boldsymbol{q}, t) := u$ with dot corresponding to the Lagrangian total time derivative. From these definitions we can see that:

$$\frac{\mathrm{d}}{\mathrm{d}t} u_i(\boldsymbol{x}(\boldsymbol{q}, t), t) = \partial_t u_i + \frac{\partial u_i}{\partial x_j} \frac{\partial x_j}{\partial t} , \tag{3.1}$$

where the Einstein sum convention is implied here and in all subsequent calculations. Therefore, we can write $\mathrm{d}\boldsymbol{u}(\boldsymbol{x}(\boldsymbol{q}, t), t)/\mathrm{d}t = \partial_t \boldsymbol{u} + (\dot{\boldsymbol{x}} \cdot \boldsymbol{\nabla}_x)\boldsymbol{u}$. Inserting this and the definition of $\boldsymbol{u}$ in Lagrangian coordinates into eq. (2.34a) yields:

$$\begin{aligned} \frac{\mathrm{d}}{\mathrm{d}t}\boldsymbol{u} - (\dot{\boldsymbol{x}} \cdot \boldsymbol{\nabla}_x)\boldsymbol{u} + (\boldsymbol{u} \cdot \boldsymbol{\nabla}_x)\boldsymbol{u} + 2H\boldsymbol{u} &= -\frac{1}{a^2}\boldsymbol{\nabla}_x \tilde{\phi} , \\ \frac{\mathrm{d}}{\mathrm{d}t}\dot{\boldsymbol{x}} - (\dot{\boldsymbol{x}} \cdot \boldsymbol{\nabla}_x)\dot{\boldsymbol{x}} + (\dot{\boldsymbol{x}} \cdot \boldsymbol{\nabla}_x)\dot{\boldsymbol{x}} + 2H\dot{\boldsymbol{x}} &= -\frac{1}{a^2}\boldsymbol{\nabla}_x \tilde{\phi} , \\ \ddot{\boldsymbol{x}} + 2H\dot{\boldsymbol{x}} &= -\frac{1}{a^2}\boldsymbol{\nabla}_x \tilde{\phi} . \end{aligned} \tag{3.2}$$

Next, we consider the mass conservation, which can be written as:

$$M = \bar{\rho}(t)[1 + \delta(\boldsymbol{x}, t)]\mathrm{d}^3 x = \bar{\rho}(t)[1 + \delta^{\mathrm{ini}}(\boldsymbol{q})]\mathrm{d}^3 q , \tag{3.3}$$

where the second equality follows from the fact that the total mass of the system does not change over time in the absence of other interactions/collisions [44]. We know that applying the 'slaving condition', see for example [37] or the previous section 2.3.6, fixes $\delta^{\mathrm{ini}} = 0$ in cases which do not include radiation. We also know that for coordinate transformations the following holds:

$$M = \int \bar{\rho}(t)[1 + \delta(\boldsymbol{x}, t)\mathrm{d}^3 x = \int \bar{\rho}(t)[1 + \delta(\boldsymbol{x}(\boldsymbol{q}, t), t)]J\mathrm{d}^3 q , \tag{3.4}$$

where $J = |\det[\boldsymbol{\nabla}_{\boldsymbol{q}}\boldsymbol{x}]|$, the determinant of the Jacobian (before shell-crossing). From this it follows that:

$$1 + \delta(\boldsymbol{x}(\boldsymbol{q},t),t) = \frac{1}{J}\,, \qquad [\delta^{\rm ini} = 0]\,. \tag{3.5}$$

This relation is physically equivalent with the mass conservation law

$$\partial_t \delta + \boldsymbol{\nabla}_{\boldsymbol{x}} \cdot [1+\delta]\boldsymbol{u} = 0\,, \qquad \Leftrightarrow \qquad \frac{\mathrm{d}}{\mathrm{d}t}(1+\delta) + (1+\delta)\boldsymbol{\nabla}_{\boldsymbol{x}} \cdot \boldsymbol{u} = 0\,. \tag{3.6}$$

To see this, one expresses the last equation in Lagrangian coordinates ($\delta(\boldsymbol{x}) \to \delta(\boldsymbol{x}(\boldsymbol{q},t))$ etc.) and multiplies the whole equation by J. This firstly leads to

$$J\frac{\mathrm{d}}{\mathrm{d}t}(1+\delta) + (1+\delta)J\boldsymbol{\nabla}_{\boldsymbol{x}} \cdot \boldsymbol{u} = 0\,. \tag{3.7}$$

Now, the second expression can be simplified by using the identity $\mathrm{d}J/\mathrm{d}t = J\boldsymbol{\nabla}_{\boldsymbol{x}} \cdot \boldsymbol{u}$, which follows from using Jacobi's matrix formula[1] leading to

$$J\frac{\mathrm{d}}{\mathrm{d}t}(1+\delta) + (1+\delta)\frac{\mathrm{d}}{\mathrm{d}t}J = 0\,, \qquad \Leftrightarrow \qquad \frac{\mathrm{d}}{\mathrm{d}t}\left([1+\delta]J\right) = 0\,. \tag{3.8}$$

Integrating the last equation in time then leads to Eq. (3.5) for $\delta^{\rm ini} = 0$, which thus concludes the demonstration. In the following we simply replace the mass conservation through this equation.

3.2 Fluid Equations in Lagrangian Space

These considerations yield the following 'mixed form' for our fluid equations, where some derivatives are still w.r. to Eulerian coordinates:

$$\ddot{\boldsymbol{x}} + 2H\dot{\boldsymbol{x}} = -\frac{1}{a^2}\boldsymbol{\nabla}_{\boldsymbol{x}}\tilde{\phi}\,, \tag{3.9a}$$

$$\delta(\boldsymbol{x}(\boldsymbol{q},t),t) + 1 = \frac{1}{J}\,, \tag{3.9b}$$

$$\boldsymbol{\nabla}_{\boldsymbol{x}}^2\tilde{\phi} = \frac{3}{2a}H_0^2\Omega_{\rm m0}\delta\,. \tag{3.9c}$$

We have also replaced the matter density in eq. (2.34c) with the cosmological energy density. By taking the divergence of eq. (3.9a) we get:

$$\begin{aligned}
\boldsymbol{\nabla}_{\boldsymbol{x}} \cdot (\ddot{\boldsymbol{x}} + 2H\dot{\boldsymbol{x}}) &= -\frac{1}{a^2}\boldsymbol{\nabla}_{\boldsymbol{x}}^2\tilde{\phi}\,, \\
\boldsymbol{\nabla}_{\boldsymbol{x}} \cdot R_{tt}\boldsymbol{x} &= -\frac{1}{a^2}\frac{3}{2a}H_0^2\Omega_{\rm m0}\delta\,, \\
\boldsymbol{\nabla}_{\boldsymbol{x}} \cdot R_{tt}\boldsymbol{x} &= \frac{3}{2}H_0^2\Omega_{\rm m0}a^{-3}\left(1 - \frac{1}{J}\right)\,,
\end{aligned} \tag{3.10}$$

where we have defined $R_{tt} := \partial_t^2 + 2H\partial_t$, used eq. (3.9c) to get to the second line and eq. (3.9b) to get to the final expression.

[1] Jacobi's formula is $\mathrm{d}J/\mathrm{d}t = J\,\mathrm{tr}(\mathbf{J}^{-1}\mathrm{d}\mathbf{J}/\mathrm{d}t)$, where $\mathbf{J} := \boldsymbol{\nabla}_{\boldsymbol{q}}\boldsymbol{x}$ is the Jacobian matrix. Next, consider $\mathrm{d}\mathbf{J}/\mathrm{d}t = \boldsymbol{\nabla}_{\boldsymbol{q}}\boldsymbol{u}$ and replace $\boldsymbol{\nabla}_{\boldsymbol{q}}$ with $\mathbf{J}\boldsymbol{\nabla}_{\boldsymbol{x}}$, leading to $\mathrm{d}\mathbf{J}/\mathrm{d}t = \mathbf{J}\boldsymbol{\nabla}_{\boldsymbol{x}}\boldsymbol{u}$. Using this relation in the RHS of the Jacobi formula then allows us to execute the trace operation, leading to $\mathrm{d}J/\mathrm{d}t = J\boldsymbol{\nabla}_{\boldsymbol{x}} \cdot \boldsymbol{u}$ as stated in the main text.

3.3 Lagrangian Perturbation Theory

In what follows, we solve these equations perturbatively up to second order. For this we define the Lagrangian displacement field $\boldsymbol{\psi}(\boldsymbol{q}, t) := \boldsymbol{x} - \boldsymbol{q}$. In LPT, the displacement can be formally expanded as:

$$\boldsymbol{\psi} = \epsilon \boldsymbol{\psi}^{(1)} + \epsilon^2 \boldsymbol{\psi}^{(2)} + O(\epsilon^3) , \tag{3.11}$$

where $\epsilon > 0$ is a bookkeeping parameter of the expansion (which is set to unity after the calculation is completed). Additionally we can use the transformation law $(\nabla_{x_i}) = (\nabla_{x_i} q_j)\nabla_{q_j}$, where $(\nabla_{x_i} q_j) = 1/(2J)\ \varepsilon_{ikl}\varepsilon_{jmn} x_{k,m} x_{l,n}$. Here the $_{,i}$ denotes the derivative w.r. to the i-th component of $\boldsymbol{q}$ and ε_{ijk} is the Levi-Civita symbol. Using this, eq. (3.10) becomes:

$$\begin{aligned}
\frac{1}{2J}\varepsilon_{ikl}\varepsilon_{jmn}x_{k,m}x_{l,n}R_{tt}x_{i,j} &= \frac{3}{2}H_0^2\Omega_{\mathrm{m}0}a^{-3}\left(1-\frac{1}{J}\right) , \\
\varepsilon_{ikl}\varepsilon_{jmn}\left(\delta_{km}+\psi_{k,m}\right)\left(\delta_{ln}+\psi_{l,n}\right)R_{tt}\left(\delta_{ij}+\psi_{i,j}\right) &= 3H_0^2\Omega_{\mathrm{m}0}a^{-3}(J-1) , \\
2\left(1+\psi_{j,j}\right)R_{tt}\psi_{i,i} - 2\psi_{j,i}R_{tt}\psi_{i,j} + O\left(\epsilon^3\right) &= 3H_0^2\Omega_{\mathrm{m}0}a^{-3}\left(J-1\right) , \\
\left(1+\psi_{j,j}\right)R_{tt}\psi_{i,i} - \psi_{j,i}R_{tt}\psi_{i,j} &= \frac{3}{2}H_0^2\Omega_{\mathrm{m}0}a^{-3}\left(J-1\right) .
\end{aligned} \tag{3.12}$$

In order to evaluate this expression in terms of the displacement ψ we also have to write J in terms of ψ:

$$\begin{aligned}
J = \det[\boldsymbol{\nabla_q x}] = \det[x_{i,j}] &= \frac{1}{6}\varepsilon_{ikl}\varepsilon_{jmn}x_{j,i}x_{m,k}x_{n,l} = \\
&= \frac{1}{6}\varepsilon_{ikl}\varepsilon_{jmn}\left[(\delta_{ji}+\psi_{j,i})(\delta_{mk}+\psi_{m,k})(\delta_{nl}+\psi_{n,l})\right] = \\
&= 1 + \psi_{i,i} + \frac{1}{2}\left(\psi_{i,i}\psi_{j,j} - \psi_{j,i}\psi_{i,j}\right) + O\left(\epsilon^3\right) ,
\end{aligned} \tag{3.13}$$

where $\boldsymbol{\nabla_q x}$ is a tensor product. Inserting our perturbative treatment of ψ:

$$J = 1 + \epsilon\psi^{(1)}_{i,i} + \epsilon^2 R_{tt}\psi^{(2)}_{i,i} + \frac{1}{2}\epsilon^2\left[\psi^{(1)}_{i,i}\psi^{(1)}_{j,j} - \psi^{(1)}_{j,i}\psi^{(1)}_{i,j}\right] + O\left(\epsilon^3\right) . \tag{3.14}$$

Doing the same for the LHS of eq.(3.12) yields:

$$\begin{aligned}
&\left[1+\epsilon\psi^{(1)}_{j,j} + O\left(\epsilon^2\right)\right]R_{tt}\left[\epsilon\psi^{(1)}_{i,i} + \epsilon^2\psi^{(2)}_{i,i}\right] - \epsilon^2\psi^{(1)}_{j,i}R_{tt}\psi^{(1)}_{i,j} = \\
&\quad \epsilon R_{tt}\psi^{(1)}_{i,i} + \epsilon^2 R_{tt}\psi^{(2)}_{i,i} + \epsilon^2\psi^{(1)}_{j,j}R_{tt}\psi^{(1)}_{i,i} - \epsilon^2\psi^{(1)}_{j,i}R_{tt}\psi^{(1)}_{i,j} .
\end{aligned} \tag{3.15}$$

Meanwhile the RHS of (3.12) looks like:

$$\begin{aligned}
&\frac{3}{2}H_0^2\Omega_{\mathrm{m}0}a^{-3}\left(J-1\right) = \\
=&\frac{3}{2}H_0^2\Omega_{\mathrm{m}0}a^{-3}\left[\epsilon\psi^{(1)}_{i,i} + \epsilon^2\psi^{(2)}_{i,i} + \frac{1}{2}\epsilon^2\left(\psi^{(1)}_{i,i}\psi^{(1)}_{j,j} - \psi^{(1)}_{j,i}\psi^{(1)}_{i,j}\right)\right] .
\end{aligned} \tag{3.16}$$

Collecting all terms of $O(\epsilon)$:

$$R_{tt}\psi_{i,i}^{(1)} = \frac{3}{2}H_0^2\Omega_{\mathrm{m}0}a^{-3}\psi_{i,i}^{(1)}\,. \tag{3.17}$$

Doing the same for the terms of $O\left(\epsilon^2\right)$ and using the relation from $O(\epsilon)$:

$$\begin{aligned} R_{tt}\psi_{i,i}^{(2)} + \psi_{j,j}^{(1)}R_{tt}\psi_{i,i}^{(1)} - \psi_{j,i}^{(1)}R_{tt}\psi_{i,j}^{(1)} &= \frac{3}{2}H_0^2\Omega_{\mathrm{m}0}a^{-3}\left[\psi_{i,i}^{(2)} + \frac{1}{2}\left(\psi_{i,i}^{(1)}\psi_{j,j}^{(1)} - \psi_{j,i}^{(1)}\psi_{i,j}^{(1)}\right)\right]\,, \\ R_{tt}\psi_{i,i}^{(2)} &= \frac{3}{2}H_0^2\Omega_{\mathrm{m}0}a^{-3}\left[\psi_{i,i}^{(2)} - \frac{1}{2}\left(\psi_{j,j}^{(1)}\psi_{i,i}^{(1)} - \psi_{j,i}^{(1)}\psi_{i,j}^{(1)}\right)\right]\,. \end{aligned} \tag{3.18}$$

We will now investigate more explicit expressions for our first and second order displacements.

3.3.1 First Order Displacement

Equations (3.17)–(3.18) are partial differential equations; to solve them, one first needs to develop a strategy which, as it turns out, changes them into ordinary differential equations that are easy to solve. For this we should first verify if the perturbative displacement contains transverse contributions. To elucidate on this, we assume that the Eulerian velocity is irrotational as customary in the literature, i.e., $\boldsymbol{\nabla}_x \times \boldsymbol{v} = \boldsymbol{0}$. In component form and employing Lagrangian coordinates, this can be written as

$$\begin{aligned} \varepsilon_{ijk}\nabla_{x_j}\partial_t x_k &= 0\,, \\ \varepsilon_{ijk}(\nabla_{x_j}q_l)\nabla_{q_l}\partial_t x_k &= 0\,, \\ \frac{1}{2J}\varepsilon_{ijk}\varepsilon_{jpq}\varepsilon_{lmn}x_{p,m}x_{q,n}\partial_t x_{k,l} &= 0\,, \\ x_{i,n}\varepsilon_{nml}x_{k,m}\partial_t x_{k,l} &= 0\,. \end{aligned} \tag{3.19}$$

To get from the second to the last row we used the standard relations of the Levi-Civita symbol and the antisymmetry of the involved terms. We can simplify this cubic equation into a quadratic equation by using an elegant method developed in [45]. By inspecting our result closely we can see that we are dealing with an equation of the form:

$$A_{ij}X_j = 0\,, \tag{3.20}$$

where $A_{ij} = x_{i,j}$ and $X_j = \varepsilon_{jml}x_{k,m}\partial_t x_{k,l}$. Multiplying by the inverse $(A^{-1})_{ij}$ on both sides we get:

$$\begin{aligned} (A^{-1})_{ki}A_{ij}X_j &= 0\,, \\ \delta_{kj}X_j &= 0\,, \\ X_i &= 0\,, \end{aligned} \tag{3.21}$$

which means that:

$$\varepsilon_{ijk}x_{p,j}\partial_t x_{p,k} = 0\,. \tag{3.22}$$

An alternative approach to achieve this result can be found in [41] and traces back to the work done in [44]. Interestingly, this result has already been derived by Cauchy 200 years ago, but has been almost forgotten in the meantime only to be rediscovered later, see [46]. Note that starting from the irrotational Eulerian velocity assumption we have not introduced any perturbative consideration, which means that this result is valid non-perturbatively. We can now insert our perturbative ansatz (i.e. apply first order lagrangian perturbation theory (1LPT)) at first order $\boldsymbol{x} = \boldsymbol{q} + \boldsymbol{\psi}^{(1)}$:

$$\begin{aligned} \varepsilon_{ijk}\left(\delta_{p,j} + \epsilon\psi^{(1)}_{p,j}\right)\partial_t\left(\delta_{p,k} + \epsilon\psi^{(1)}_{p,k}\right) = 0\,, \\ \varepsilon_{ijk}\dot{\psi}^{(1)}_{j,k}\epsilon + O(\epsilon^2) = 0\,, \\ \varepsilon_{ijk}\psi^{(1)}_{j,k} = w_i^{\mathrm{ini}}\,. \end{aligned} \tag{3.23}$$

Assuming vanishing initial vorticity, we have $w_i^{\mathrm{ini}} \to 0$. From this it immediately follows that there exists a potential $\Phi^{(1)}$ such that at first order:

$$\boldsymbol{\psi}^{(1)} = -\boldsymbol{\nabla}_{\boldsymbol{q}}\Phi^{(1)}(\boldsymbol{q},t) = -D(t)\boldsymbol{\nabla}_{\boldsymbol{q}}\varphi^{\mathrm{ini}}(\boldsymbol{q})\,. \tag{3.24}$$

See also [47] for this result. The split into a temporal and spatial part can be justified from the fact that all differential equations which involve $\boldsymbol{\psi}^{(1)}$ are either purely temporal (3.17) or purely spatial like above. Considering only the temporal part and inserting into (3.17) we get back the general form of our D-time ODE (2.40) that we derived by linearising the Euler-Poisson system of equations (2.34):

$$\left[R_{tt} - \frac{3}{2}H_0^2\Omega_{\mathrm{m0}}a^{-3}\right]D(t) = 0\,, \tag{3.25}$$

and it follows that

$$\boldsymbol{\nabla}_{\boldsymbol{q}}\cdot\boldsymbol{\psi}^{(1)} = -D\varphi^{\mathrm{ini}}_{,ll}\,. \tag{3.26}$$

More importantly this implies that at first order the displacement field is purely longitudinal, i.e. $\boldsymbol{\nabla}_{\boldsymbol{q}}\times\boldsymbol{\psi}^{(1)} = \boldsymbol{0}$. Let us now move on to the second order.

3.3.2 Second Order Displacement

We can now repeat the same calculation up to second order (i.e. appy second order Lagrangian perturbation theory (2LPT)); we first have

$$\begin{aligned} \varepsilon_{ijk}\left(\delta_{lj} + \epsilon\psi^{(1)}_{l,j} + \epsilon^2\psi^{(2)}_{l,j}\right)\partial_t(\epsilon\psi^{(1)}_{l,k} + \epsilon^2\psi^{(2)}_{l,k}) = 0\,, \\ \epsilon_{ijk}\psi^{(1)}_{l,j}\dot{\psi}^{(1)}_{l,k} + \varepsilon_{ijk}\dot{\psi}^{(2)}_{j,k} = 0\,. \end{aligned} \tag{3.27}$$

Now let us examine the first term more closely by inserting our previous result (3.24) into it:

$$\begin{aligned} &\varepsilon_{ijk}(-D(t)\nabla_{q_j}\nabla_{q_l}\varphi^{\mathrm{ini}})(-\dot{D}(t)\nabla_{q_k}\nabla_{q_l}\varphi^{\mathrm{ini}}) = \\ &= D(t)\dot{D}(t)\varepsilon_{ijk}\nabla_{q_j}(\nabla_{q_l}\varphi^{\mathrm{ini}})\nabla_{q_k}(\nabla_{q_l}\varphi^{\mathrm{ini}}) = 0\,, \end{aligned} \tag{3.28}$$

where, in the last line, we have used that the derivatives are symmetric but the epsilon tensor is antisymmetric. From this it follows that $\varepsilon_{ijk}\dot{\psi}^{(2)}_{j,k} = 0$ and, similarly to the first order case, we can define a potential such that:

$$\boldsymbol{\psi}^{(2)} = -\boldsymbol{\nabla}_{\boldsymbol{q}}\Phi^{(2)}(\boldsymbol{q}, t)\,. \tag{3.29}$$

Having established the (well-known) result that the displacement is given by a potential in Lagrangian coordinates up to second order, we can now insert all our results into the PDE for the second order perturbation (3.18):

$$\begin{aligned}
R_{tt}\psi^{(2)}_{i,i} &= \frac{3}{2}H_0^2\Omega_{\mathrm{m}0}a^{-3}\left[\psi^{(2)}_{i,i} - \frac{1}{2}\left(\psi^{(1)}_{i,i}\psi^{(1)}_{j,j} - \psi^{(1)}_{j,i}\psi^{(1)}_{i,j}\right)\right],\\
\left[R_{tt} - \frac{3}{2}H_0^2\Omega_{\mathrm{m}0}a^{-3}\right]&\boldsymbol{\nabla}^2_{\boldsymbol{q}}\Phi^{(2)}(\boldsymbol{q}, t) =\\
-\frac{3}{4}\Omega_{\mathrm{m}0}H_0^2a^{-3}D^2(t)&\left[(\boldsymbol{\nabla}^2_{\boldsymbol{q}}\varphi^{\mathrm{ini}}(\boldsymbol{q}))^2 - (\boldsymbol{\nabla}_{\boldsymbol{q}}\boldsymbol{\nabla}_{\boldsymbol{q}}\varphi^{\mathrm{ini}}(\boldsymbol{q}))_{ij}(\boldsymbol{\nabla}_{\boldsymbol{q}}\boldsymbol{\nabla}_{\boldsymbol{q}}\varphi^{\mathrm{ini}}(\boldsymbol{q}))_{ji}\right],\\
\left[R_{tt} - \frac{3}{2}H_0^2\Omega_{\mathrm{m}0}a^{-3}\right]&\boldsymbol{\nabla}^2_{\boldsymbol{q}}\Phi^{(2)}(\boldsymbol{q}, t) = -L(t)\mu_2(\boldsymbol{q})\,,
\end{aligned} \tag{3.30}$$

with $L(t) = (3/2)\Omega_{\mathrm{m}0}H_0^2a^{-3}D^2(t)$ and

$$\mu_2 = (1/2)\left[(\boldsymbol{\nabla}^2_{\boldsymbol{q}}\varphi^{\mathrm{ini}}(\boldsymbol{q}))^2 - (\boldsymbol{\nabla}_{\boldsymbol{q}}\boldsymbol{\nabla}_{\boldsymbol{q}}\varphi^{\mathrm{ini}}(\boldsymbol{q}))_{ij}(\boldsymbol{\nabla}_{\boldsymbol{q}}\boldsymbol{\nabla}_{\boldsymbol{q}}\varphi^{\mathrm{ini}}(\boldsymbol{q}))_{ji}\right]\,. \tag{3.31}$$

As we can see the RHS is factorizable into a temporal and spatial part. Using an Ansatz of the form $\Phi^{(2)}(\boldsymbol{q}, t) = E(t)\varphi^{(2)}(\boldsymbol{q})$ we can then solve the resulting ODEs:

$$\left[R_{tt} - \frac{3}{2}H_0^2\Omega_{\mathrm{m}0}a^{-3}\right]E(t) = -\frac{3}{2}H_0^2\Omega_{\mathrm{m}0}a^{-3}D^2(t)\,, \tag{3.32}$$

$$\boldsymbol{\nabla}^2_{\boldsymbol{q}}\varphi^{(2)}(\boldsymbol{q}) = \mu_2(\boldsymbol{q})\,, \tag{3.33}$$

where we remind the reader that $R_{tt} := \partial_t^2 + 2H\partial_t$. This means for the displacement:

$$\psi^{(2)} = E(t)\boldsymbol{\nabla}^{-1}_{\boldsymbol{q}}\mu_2(\boldsymbol{q})\,, \tag{3.34}$$

where we have defined $\boldsymbol{\nabla}^{-1}_{\boldsymbol{q}} = \boldsymbol{\nabla}_{\boldsymbol{q}}\boldsymbol{\nabla}^{-2}_{\boldsymbol{q}}$, with the inverse Laplace operator $\boldsymbol{\nabla}^{-2}_{\boldsymbol{q}}$. These results are very well established in the literature [48, 49, 47], albeit not always in the same time variable as here, and not always using the formulation with energy densities of the universe.

3.3.3 ODEs in kDDE

We have already discussed the first order growth ODE (3.25) in detail in the chapters 2.3.4 and 2.3.5 as formulated in the a-time. Using the knowledge from these, we can derive the following expression:

$$\begin{aligned}
&\left(1 + f_{\mathrm{DE}0}a^{-3(w_0+w_a)}\mathrm{e}^{3w_a(a-1)} + f_{\mathrm{k}0}a\right)\left(\partial_a^2E(a) + \frac{3}{2a}\partial_aE(a)\right) + \frac{1}{2}f_{\mathrm{k}0}\partial_aE(a) +\\
&+\frac{3}{2a}\left[aw_a - (w_0 + w_a)\right]f_{\mathrm{DE}0}a^{-3(w_0+w_a)}\mathrm{e}^{3w_a(a-1)}\partial_aE(a) - \frac{3}{2a^2}E(a) = -\frac{3}{4a^2}D^2(a)\,.
\end{aligned} \tag{3.35}$$

For the sake of comparison we repeat the ODE for the first order growth:

$$\left(1 + f_{\mathrm{DE0}} a^{-3(w_0+w_a)} \mathrm{e}^{3w_a(a-1)} + f_{\mathrm{k0}} a\right) \left(\partial_a^2 D(a) + \frac{3}{2a} \partial_a D(a)\right) + \frac{1}{2} f_{\mathrm{k0}} \partial_a D(a) + \\ + \frac{3}{2a} \left[a w_a - (w_0 + w_a)\right] f_{\mathrm{DE0}} a^{-3(w_0+w_a)} \mathrm{e}^{3w_a(a-1)} \partial_a D(a) - \frac{3}{2a^2} D(a) = 0\,. \tag{3.36}$$

The similarity between these two is striking; the only true difference is in the RHS and that we are dealing with the second order growth, which is also to be expected, as it is built upon the 1LPT result. It should be noted, that the ODE for the first order growth looks exactly like the ODE we derived by linearising the Euler-Poisson system of equations, which yielded the following (2.84). This is also as anticipated, since it is the linear contribution of the time evolution in LPT and should thus be consistent with the linear contribution to the time evolution of the linearised Euler-Poisson system of equations. Note that this specific ODE for the second order growth has not been documented within the literature. How this is implemented into the numerical integrator, will be discussed in chapter 4.2.2 and the indirect investigation through N-body simulations is to be found in 5.

4 N-Body Simulations

The most commonly used discretization technique in the state of the art cosmological CDM simulations is the N-body method. The principle idea is as follows: One discretizes the continuous matter distribution into a number of N particles, which are sampled from the density field. Through this, the Hamiltonian equations of motion for the N-particle system can be time-integrated to make predictions about the evolution of the density distribution.

This discretization comes with its own set of complications, like the fact that the mass distribution is extended infinitely and the choice of the N particles ICs once they have been sampled. Current challenges of this approach reside in discreteness effects, which are particularly strong when the resolution of the mass and force suffers a mismatch. At this point the discrete particle dynamics deviate from the continuous dynamics of the distribution. This effect can be softened by various techniques. More details regarding N-body simulations in cosmology and recent developments can be found in [19].

More importantly for the topic at hand is the fact, that the dynamics are determined by a Hamiltonian, which allows us to time-integrate the equations of motion with various techniques.

4.1 Symplectic Integrators

In the context of cosmology Hamiltonians are separable, which means that they take the following form:

$$\mathcal{H} = \alpha(t)T(\boldsymbol{p}_1, \boldsymbol{p}_2, ..., \boldsymbol{p}_N) + \beta(t)U(\boldsymbol{x}_1, ..., \boldsymbol{x}_N)\,. \tag{4.1}$$

Following the derivation from [19] we introduce the superconformal time $d\tilde{t} = a^{-2}dt$ and group the momentum and position of each respective particle $\boldsymbol{\Gamma}_i = (\boldsymbol{x}, \boldsymbol{p})_i$ together. The equations of motion can be written as $\dot{\boldsymbol{x}} = \{\boldsymbol{x}, \mathcal{H}\}$ and $\dot{\boldsymbol{p}} = \{\boldsymbol{p}, \mathcal{H}\}$, where we have used the Poisson bracket $\{\cdot, \cdot\}$. Alternatively, we can introduce a Hamiltonian operator:

$$\hat{\mathcal{H}}(t) = \{\cdot, \mathcal{H}(t)\} = \{\cdot, \alpha(t)T\} + \{\cdot, \beta(t)U\} =: \hat{D}(t) + \hat{K}(t)\,, \tag{4.2}$$

through which we can also define the so-called Drift- and Kick operators $\hat{D}$ and $\hat{K}$. Using this, we can write the equations of motion as the follows:

$$\dot{\boldsymbol{\Gamma}}_i = \hat{\mathcal{H}}(t)\boldsymbol{\Gamma}_i\,. \tag{4.3}$$

This first order operator equations can be solved by using Dyson's time ordering operator $\mathcal{T}$:

$$\boldsymbol{\Gamma}_i(t) = \mathcal{T}\exp\left(\int_0^t \hat{\mathcal{H}}(t')dt'\right)\boldsymbol{\Gamma}(0)\,. \tag{4.4}$$

Note that $\hat{D}$ acts only on momenta and $\hat{K}$ acts only on positions. This important property allows us to find time-explicit operator factorizations, which have the following form:

$$\mathcal{T}\exp\left(\int_t^{t+\epsilon}\hat{\mathcal{H}}(t')dt'\right) \simeq \exp\left(\epsilon_n\hat{K}\right)...\exp\left(\epsilon_3\hat{D}\right)\exp\left(\epsilon_2\hat{K}\right)\exp\left(\epsilon_1\hat{D}\right) + O(\epsilon^m)\,, \tag{4.5}$$

where the order of the error exponent m is determined by the choice of the coefficients ϵ_i. When both α and β are time-dependent one can achieve an error of $O(\epsilon^3)$ in the most beneficial case. Here the choice of superconformal time is particularly useful: in cosmic time t, $\alpha(t) = a(t)^{-2}$ and $\beta(t) = a(t)^{-1}$, while in superconformal time $\tilde{t}$ they turn to $\alpha(\tilde{t}) = 1$ and $\beta(\tilde{t}) = a(\tilde{t})$. We will now explain how to construct an extendend phase space integrator. For this we take the following set of coordinates $(\boldsymbol{x}_i, a)$ and momenta $(\boldsymbol{p}_i, p_a)$, which now have an additional scale factor a and momentum p_a in contrast to earlier. With this, we have a new extended phase space Hamiltonian, given in superconformal time:

$$\tilde{\mathcal{H}} = \sum_i \frac{\boldsymbol{p}_i^2}{2M} + aU(\boldsymbol{x}_1, ..., \boldsymbol{x}_N) + a^2\tilde{H}(a)p_a\,, \tag{4.6}$$

where $\tilde{H} = \partial_t a$ is the Hubble function in conformal time. The last term arises from $\mathrm{d}a/\mathrm{d}\tilde{t} = a^2\tilde{H}$. When we now pick $\epsilon_1 = \epsilon_3 = \epsilon/2$ and $\epsilon_2 = \epsilon$ and all higher $\epsilon_i = 0$ and expand the exponential functions up to first order we arrive at the following expression:

$$\boldsymbol{\Gamma}_i(\tilde{t}+\epsilon) = \left(\mathbb{1} + \frac{\epsilon}{2}\hat{D}\right)\left(\mathbb{1} + \epsilon\hat{K}\right)\left(\mathbb{1} + \frac{\epsilon}{2}\hat{D}\right)\boldsymbol{\Gamma}_i(\tilde{t}) + h.o.t.\,. \tag{4.7}$$

This can also be written explicitly, which we do in the following, as it is also the way one would usually realise this in a code:

$$\boldsymbol{x}_i\left(\tilde{t}+\frac{\epsilon}{2}\right) = \boldsymbol{x}_i(\tilde{t}) + \frac{\epsilon}{2M}\boldsymbol{p}_i(\tilde{t})\,, \tag{4.8a}$$

$$\boldsymbol{p}_i(\tilde{t}+\epsilon) = \boldsymbol{p}_i(\tilde{t}) - \epsilon a\left(\tilde{t}+\frac{\epsilon}{2}\right)\nabla_{\boldsymbol{x}_i}U\left[\boldsymbol{x}_1\left(\tilde{t}+\frac{\epsilon}{2}\right), ..., \boldsymbol{x}_N\left(\tilde{t}+\frac{\epsilon}{2}\right)\right]\,, \tag{4.8b}$$

$$\boldsymbol{x}_i(\tilde{t}+\epsilon) = \boldsymbol{x}_i\left(\tilde{t}+\frac{\epsilon}{2}\right) + \frac{\varepsilon}{2M}\boldsymbol{p}_i(\tilde{t}+\epsilon)\,, \tag{4.8c}$$

$$a\left(\tilde{t}+\frac{\epsilon}{2}\right) = a(\tilde{t}) + \frac{\epsilon}{2}a(\tilde{t})^2\tilde{H}(a(\tilde{t}))\,, \tag{4.8d}$$

$$a(\tilde{t}+\epsilon) = a\left(\tilde{t}+\frac{\epsilon}{2}\right) + \frac{\epsilon}{2}a\left(\tilde{t}+\frac{\epsilon}{2}\right)^2\tilde{H}\left[a\left(\tilde{t}+\frac{\epsilon}{2}\right)\right]\,. \tag{4.8e}$$

These equations give us the so-called drift-kick-drift (DKD) form of a second order "leap frog" integrator, which is the most commonly used scheme in cosmological simulations.

4.2 Fast Time-integrating Methods/D-time Integrators

The main drawback of the the previously introduced type of symplectic integrators is that they require a large amount of timesteps to accurately integrate the Hamiltonian dynamics of the system, even during the early stages of structure formation, when their behaviour is almost linear.

One way to overcome this issue is by working with so-called "D-time integrators" (originally introduced as Π integrators in [13]), which do not use the canonical conjugate momentum of $\boldsymbol{x}$, but use a momentum defined by the D-time $\boldsymbol{V} = \partial_D \boldsymbol{x}$ instead. One general timestep, using the D-time, $D : D_n \longrightarrow D_{n+1}$, is then realised as follows [13]:

$$\boldsymbol{x}_{n+1/2} = \boldsymbol{x}_n + \frac{\Delta D}{2} \boldsymbol{V}_n \,, \tag{4.9a}$$

$$\boldsymbol{V}_{n+1} = \alpha \boldsymbol{V}_n + \beta D^{-1}_{n+1/2} \boldsymbol{A}(\boldsymbol{x}_{n+1/2}) \,, \tag{4.9b}$$

$$\boldsymbol{x}_{n+1} = \boldsymbol{x}_{n+1/2} + \frac{\Delta D}{2} \boldsymbol{V}_{n+1} \,, \tag{4.9c}$$

where $\boldsymbol{A} = -\boldsymbol{\nabla}_x \varphi$ and φ is the gravitational potential. Note that we have omitted the index $i = 1, .., N$, but of course this timestepping scheme applies to all N particles of the simulation and is analogous to (4.8). We would like to solve this acceleration along 1LPT and 2LPT trajectories, starting from [15]:

$$(\boldsymbol{\nabla}_x \cdot \boldsymbol{A})|_{\boldsymbol{x}=\boldsymbol{x}^{\text{1LPT}}} = \delta(\boldsymbol{x}^{\text{1LPT}}) \,. \tag{4.10}$$

Using the mass conservation equivalent expression (3.9b) and the transformation law for the derivative from comoving to Lagrangian spatial coordinates $(\nabla_{x_i}) = (\nabla_{x_i} q_j)\nabla_{q_j}$, where $(\nabla_{x_i} q_j) = 1/(2J)\ \varepsilon_{ikl}\varepsilon_{jmn} x_{k,m} x_{l,n}$, the above expression turns into this semi Lagrangian form:

$$\frac{1}{2}\left(\varepsilon_{ikl}\varepsilon_{jmn} x_{k,m} x_{l,n} A_{i,j}\right)|_{\boldsymbol{x}^{\text{1LPT}}} = J_{\text{1LPT}} - 1 \,. \tag{4.11}$$

The RHS can be rewritten using a relation we have derived before (3.13). By transforming both sides fully into Lagrangian coordinates this equation then turns into:

$$\begin{aligned} &\left[(1+\psi_{l,l})\delta_{ij} - \psi_{j,i} + \varepsilon_{ikl}\varepsilon_{jmn}\psi_{k,m}\psi_{l,n}\right] A_{i,j}|_{\boldsymbol{x}^{\text{1LPT}}} = \\ &= \left[\psi_{i,i} + \frac{1}{2}\left(\psi_{i,i}\psi_{j,j} - \psi_{j,i}\psi_{i,j}\right) + h.o.t.\right] A_{i,j}|_{\boldsymbol{x}^{\text{1LPT}}} \,. \end{aligned} \tag{4.12}$$

Note that the trajectory has not yet been evaluated at this point, so up until now this calculation is analogous to 2LPT. We now take the 1LPT trajectory as our input for A and ψ. We can again introduce a parameter ϵ, similarly to chapter 3. Since we are interested in the 1LPT trajectory this means that we take $\psi = \epsilon \psi^{(1)}$ and we additionally expand $A^{\text{1LPT}} = \epsilon A^{(1)} + \epsilon^2 A^{(2)} + O(\epsilon^3)$. We insert this into the above equation and group all terms of the same order together up to (i.e. including) ϵ^2. Lastly, we use the expression for $\psi^{(1)} = -D\boldsymbol{\nabla}_{\boldsymbol{q}}\varphi^{\text{ini}}$, which we have derived in the previous chapter 3.3.1. This combined finally yields:

$$\boldsymbol{A}^{\text{1LPT}} = -D\boldsymbol{\nabla}_{\boldsymbol{q}}\varphi^{\text{ini}} - D^2 \boldsymbol{\nabla}_{\boldsymbol{q}}^{-1} \mu_2(\boldsymbol{q}) \,, \tag{4.13}$$

where we remind the reader that $\boldsymbol{\nabla}_{\boldsymbol{q}}^{-1} = \boldsymbol{\nabla}_{\boldsymbol{q}} \boldsymbol{\nabla}_{\boldsymbol{q}}^{-2}$ with $\boldsymbol{\nabla}_{\boldsymbol{q}}^{-2}$ the inverse Laplace operator. For 2LPT, this calculation is analogous, except for the fact that we use $\psi = \epsilon\psi^{(1)} + \epsilon^2\psi^{(2)}$ and additionally use the information that $\psi^{(2)} = -E\boldsymbol{\nabla}_{\boldsymbol{q}}^{-1}\mu_2(\boldsymbol{q})$, which we know from section 3.3.2.

$$\boldsymbol{A}^{\text{2LPT}} = -D\boldsymbol{\nabla}_{\boldsymbol{q}}\varphi^{\text{ini}} - (E + D^2)\boldsymbol{\nabla}_{\boldsymbol{q}}^{-1}\mu_2(\boldsymbol{q}) \,. \tag{4.14}$$

Note that this calculation differs from standard LPT computations, since we take the approximate trajectories as inputs and truncate the acceleration arbitrarily at the second order. A similar derivation can be found in [15].

The difference between various D-time integrators lies now in the choice of α and β. We will discuss two possible choices of these temporal weights in the following sections.

4.2.1 FastPM

A very popular choice of weights in cosmological simulations [19] is given by FastPM [50]. It is a symplectic, 1LPT consistent after each finished time step and second order accurate integrator. 1LPT consistent means that it is the condition $\alpha + \beta = 1$ is satisfied and symplectic means that the integrator of the discrete Hamiltonian captures all of the relevant symmetries of the continuous Hamiltonian like energy conservation for a time independent Hamiltonian. The difference between this discrete and continuous Hamiltonian is again a so-called error Hamiltonian, and if it is small enough, the majority of stable orbits in the continuous system will translate to stable orbits in the discrete system [51].

The symplecticity of FastPM stems from the fact that its choice weights, was originally derived from canonical variables, which is how one arrives at α^{FastPM}, and then β^{FastPM} is obtained by imposing $\alpha^{\text{FastPM}} + \beta^{\text{FastPM}} = 1$. This is also the unique choice of weights that results in a symplectic D-time integrator.

Interestingly [51] already derived a not-symplectic integrator in the appendix, which goes into the direction of the BullFrog integrator, though they make a canonical transformation to achieve symplecticity again.

The weights for FastPM are explicitly given by

$$\alpha^{\text{FastPM}} = \frac{B_n}{B_{n+1}}, \qquad \beta^{\text{FastPM}} = 1 - \alpha^{\text{FastPM}}, \tag{4.15}$$

where $B(a) = a^3 H \partial_a D$ and $B_n = B(a(D))|_{D=D_n}$. We can arrive at this function by considering $\boldsymbol{p} = a^2 \partial_t \boldsymbol{x} = B \partial_D \boldsymbol{x}$. All D-time integrators can be initialised at $D = 0$, which corresponds to the Big Bang [15][14], however FastPM is being set back in its accuracy due to a mismatch in the 2LPT term [15].

4.2.2 BullFrog

The recently introduced BullFrog integrator [15] comes with a different choice of temporal weights, which, before shell-crossing, allow it to be 2LPT consistent after each completed time step, up to higher order terms. This can be thought of as a 2LPT extension to FastPM. This choice is unique for these D-time integrators. We will first show how to calculate the weights first time-step and then how it is done for an arbitrary time step.

First Time Step During the first time step $n : 0 \to 1$ we have that $\boldsymbol{x}_0 = \boldsymbol{q}$, per definition, since we defined $\boldsymbol{q}$ to be the initial position and $\boldsymbol{\psi}$ the displacement, when discussing LPT in chapter 3.3. From the slaving argument 2.109 we also get the initial velocity $\partial_D \boldsymbol{x}_0 = \boldsymbol{V}_0 = -\boldsymbol{\nabla}_{\boldsymbol{q}} \varphi^{\text{ini}}$, where

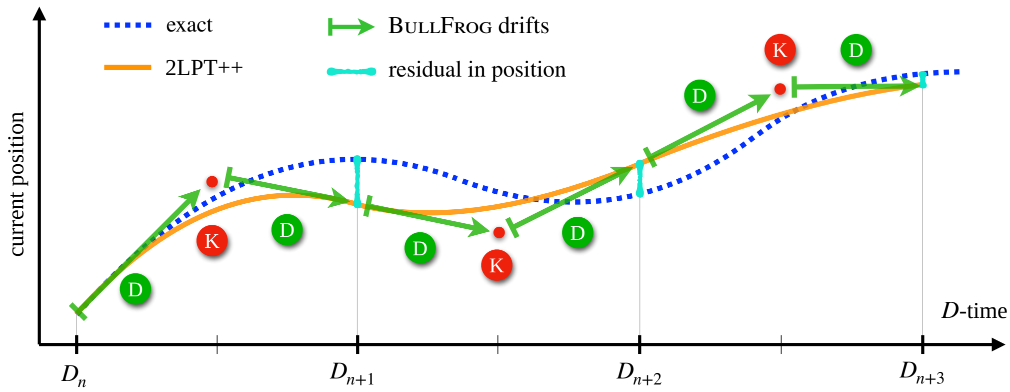

Figure 4.1: Outline of the position calculation in the BullFrog time integration scheme. After every half-drift ("D" in green) the velocity is updated with a kick ("K" in red) in such a way that the particle's position is consistent with 2LPT after each second half-drift (or after each full step). This is done by taking the acceleration as an input and choosing the weights α and β accordingly. The difference in positions between the "true" solution and the one calculated by BullFrog reduces with the reduction of the step size. The figure is from Rampf et al. [15].

the use of $\boldsymbol{\nabla}_{\boldsymbol{q}}$ follows from the fact that at the inital time $\boldsymbol{x} = \boldsymbol{q}$. When inserting this into (4.9c) we get:

$$\boldsymbol{x}_{1/2} = \boldsymbol{x}_0 + \frac{\Delta D}{2}\boldsymbol{V}_0\,, \tag{4.16a}$$

$$\boldsymbol{V}_1 = \alpha^{\rm BF}\boldsymbol{V}_0 + \beta^{\rm BF}(\Delta D/2)^{-1}\boldsymbol{A}(\boldsymbol{x}_{1/2})\,, \tag{4.16b}$$

$$\boldsymbol{x}_1 = \boldsymbol{x}_{1/2} + \frac{\Delta D}{2}\boldsymbol{V}_1\,. \tag{4.16c}$$

If we now evaluate $\boldsymbol{A}$ along the trajectory, as we did for 1LPT earlier starting from (4.10) we get the following expression:

$$\boldsymbol{A}(\boldsymbol{x}_{1/2}) = -\frac{\Delta D}{2}\boldsymbol{\nabla}_{\boldsymbol{q}}\varphi^{\rm ini} - \left(\frac{\Delta D}{2}\right)^2\boldsymbol{\nabla}_{\boldsymbol{q}}^{-1}\mu_2\,, \tag{4.17}$$

which is equivalent to $\boldsymbol{A}^{\rm 1LPT}$ (4.13)! This is a consequence of our ICs. In order to get an expression for the weights, we now use that $\partial_D \boldsymbol{x}^{\rm 2LPT} = \boldsymbol{V}^{\rm 2LPT} = \partial_D\boldsymbol{\psi}^{(1)} + \partial_D\boldsymbol{\psi}^{(2)} = -\boldsymbol{\nabla}_{\boldsymbol{q}}\varphi^{\rm ini} + \partial_D E\boldsymbol{\nabla}_{\boldsymbol{q}}^{-1}\mu_2$ and match this to the expression in (4.16b), evaluated at $D = \Delta D$, which gives us the following expression:

$$(-\boldsymbol{\nabla}_{\boldsymbol{q}}\varphi^{\rm ini} + \partial_D E\boldsymbol{\nabla}_{\boldsymbol{q}}^{-1}\mu_2)|_{D=\Delta D} = -\alpha^{\rm BF}\boldsymbol{\nabla}_{\boldsymbol{q}}\varphi^{\rm ini} - \beta^{\rm BF}\left[\boldsymbol{\nabla}_{\boldsymbol{q}}\varphi^{\rm ini} + \frac{\Delta D}{2}\boldsymbol{\nabla}_{\boldsymbol{q}}^{-1}\mu_2\right]. \tag{4.18}$$

Matching all terms $\propto \nabla_{\boldsymbol{q}}\varphi^{\mathrm{ini}}$ and all the ones $\propto \nabla_{\boldsymbol{q}}^{-1}\mu_2$ together we naturally arrive at the 1LPT condition $\alpha + \beta = 1$ and from this we also get the following expressions:

$$\alpha^{\mathrm{BF}} = 1 - \beta^{\mathrm{BF}} = 1 + \frac{2}{\Delta D}E_1' \,, \tag{4.19}$$

$$\beta^{\mathrm{BF}} = -\frac{2}{\Delta D}E_1' \,, \tag{4.20}$$

where $E_1'(\Delta D) = \partial_D E(D)|_{D=\Delta D}$. These weights then yield 2LPT consistency, at least for ΛCDM [15].

Arbitrary Time Step We now want to generalise the previous procedure to all subsequent time steps $n : n \longrightarrow n+1$, which means that we can safely assume that the previous step was 2LPT consistent. The first half-drift for an arbitrary timestep is then given by inserting all known quantities into (4.9a):

$$\boldsymbol{x}_{n+1/2} = \boldsymbol{q} - \left(D_n + \frac{\Delta D}{2}\right)\nabla_{\boldsymbol{q}}\varphi^{\mathrm{ini}} + \left(E_n + \frac{\Delta D}{2}E_n'\right)\nabla_{\boldsymbol{q}}^{-1}\mu_2 + h.o.t.\,. \tag{4.21}$$

Evaluating the acceleration along the $\boldsymbol{x}_{n+1/2}$ trajectory we then get:

$$\boldsymbol{A}(\boldsymbol{x}_{n+1/2}) = -\left(D_n + \frac{\Delta D}{2}\right)\nabla_{\boldsymbol{q}}\varphi^{\mathrm{ini}} + \left[E_n + \frac{\Delta D}{2}E_n' - \left(D_n + \frac{\Delta D}{2}\right)^2\right]\nabla_{\boldsymbol{q}}^{-1}\mu_2\,. \tag{4.22}$$

While very similar in form to $\boldsymbol{A}^{\mathrm{2LPT}}$ (4.14), it yields slightly different results, which we expect, as we are not moving along the 2LPT trajectory, after the first half drift. It is the kick which always brings us back to the 2LPT trajectory after the second half drift. As for the initial time step we plug this into the "kick" 4.9b and demand that it coincides with the 2LPT velocity at the time $D_{n+1} = D_n + \Delta D$, we get the following condition on our temporal weights:

$$-\nabla_{\boldsymbol{q}}\varphi^{\mathrm{ini}} + E_{n+1}'\nabla_{\boldsymbol{q}}^{-1}\mu_2 = -(\alpha^{\mathrm{BF}} + \beta^{\mathrm{BF}})\nabla_{\boldsymbol{q}}\varphi^{\mathrm{ini}} + (\alpha^{\mathrm{BF}}E_n' + \beta^{\mathrm{BF}}F_{n+1/2})\nabla_{\boldsymbol{q}}^{-1}\mu_2\,, \tag{4.23}$$

where $F_{n+1/2} = (D_{n+1/2})^{-1}[E_n + (\Delta D/2)E_n'] - D_{n+1/2}$ and $E_n' = \partial_D E|_{D=D_n+\Delta D}$. By comparing coefficients we again get the 1LPT consistency $\alpha + \beta = 1$ from the first term. Using this in the second term, we arrive at the expressions for temporal weights :

$$\alpha^{\mathrm{BF}} = \frac{E_{n+1}' - F_{n+1/2}}{E_n' - F_{n+1/2}}\,, \quad \beta^{\mathrm{BF}} = \frac{E_{n+1}' - E_n'}{F_{n+1/2} - E_n'}\,, \tag{4.24}$$

We can see that the entire information about the chosen cosmological model is then encoded in these temporal weights, which are related to the LPT of the model. This particular choice makes the particle momenta and positions 2LPT consistent after each completed timestep, allows for UV-completeness and converges quadratically against the true solution in the ΛCDM case, if the exact growth function D is chosen. The 2LPT consistency follows from the unique choice to match the degrees of freedom in the "kick" update to the 1LPT and 2LPT prediction.

What seems like an intentional setback of BullFrog, is its lack of symplecticity, which should, at least in theory, make it less qualified than FastPM to simulate virialised systems, like for example halos. Since energy is not conserved on the large scales, as consequence of the Hubble drag term in (2.34a), which acts similarly to a friction on the system, it is not a very important property for the predictions of the LSS. However, FastPM, as a representative of symplectic solvers, was also previously compared against other LPT informed integrators, where it was shown that it requires more time steps in order to converge towards the correct solution, even on smaller scales, where simplecticity should be more impactful [13]. The precise reason for this is still unknown. For the large scales BullFrog shows an improvement in efficiency by a factor of 2-3 for accurate LSS predictions [15][13], when compared with FastPM. Despite its recent introduction, the BullFrog scheme has already been used for cosmological inference [52].

4.3 Initial Conditions

In order to generate the initial conditions for the numerical setup one can use a variety of techniques, which have been developed over the years and have been discussed in more detail in [19]. Here we will give a short summary of two alternatives to the approach we have used and then discuss the approach which is part of our implementation. The strongly non-linear structures, which we can observe on the small scales in the universe today, are a consequence of small perturbations in the early universe which are augmented by gravitational interactions. On the large scales and for early times these perturbations remain small which allows for perturbative calculations of the non-linear coupled equations [53]. This analytical approach loses its validity due to non-linearities and shell crossing. While perturbation theory can be extended somewhat beyond shell crossing [54, 55, 56], one usually approaches the non-linear regime through N-body approaches with an input from perturbation theory in the initial conditions.

Since the early phase of the universe consists of a plasma which is coupled to radiation and interacts gravitationally with dark matter, and posseses only small density perturbations, one can approach its evolution by leading order perturbation theory. This is done through so-called linear-order Einstein-Boltzmann (EB) codes, which integrate this complex system through first order perturbation theory. Examples of these are Class [57, 58] and Camb [59]. The output of these EB codes can then be used to set up the ICs of N-body simulations in different ways, which we discuss below. The N-body simulations can then effectively capture the non-linearities, while the EB codes captures the effect the different species have on one another. The challenge lies then in finding a good balance between including all of the physics, while still capturing the non-linearities that matter produces.

4.3.1 Forward Method

In the forward method one takes the output of the EB code at $a = a_{\text{ini}} \lesssim 10^{-2}$ and then continues on to simulate all non-linearities through the N-body simulation. The limitation of this approach is the fact that it is incompatible with higher order LPT, since the EB code yields only linear quantities at a_{ini}. This also means that a_{ini} has to be as early as possible in order to limit the arising inaccuracies, which stem from non-linearities in the simulation[19].

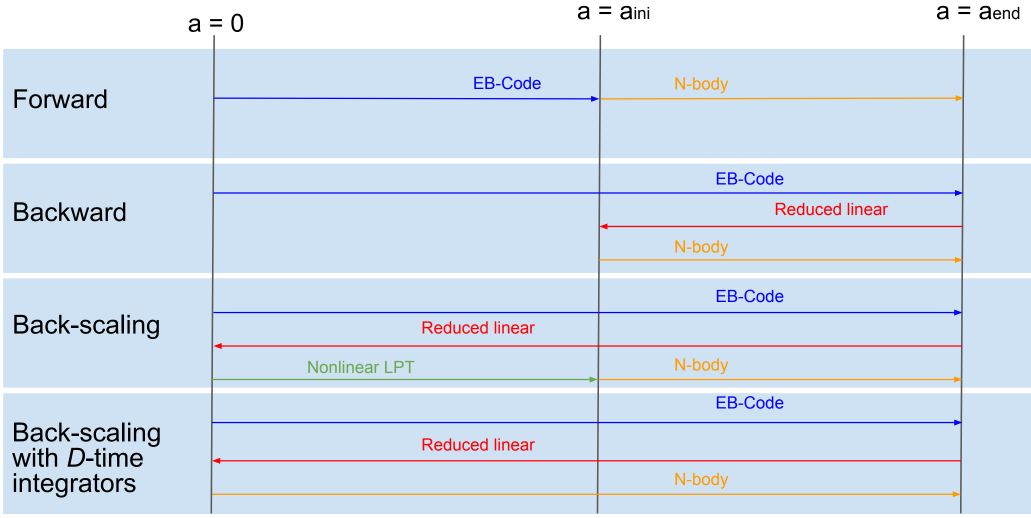

Figure 4.2: Different approaches to arrive at initial conditions for N-body simulations. "EB-Code" gives the linear evolution of all particle species, but misses the non-linearities from the N-body code, "reduced linear" represents the linearised version of the physics solved by the N-body code and is used to evolve the system backwards, "nonlinear LPT" describes the progression of the system, as given by some finite order of LPT and "N-body" is the full non-linear evolution as calculated by the N-body code. The figure is inspired by [19].

4.3.2 Backward Method

Alternatively, one can take the EB code output at $a = a_{\text{today}}$, evolve the backwards in time using the linearised N-body code physics to a_{ini} and then use the density contrast δ_{EB} to provide ICs to the simulation. The backdraw of this approach is that, just like for the forward method, only linear fields are known, and also one has to make sure that decaying modes at a_{ini} are very small [19].

4.3.3 Back-Scaling Method

Knowledge of the growth factor D allows a rather simple approach, where we just evolve the density contrast δ_{EB} back in time, through the D-function:

$$\varphi^{\text{ini}}(\boldsymbol{q}) = D^{-1}(a_{\text{today}})\boldsymbol{\nabla}_{\boldsymbol{q}}^{-2}\delta_{\text{EB}}(\boldsymbol{q}, a_{\text{today}})\,. \tag{4.25}$$

Afterwards one can use LPT to generate ICs at a_{ini} [19]. This is not necessary for D-time integrators, which can be initialised at $a = 0$ directly [14] and therefore this also applies to BullFrog [15] and FastPM [50], although it turns out that, while in principle possible, it is not recommended to do so for FastPM, as it differs from 2LPT for $a \to 0$ [14, 15]. Back-scaling is is the most commonly employed approach [19], and also the one we are using in our implementation.

4.3.4 White Noise Field

The Fourier transform of the field amplitude $\tilde{\varphi}^{\text{ini}}(\boldsymbol{k})$ that is computed from the EB-code potential is then convolved with a complex valued three dimensional white noise field $\tilde{W}(\boldsymbol{k})$, which results in a real Gaussian homogenous and isotropic random field:

$$F(\boldsymbol{x}) = \frac{1}{(2\pi)^3} \int_{\mathbb{R}^3} d^3k \mathrm{e}^{i\boldsymbol{k}\cdot\boldsymbol{x}} \tilde{\varphi}(\boldsymbol{k}) \tilde{W}(\boldsymbol{k}) \,. \tag{4.26}$$

$\tilde{W}$ gets its name from the fact that it is k indepentent and satisfies the following properties:

$$\tilde{\boldsymbol{W}}(\boldsymbol{k}) = \tilde{\boldsymbol{W}}^*(-\boldsymbol{k}) \,, \quad \langle \tilde{\boldsymbol{W}}(\boldsymbol{k}) \rangle = 0 \,, \quad \langle \tilde{\boldsymbol{W}}(\boldsymbol{k}) \tilde{\boldsymbol{W}}^*(\boldsymbol{k}') \rangle = \delta_D(\boldsymbol{k} - \boldsymbol{k}') \,, \tag{4.27}$$

where $\boldsymbol{k}$, $\boldsymbol{k}'$ are wave vectors, δ_D is the (3 dimensional) Dirac delta function and the * denotes the complex conjugation. This field F is then the starting point of the simulations.

4.4 Power Spectrum

We conclude this chapter by explaining the power spectrum, which our main tool for testing the validity of the BullFrog integrator and a very common tool in LSS cosmology [19, 53]. It is defined as the Fourier transform of the two-point correlation function ξ. The latter is given by:

$$\xi(r) = \langle \delta(\boldsymbol{x}_1) \delta(\boldsymbol{x}_2) \rangle = \frac{1}{V} \int_V d^3x \; \delta(\boldsymbol{x}) \delta(\boldsymbol{x} + \boldsymbol{r}) \,, \tag{4.28}$$

where $\boldsymbol{r} = \boldsymbol{x}_1 - \boldsymbol{x}_2$ and $r = |\boldsymbol{r}|$ and we note that due to homogeneity $\langle \delta(\boldsymbol{x}) \rangle = 0$ [53]. By Fourier transforming this result we can then arrive at the powerspectrum:

$$P(k) = \int d^3r \; \mathrm{e}^{-i\boldsymbol{k}\cdot\boldsymbol{r}} \xi(r) \,, \tag{4.29}$$

up to a factor of $(2\pi)^3$, which is, as commonly emphasized in the literature, a matter of convention [4, 53]. To reduce the impact of the fluctuations in the power spectrum of the white noise field $\tilde{W}$ (i.e. the cosmic variance) one can "fix" its amplitude to its expectation value. This reduces degrees of freedom and introduces non-Gaussianities, which turn out to be far smaller than other biases in the power spectrum and therefore unproblematic [19, 60]. In practice, one evaluates the power spectrum in discrete bins of k.

5 Simulation Results and Comparisons

In order to confirm the validity of our results we compare our implementation of BullFrog with the "COsmological N-body CodE in PyThon" (CONCEPT) [17] and the cosmological neural-network emulators for large-scale structure statistics "baccoemu" [18], which we will refer to as Bacco. In both cases our linear matter power spectrum is obtained from Bacco and CONCEPT and used as an input for back-scaling in our BullFrog implementation in order to achieve consistent results. We also add linear power spectra from simulations which used FastPM choices of weights.

Numerical and Cosmological parameters All of our N-body simulations are conducted with $N = 256^3$ particles, with a box size of $L = 1.024$ Gpc/h, where $h = 0.67$ is the reduced Hubble's constant. For the BullFrog and FastPM force calculation we have used the particle-mesh (PM) method with a grid resolution of 512^3 and double precision computation. We note that our matter energy density Ω_{m0}, consists of a baryonic matter contribution $\Omega_{\mathrm{b}} = 0.049$ and a CDM contribution $\Omega_{\mathrm{c}} = 0.251$, which then unify as $\Omega_{\mathrm{m0}} = \Omega_{\mathrm{b}} + \Omega_{\mathrm{c}} = 0.3$, as specified in the table 2.1. This is irrelevant for the simulation itself, as we treat baryonic matter to behave collisionless within our N-body simulation, it is however relevant for an EB solver input and for the generation of power spectra using Bacco. In all cases we have used a spectral index of $n_{\mathrm{s}} = 0.96$.

We use 10 BullFrog steps and 100 FastPM steps respectively in each simulation, conduct 20 simulations of each respectively and average over all 20 in order to reduce the impact from cosmic variance. As already mentioned in chapter 4, all D-time integrators can be initialised at $a = 0$, however it is not as advisable for FastPM. To ensure a good comparison, we therefore utilise the standard back-scaling approach and use 2LPT to get initial conditions at $a = 0.02$ or $z = 49$ for both BullFrog and FastPM. The standard deviation of BullFrog is then shown as a light-blue background in each graph. To reduce discreteness problems we also employ de-aliasing through grid interlacing [61]. All simulatons were run using a GPU.

5.1 Comparison with Bacco

Bacco is a python package containing several neural network emulators for power spectra of the cosmic large scale structure. It allows the inclusion of various contributions in cosmology like DE with the CPL parametrisation, massive neutrinos, etc. It is therefore well-suited for our comparison with the BullFrog time-stepping scheme.

To make an accurate comparison, we first use the linear power spectrum from Bacco at $a = 1$ as an input for back-scaling in our simulations, and then compare the resulting simulations to the non-linear power spectrum from Bacco. All Bacco power spectra use $\sigma_8 = 0.792$, which is therefore also the σ_8 used in our BullFrog and FastPM simulations. The remaining cosmological parameters can be found in table 2.1. Since the power spectrum is evaluated using different bins in Bacco than in our BULLFROG implementation, we interpolate the 100 Bacco power spectrum values onto the 22 BULLFROG k bins in logarithmic space.

We start by comparing with ΛCDM parameters and then continue to contrast it with DE models of various "strengths", where DDE4 shows the strongest time dependence. In our comparison of

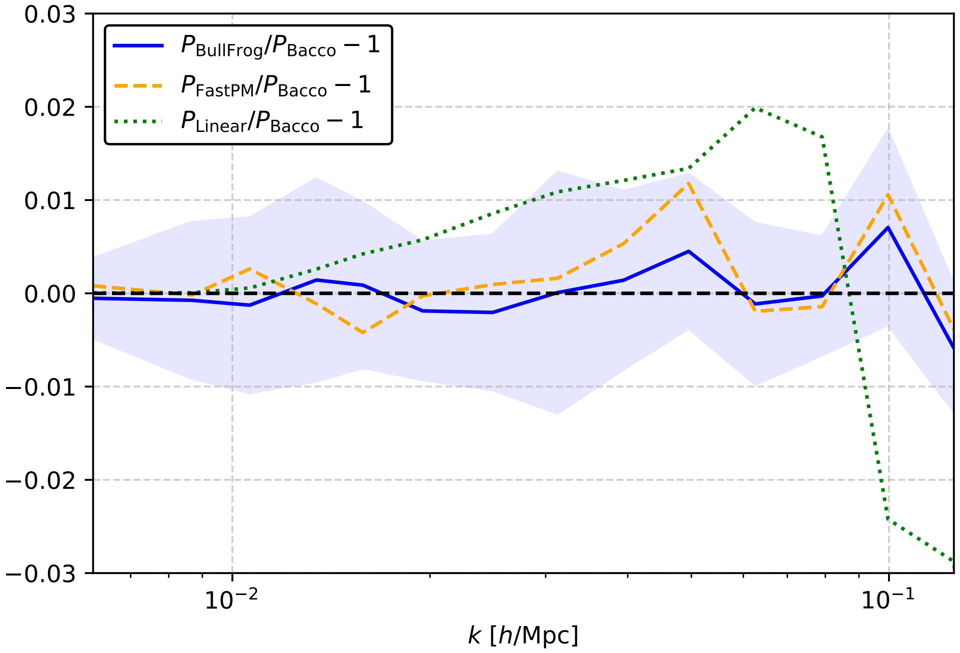

Figure 5.1: Comparison of BULLFROG, FASTPM and Bacco in the ΛCDM model. BULLFROG is consistent with Bacco up to 1% on linear scales.

ΛCDM we achieve sub percent level consistency with the non-linear Bacco power spectrum on linear scales as can be seen in 5.1. Deviations in the non-linear regime are to be expected in any comparison, however the linear regimes of the non-linear power spectra should be consistent, if the same cosmology was used. When considering the DDE models in 5.2, 5.3 and 5.4, we can see that we again achieve sub-percent level deviations from Bacco's non-linear power spectrum, except at $k = 0.1$. This peak does not seem to depend on the strength of the DE and is most likely an artifact from the interpolation, since 22 bins for the BULLFROG power spectrum is a comparatively small number. Apart from the $k = 0.1$ bin, the power spectrum line from BULLFROG is always within standard deviation. This comparison with Bacco therefore shows good agreement with our BULLFROG implementation.

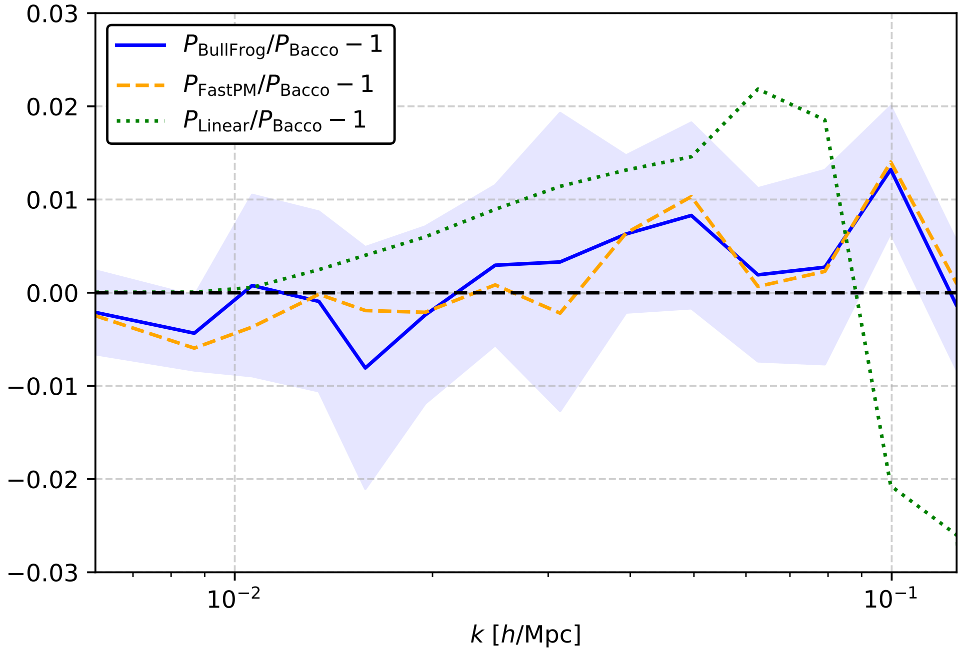

Figure 5.2: Comparison of BULLFROG, FASTPM and Bacco in the DDE4 model. Sub percent accuracy has been achieved at almost the entire linear scale, with the exception of a peak at $k = 0.1$.

5.2 Comparison with CO*N*CEPT

CO*N*CEPT is a simulation code for cosmic structure formation, which can incorporate a variety of different particle species, and is consistent with general relativistic perturbation theory [17].

For our comparison we create initial conditions in CO*N*CEPT and use the linear power spectrum output of CO*N*CEPT at $a = 1$ as the input for our simulations. The CO*N*CEPT initial conditions are created using a primordial scalar fluctuations amplitude of $A_s = 2.1 \cdot 10^{-9}$, which is also the CO*N*CEPT default value. The σ_8 for BULLFROG and FASTPM was then calculated from the linear power spectrum of CO*N*CEPT (since A_s and σ_8 are not independent of one another). For the force computation in CO*N*CEPT we have used a P3M method with a grid resolution of 512^3. We again begin our comparison with a ΛCDM model and then move on to compare with various DE cosmologies, that are based one the DESI data release [7]. For the number of time steps in our CO*N*CEPT simulations we have used the default number of 150.

For the power spectrum comparison we again interpolate 49 values from CO*N*CEPT onto the 22 k bins of our BULLFROG implementation. We can see that the deviations are far larger than in our comparison with Bacco. This can be attributed to a variety of reasons: Most importantly, the CO*N*CEPT simulations do not use the same initial white noise field as our BULLFROG simulations, and we have only conducted one CO*N*CEPT simulation per model. Therefore the CO*N*CEPT

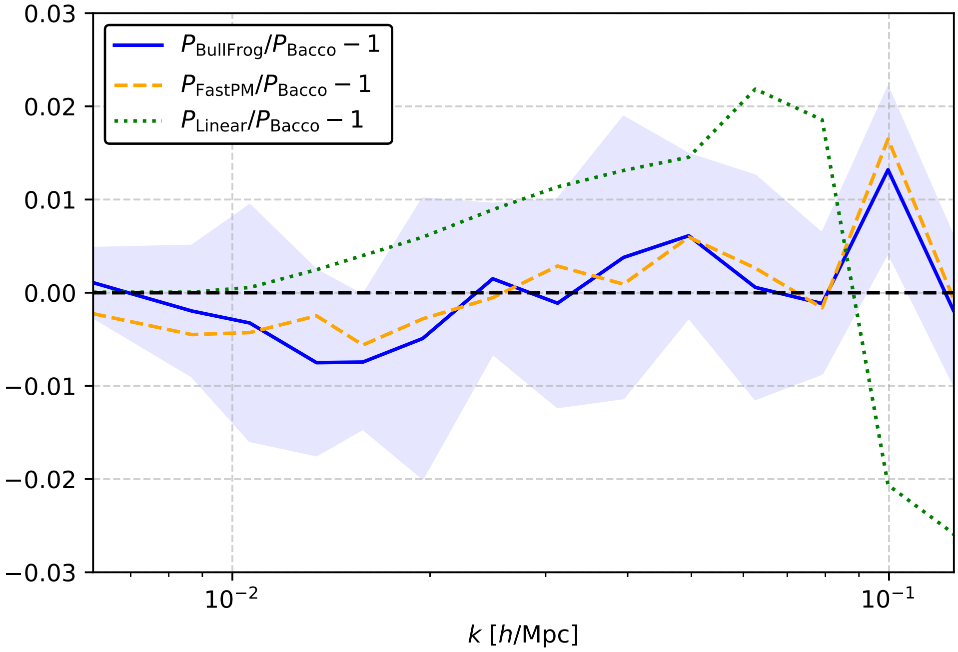

Figure 5.3: Comparison of BULLFROG, FASTPM and Bacco in the DDE5 model. As in the case of DDE4 5.2 BULLFROG is consistent with Bacco up to the deviation at $k = 0.1$.

simulations suffer from a strong cosmic variance. Additionally, we interpolate half as many CO*N*CEPT values onto the BULLFROG k bins which introduces further inaccuracies. When looking through all considered models in figures 5.5, 5.6, 5.7 and 5.8, we can see that the deviation from CO*N*CEPT remains consistent in its amplitude, which is reassuring, as it does not seem to depend on the choice of cosmology.

5.3 Numerical Convergence

Lastly, we conclude our investigation by looking at the convergence of BULLFROG towards a reference solution. For this we use the same realisation of the universe (i.e. the same white noise field seed) for all runs and we do the comparison with the DDE4 model. Our reference solution is a BULLFROG simulation with 200 steps. The full relative difference can be seen in figure 5.9. There we can see that the error at non-linear scales is at most less than 1% (but close to it). When trying to model non-linear structure it is therefore advisable to use at least 50 BULLFROG steps, or 100 would be even better. In each case BULLFROG with a certain amount of steps performs better than its FASTPM counterpart. To better investigate the impact on linear scales we have restricted the x and y axis and visualised the result in 5.10. We can see that using 10 BULLFROG steps introduces an error of 0.2% at most, with the peak residing at $k = 0.1$. While this coincides with the error peak in our comparison to Bacco, it is most likely not the main reason of the

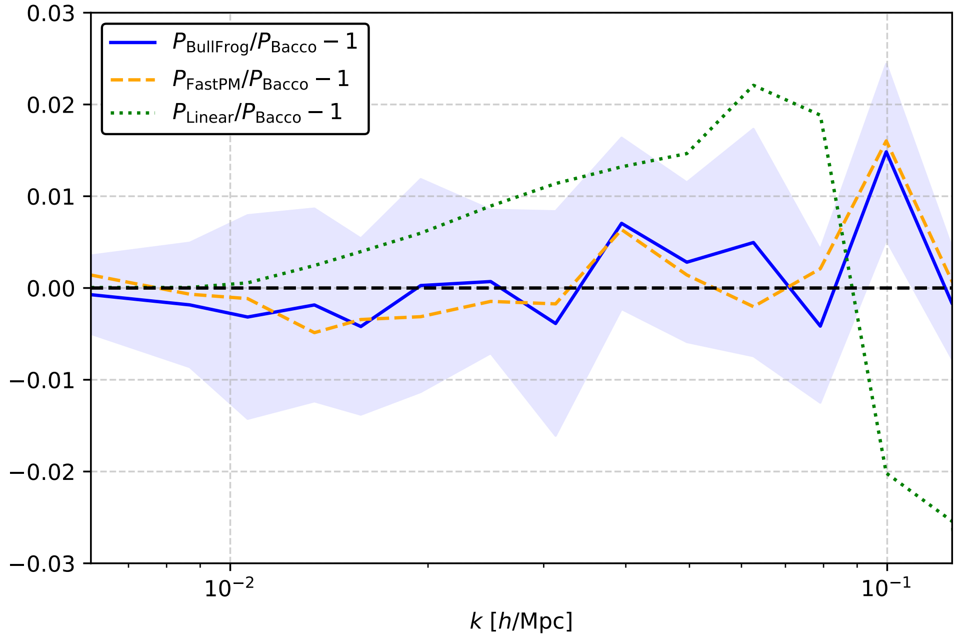

Figure 5.4: Comparison of BullFrog, FastPM and Bacco in the DDE6 model. The same trend as in both previous models is observable here, where BullFrog is consistent with Bacco everywhere, except at $k = 0.1$.

deviation. While no rigorous analysis of simulation lengths were conducted, a rough estimate yields that a BullFrog simulation requires $\approx$ 30s, while a FastPM simulation with 100 steps (which corresponds to a slightly worse accuracy) requires $\approx$ 1min.

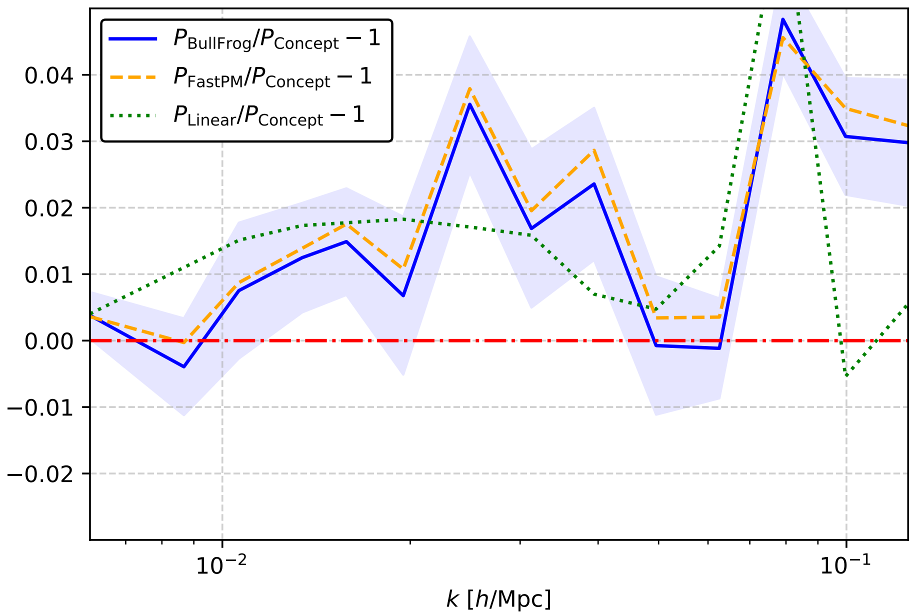

Figure 5.5: Comparison of BullFrog, FastPM and Concept in the ΛCDM model.

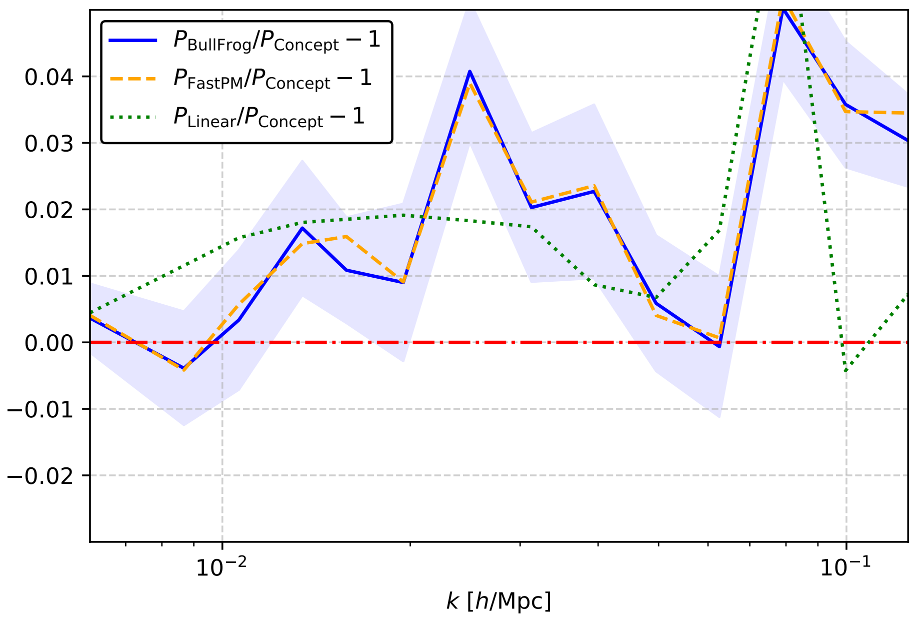

Figure 5.6: Comparison of BullFrog, FastPM and Concept in the DDE1 model. Similarly to the ΛCDM model the error is $\approx 5\%$.

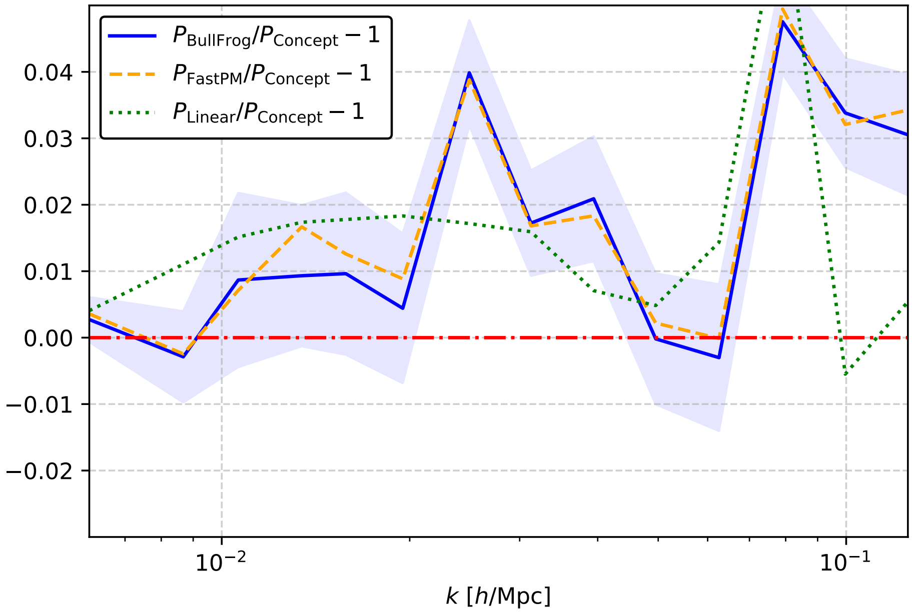

Figure 5.7: Comparison of BULLFROG, FASTPM and Concept in the DDE2 model.

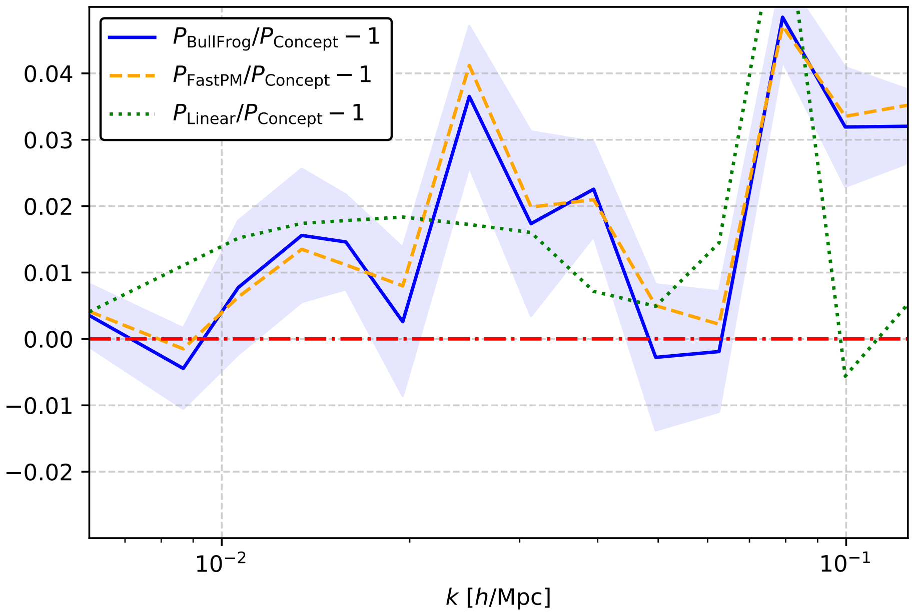

Figure 5.8: Comparison of BULLFROG, FASTPM and Concept in the DDE3 model.

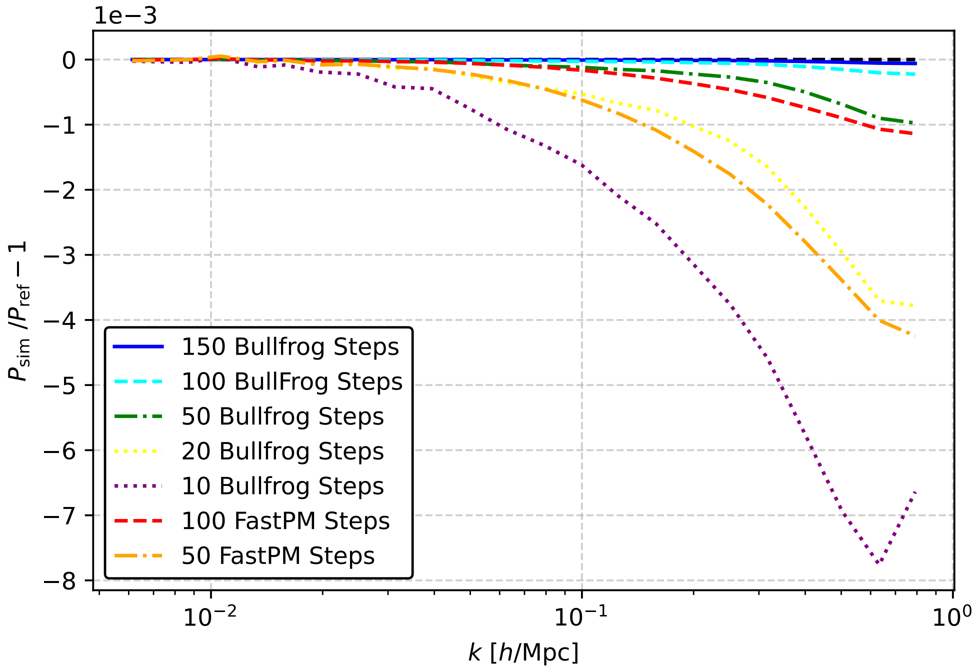

Figure 5.9: Numerical convergence analysis of the full non-linear power spectrum. One can see that BullFrog converges towards the reference solution with significantly fewer steps. The maximum error introduced by the lowest amount of steps in this case (10) is less than 1% even strongly non-linear scales.

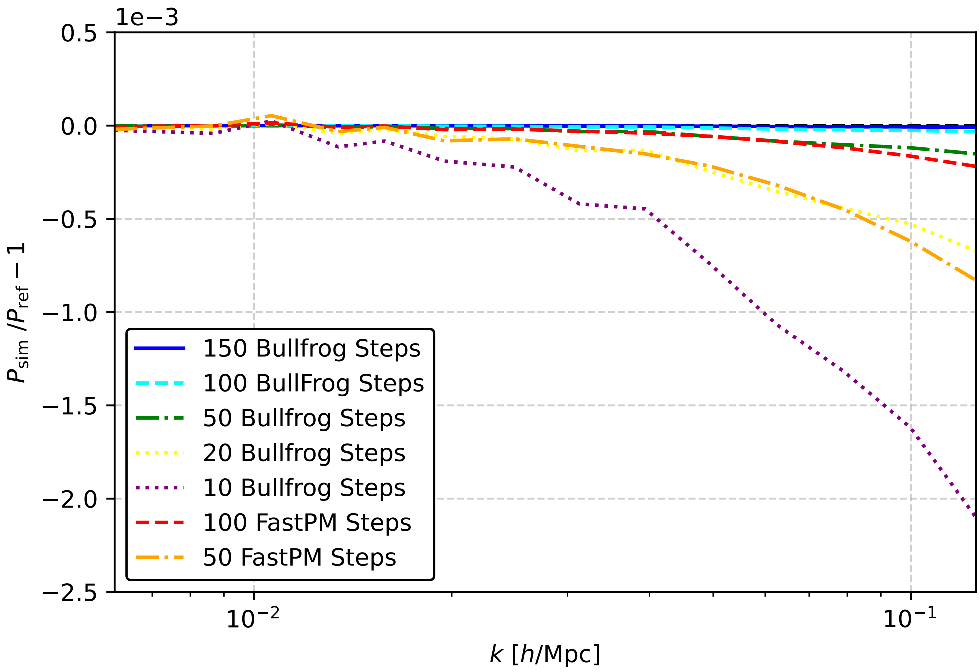

Figure 5.10: Numerical convergence analysis in the linear regime. The linear regime is the most important one for our comparisons with Bacco and CO*N*CEPT. Here errors introduced by using 10 BullFrog steps (as was done in the other simulations) is of order 0.2‰ at $k = 0.1$ and should therefore only have a miniscule impact on the overall accuracy of our simulation results.

6 Discussion and Conclusion

The main results of thesis can be loosely split into two parts:

1. The theoretical insights about the time evolution of large scale structure perturbations, through the first and second order growth function, in various cosmological models.

2. The state-of-the art fast integrator BULLFROG for beyond ΛCDM models.

We first discuss the theoretical findings and the time integrator afterwards, although both of these are of course closely related and intertwined. We then give an outlook on possible avenues for future work.

Theoretical Insights We have started by rederiving the equations which describe the time evolution of the background spacetime if one assumes that the universe consists of CDM, DE and possesses non-zero curvature in section 2.1. We have also discussed why including radiation, if one assumes that it interacts negligibly with matter, will affect the background evolution only. Next we derived the fluid equations in an expanding universe, which govern the dynamics of matter and linearised them, in order to turn our complex PDE for the dynamics of matter into an ODE for the time evolution of the matter density perturbations at the start of section 2.3. We frequently referred to this growth factor as the D-time.

The analytical solutions to the D-time ODE for EdS, ΛCDM and M+R cosmological models were already well known [37][39] and re-derived in sections 2.3.1, 2.3.2 and 2.3.3 respectively, however, all of these models suffer from divergences at $a = 0$ at the level of the Euler-Poisson system of equations. This issue can be resolved through choices of initial conditions (also known as the slaving argument) for EdS and ΛCDM, but was thought not possible when one includes a radiation term in the Friedmann equation [37]. As we have shown in section 2.3.3, finding a slaving argument for M+R is possible, although it is different from the EdS/ΛCDM one. While this is not implemented into the time integrator for beyond ΛCDM models, as it would have been beyond the scope of this project, it builds the foundation of possible future work and presents a previously unknown result.

Another important insight is the derivation and analysis of the D-time ODE for the kDDE model, which is the core part of this thesis. An analytical solution to the full kDDE ODE could not be found. We have investigated numerically how different contributions, like varying strength of dark energy and inclusion of curvature, affects the time evolution of the density perturbations in the linearised system, for realistic choices of the w_0 and w_a dark energy parameters in 2.3.4. Additionally, we discussed how this ODE behaves for early times in section 2.3.5, using multiple avenues, which is important for initialisation of BULLFROG, as it needs to be started precisely in the growing mode. We then used this early time solution to derive a slaving argument for kDDE in section 2.3.6, which turns out to be the same one as for ΛCDM and EdS.

Lastly, we have generalised 2LPT towards the kDDE model, and discussed several technical details, which are usually left out in the literature.

BullFrog We have shown that BullFrog is in very good agreement with Bacco in the DDE regime with discrepancies $< 1\%$ in the linear regime. The only oddity in this comparison is the consistent deviation-peak at $k = 0.1$, which is most likely due to the small number of bins onto which we interpolate, but might also be related to the inaccuracies introduced by using only 10 BullFrog steps in our simulations.

Our comparison with CONCEPT shows deviations of up to 5%, which is far larger, but also to be expected as the simulations both start from different white noise fields and therefore realisations of the universe. Since we also only conducted one CONCEPT run in each comparison and did not average over them like for BullFrog or FastPM, the CONCEPT power spectra suffer from high cosmic variance, which further increases the discrepancy.

We concluded with a test of numerical convergence, where we saw that BullFrog converges towards the reference solution with fewer timesteps than FastPM in the case of DDE, a result already shown for ΛCDM in [15]. This corresponds to an overall shorter simulation time, with 100 FastPM steps corresponding to $\approx$ 1min, while 50 BullFrog steps induced a simulation length of $\approx$ 30s, where the BullFrog power spectrum was slightly more accurate.

Outlook The BullFrog "project" can now be further pursued through four avenues:

1. Further/more sophisticated validation of the current implementation.

2. Justification of the full parameter space.

3. Inclusion of further species (radiation and massive neutrinos) into the kDDE model.

4. Implementation of simulations in a curved space.

For further tests of the current implementation it would be beneficial to compare it to another N-body simulation code as a test of its validity. Additionally, simulations with a larger number of particles would allow for more fine-grained binning of the BullFrog power spectrum and allow for more accurate interpolations. Alternatively, one could also evaluate the power spectrum with equal bins, therefore discarding the need for interpolation altogether. Another interesting test would be to run simulations throughout the entire parameter space, to see if deviations can be found and if they are dependent on some specific parameters.

When deriving our early time solution and the slaving condition for the kDDE model we made two restricting assumptions: First, we assumed that $w_0 + w_a < 0$, without which the derivation would not be valid, and second, we assumed that Λ_{K0} is always small enough, such that does not cause additional divergent terms at early times. While both of these assumptions are consistent with current measurements [7, 28], they still restrict the parameter space, which one would like to keep as open as possible, for general parameter inference methods. If our analysis is not extendable towards the remaining parameter space, it would still be desirable to quantify the precise range of validity.

The inclusion of radiation into the kDDE framework is an obvious next step, since the groundwork was already laid here through derivation of the slaving argument in the M+R model and the early time solution of kDDE. One can therefore conjecture that the early time solution in such a kDDE+R model will be of the form:

$$D(a) = \frac{2}{3}\Lambda_{\mathrm{R0}} + a - \frac{4}{7}\Lambda_{\mathrm{k0}}a^2 + O(a^3)\,, \tag{6.1}$$

and the slaving argument will look precisely like in the M+R case. Of course this has to be rigorously derived and studied numerically, as was done for the kDDE model in this thesis. A potentially very non-trivial aspect will then be introduced to the LPT discussion: while in the case of kDDE, the derivation of the 1LPT and 2LPT displacements were analogous to known derivations in the literature, this might change when one includes radiation. In section 3.1, when we replaced the mass conservation equation, we have used the slaving argument to fix $\delta^{\mathrm{ini}} = 0$, which simplified the resulting equation (3.5). Changing the slaving argument might have an impact on the subsequent derivation, which would be a crucial point to be investigated. To include massive neutrinos into this framework, one would have to accurately model their evolution from relativistic particles with a density $\propto a^{-4}$ to particles with a density $\propto a^{-3}$ at the level of the Friedmann equation. How this would impact the early time solution is unclear at this stage, but it should not cause divergences at the level of the D function since only terms which fall faster than a^{-4} should yield these.

Finally, the most challenging extension of this work, would be the proper implementation of a curved background into the simulations. While the effect of curvature on the growth factor is included in our simulations, this is only one of many, as our simulations are still conducted in a flat box. Pioneering work in this direction has recently been done in [62], although other approaches might also be feasible.

Bibliography

[1] P.J.E. Peebles, *The Large-Scale Structure of the Universe*, Princeton University Press (1980), 10.2307/j.ctvxrpz4n.

[2] S.M. Carroll, *Spacetime and Geometry: An Introduction to General Relativity*, Cambridge University Press (2019), 10.1017/9781108770385.

[3] P. Bull, Y. Akrami, J. Adamek, T. Baker, E. Bellini, J. Beltrán Jiménez et al., *Beyond lcdm: Problems, solutions, and the road ahead*, *Physics of the Dark Universe* **12** (2016) 56–99 [1512.05356].

[4] D. Huterer, *A Course in Cosmology: From Theory to Practice*, Cambridge University Press (2023), 10.1017/9781009070232.

[5] L. Perivolaropoulos and F. Skara, *Challenges for lcdm: An update*, *New Astronomy Reviews* **95** (2022) 101659 [2105.05208].

[6] E. Abdalla, G.F. Abellán, A. Aboubrahim, A. Agnello, O. Akarsu, Y. Akrami et al., *Cosmology Intertwined: A Review of the Particle Physics, Astrophysics, and Cosmology Associated with the Cosmological Tensions and Anomalies*, *Journal of High Energy Astrophysics* **34** (2022) 49.

[7] A. Adame, J. Aguilar, S. Ahlen, S. Alam, D. Alexander, C. Allende Prieto et al., *Desi 2024 vii: cosmological constraints from the full-shape modeling of clustering measurements*, *Journal of Cosmology and Astroparticle Physics* **2025** (2025) 028 [2411.12022].

[8] M. Kamionkowski and A.G. Riess, *The Hubble Tension and Early Dark Energy*, *Annual Review of Nuclear and Particle Science* **73** (2023) 153.

[9] D. Huterer and D.L. Shafer, *Dark energy two decades after: Observables, probes, consistency tests*, *Reports on Progress in Physics* **81** (2018) 016901.

[10] S. Tassev, M. Zaldarriaga and D.J. Eisenstein, *Solving large scale structure in ten easy steps with COLA*, *Journal of Cosmology and Astroparticle Physics* **2013** (2013) 036 [1301.0322].

[11] C. Howlett, M. Manera and W.J. Percival, *L-PICOLA: A parallel code for fast dark matter simulation*, *Astronomy and Computing* **12** (2015) 109 [1506.03737].

[12] A.E. Bayer, A. Banerjee and Y. Feng, *A fast particle-mesh simulation of non-linear cosmological structure formation with massive neutrinos*, *Journal of Cosmology and Astroparticle Physics* **2021** (2021) 016 [2007.13394].

[13] F. List and O. Hahn, *Perturbation-theory informed integrators for cosmological simulations*, *Journal of Computational Physics* **513** (2024) 113201 [2301.09655].

[14] F. List, O. Hahn and C. Rampf, *Starting cosmological simulations from the big bang*, *Physical Review Letters* **132** (2024) 131003 [2309.10865].

[15] C. Rampf, F. List and O. Hahn, *Bullfrog: multi-step perturbation theory as a time integrator for cosmological simulations*, *Journal of Cosmology and Astroparticle Physics* **2025** (2025) 020 [2409.19049].

[16] M. Chevallier and D. Polarski, *Accelerating universes with scaling dark matter*, *International Journal of Modern Physics D* **10** (2001) 213 [gr-qc/0009008].

[17] J. Dakin, S. Hannestad and T. Tram, *The cosmological simulation code concept 1.0*, *Monthly Notices of the Royal Astronomical Society* **513** (2022) 991–1014 [2112.01508].

[18] G. Arico', R. Angulo and M. Zennaro, *Accelerating large-scale-structure data analyses by emulating boltzmann solvers and lagrangian perturbation theory*, *Open Research Europe* **1** (2022) 152 [2104.14568].

[19] R.E. Angulo and O. Hahn, *Large-scale dark matter simulations*, *Living Reviews in Computational Astrophysics* **8** (2022) .

[20] P. Jones, *Mesopotamian cosmic geography*, *The Jewish Quarterly Review* **91** (2001) 485.

[21] B. Eastwood, *Ordering the Heavens: Roman Astronomy and Cosmology in the Carolingian Renaissance*, Brill, Leiden, The Netherlands (2007), 10.1163/ej.9789004161863.i-453.

[22] N. Copernicus, *De Revolutionibus Orbium Coelestium*, Johannes Petreius, Nuremberg (1543).

[23] R. Berendzen, *Geocentric to heliocentric to galactocentric to acentric: the continuing assault to the egocentric*, *Vistas in Astronomy* **17** (1975) 65.

[24] E. Hubble, *A relation between distance and radial velocity among extra-galactic nebulae*, *Proceedings of the National Academy of Sciences* **15** (1929) 168.

[25] M.S. Turner, *Two theorists never in doubt*, *Physics Today* **54** (2001) 10.

[26] J.C. Mather, E.S. Cheng, D.A. Cottingham, R.E. Eplee, Jr., D.J. Fixsen, T. Hewagama et al., *Measurement of the Cosmic Microwave Background Spectrum by the COBE FIRAS Instrument*, *Astrophysical Journal* **420** (1994) 439.

[27] C.L. Bennett, D. Larson, J.L. Weiland, N. Jarosik, G. Hinshaw, N. Odegard et al., *Nine-year wilkinson microwave anisotropy probe (wmap) observations: Final maps and results*, *The Astrophysical Journal Supplement Series* **208** (2013) 20 [1212.5225].

[28] Planck collaboration, *Planck 2018 results. VI. Cosmological parameters*, *Astronomy & Astrophysics* **641** (2020) A6 [1807.06209].

[29] H. Aihara, R. Armstrong, S. Bickerton, J. Bosch, J. Coupon, H. Furusawa et al., *First data release of the hyper suprime-cam subaru strategic program*, *Publications of the Astronomical Society of Japan* **70** (2017) S8 [1702.08449].

[30] R. Laureijs, J. Amiaux, S. Arduini, J.-L. Augueres, J. Brinchmann, R. Cole et al., *Euclid definition study report*, *Euclid Consortium* (2011) [1110.3193].

[31] L.S. Collaboration, P.A. Abell, J. Allison, S.F. Anderson, J.R. Andrew, J.R.P. Angel et al., *Lsst science book, version 2.0*, *LSST Corporation* (2009) [0912.0201].

[32] S. Weinberg, *Cosmology*, Oxford University Press (2008).

[33] R.M. Wald, *General Relativity*, The University of Chicago Press (1984), 10.7208/chicago/9780226870373.001.0001.

[34] P. Chrusciel, *Elements of General Relativity*, Compact Textbooks in Mathematics, Birkhäuser, Switzerland (Mar., 2020), 10.1007/978-3-030-28416-9.

[35] W. Rindler, *Relativity: Special, General, And Cosmological Second Edition*, Oxford University Press (04, 2006), 10.1093/oso/9780198567318.001.0001.

[36] J.A. Vazquez Gonzalez, L.E. Padilla and T. Matos, *Inflationary cosmology: from theory to observations*, *Revista Mexicana de Física E* **17** (2020) 73–91 [1810.09934].

[37] C. Rampf, B. Villone and U. Frisch, *How smooth are particle trajectories in a ΛCDM Universe?*, *Monthly Notices of the Royal Astronomical Society* **452** (2015) 1421 [1504.00032].

[38] D. Baumann, *Cosmology*, Cambridge University Press (2022), 10.1017/9781108937092.

[39] M. Demianski, Z.A. Golda and A. Woszczyna, *Evolution of density perturbations in a realistic universe*, *General Relativity and Gravitation* **37** (2005) 2063 [gr-qc/0504089].

[40] Y. Brenier, U. Frisch, M. Henon, G. Loeper, S. Matarrese, R. Mohayaee et al., *Reconstruction of the early universe as a convex optimization problem*, *Monthly Notices of the Royal Astronomical Society* **346** (2003) 501 [astro-ph/0304214].

[41] V. Zheligovsky and U. Frisch, *Time-analyticity of Lagrangian particle trajectories in ideal fluid flow*, *Journal of Fluid Mechanics* **749** (2014) 404 [1312.6320].

[42] S. Nesseris, Y. Akrami and G.D. Starkman, *To cpl, or not to cpl? what we have not learned about the dark energy equation of state*, 2503.22529.

[43] J. Moser, *The order of a singularity in Fuchs' theory*, *Mathematische Zeitschrift* **72** (1959) 379.

[44] C. Rampf, *The recursion relation in Lagrangian perturbation theory*, *Journal of Cosmology and Astroparticle Physics* **12** (2012) 004 [1205.5274].

[45] T. Matsubara, *Recursive Solutions of Lagrangian Perturbation Theory*, Physical Review D **92** (2015) 023534 [1505.01481].

[46] U. Frisch and B. Villone, *Cauchy's almost forgotten lagrangian formulation of the euler equation for 3d incompressible flow*, The European Physical Journal H **39** (2014) 325 [1402.4957].

[47] T. Matsubara, *On Second-Order Perturbation Theories of Gravitational Instability in Friedmann-Lemaître Models*, Progress of Theoretical Physics **94** (1995) 1151 [astro-ph/9510137].

[48] F.R. Bouchet, R. Juszkiewicz, S. Colombi and R. Pellat, *Weakly Nonlinear Gravitational Instability for Arbitrary Omega*, Astrophysical Journal Letters **394** (1992) L5.

[49] T. Buchert and J. Ehlers, *Lagrangian theory of gravitational instability of Friedman-Lemaitre cosmologies – second-order approach: an improved model for non-linear clustering*, Monthly Notices of the Royal Astronomical Society **264** (1993) 375.

[50] Y. Feng, M.-Y. Chu, U. Seljak and P. McDonald, *Fastpm: a new scheme for fast simulations of dark matter and haloes*, Monthly Notices of the Royal Astronomical Society **463** (2016) 2273–2286 [1603.00476].

[51] T. Quinn, N. Katz, J. Stadel and G. Lake, *Time stepping n-body simulations*, astro-ph/9710043.

[52] H. Simon-Onfroy, F. Lanusse and A. de Mattia, *Benchmarking field-level cosmological inference from galaxy redshift surveys*, 2504.20130.

[53] F. Bernardeau, S. Colombi, E. Gaztañaga and R. Scoccimarro, *Large-scale structure of the universe and cosmological perturbation theory*, Physics Reports **367** (2002) 1–248 [astro-ph/0112551].

[54] A. Taruya and S. Colombi, *Post-collapse perturbation theory in 1d cosmology – beyond shell-crossing*, Monthly Notices of the Royal Astronomical Society **470** (2017) 4858–4884 [1701.09088].

[55] M. Pietroni, *Structure formation beyond shell-crossing: nonperturbative expansions and late-time attractors*, Journal of Cosmology and Astroparticle Physics **2018** (2018) 028–028 [1804.09140].

[56] C. Rampf, U. Frisch and O. Hahn, *Unveiling the singular dynamics in the cosmic large-scale structure*, Monthly Notices of the Royal Astronomical Society: Letters **505** (2021) L90–L94 [1912.00868].

[57] J. Lesgourgues, *The cosmic linear anisotropy solving system (class) i: Overview*, 1104.2932.

[58] D. Blas, J. Lesgourgues and T. Tram, *The cosmic linear anisotropy solving system (class). part ii: Approximation schemes*, *Journal of Cosmology and Astroparticle Physics* **2011** (2011) 034–034 [1104.2933].

[59] A. Lewis, A. Challinor and A. Lasenby, *Efficient computation of cosmic microwave background anisotropies in closed friedmann-robertson-walker models*, *The Astrophysical Journal* **538** (2000) 473–476 [astro-ph/9911177].

[60] R.E. Angulo and A. Pontzen, *Cosmological n-body simulations with suppressed variance*, *Monthly Notices of the Royal Astronomical Society: Letters* **462** (2016) L1 [1603.05253].

[61] R. Hockney and J. Eastwood, *Computer Simulation Using Particles*, CRC Press (2021), 10.1201/9780367806934.

[62] J. Adamek and R. Boschetti, *Incorporating curved geometry in cosmological simulations*, 2508.20606.